universität wien

MASTERARBEIT / MASTER'S THESIS

Titel der Masterarbeit / Title of the Master's Thesis

Topographic mapping of the connectivity between different classes of neurons and tanycytic subtypes distributed along the rostro-caudal extension of the hypothalamic III-ventricle

verfasst von / submitted by

Sophie Franzmeier, BSc

angestrebter akademischer Grad / in partial fulfilment of the requirements for the degree of

Master of Science (MSc)

Wien, 2020 / Vienna, 2020

Studienkennzahl lt. Studienblatt / degree programme code as it appears on the student record sheet:	UA 066 834
Studienrichtung lt. Studienblatt / degree programme as it appears on the student record sheet:	Molekulare Biologie (Master) / Master's degree programm Molecular Biology
Betreut von / Supervisor:	Univ. Prof. Dr. Tibor Harkany

Affidativ

I hereby declare that I am the sole author of this master thesis, that I indicated all material and that I have not used any other sources than those listed in the bibliography and identified as references. I further declare that I have not submitted this thesis at any other institution and that the text document uploaded to University of Vienna online is identical to the present master's thesis.

_____ _____

08.04.2020

Abstract

Tanycytes are highly specialized, bipolar ependymal cell residing in the tuberal region of the hypothalamus. While the cylindric cell bodies border the III-ventricular walls their long, radial process is targeting deeply into the brain parenchyma where it establishes contacts with hypothalamic-hypophyseal portal blood capillaries. In this way, tanycytes link the CSF circulating inside the ventricular system with the peripheral blood system and thus are regarded as modulators of the exchange of hormones and other biologically active substances between the CSF and the blood. Due to this advantageous location and unique morphology tanycytes emerge as pivotal components of a variety of important hypothalamic processes. Moreover, it has been suggested that tanycytes establish so-called 'neurono-glial synaptoid contacts' with neurosecretory axons at the area of the ME. In this study, I investigated the hypothesis that tanycytes are capable of transducing neuronal electrochemical signaling by detecting and further quantifying the amount of excitatory and inhibitory synaptic inputs of neurons onto tanycytes in topographically distinct regions around the hypothalamic III-ventricle. To approach this, I used immunolabeled coronal brain sections from WT, CRH-Cre-tdTomato and RAX-Cre-ER^{T2}-tdTomato mice, evaluated the sections by acquiring confocal micrographs of 13 defined regions of interest alongside the III-ventricle and established a suitable and reliable reconstruction workflow by using IMARIS to 3-dimensionally reconstruct tanycytic processes emerging from the III-ventricular walls and detect synaptic inputs. Using this newly developed reconstruction method, I successfully showed that tanycytic process do receiving synaptic inputs from adjacent hypothalamic neurons. By investigating the entire rostro-caudal extension of the hypothalamus I observed a slight overall trend towards higher amounts of synaptic inputs at caudal regions where some main hypothalamic nuclei can be found like the DMH, the VMH, the ArcN and the ME. Surprisingly, at all positions examined just a fraction of the total number of detected tanycytes receive neuronal inputs. Moreover, the use of different tanycytic markers revealed that RAX+ tanycytes are located at more caudal hypothalamic regions whereas GFAP+ tanycytes were detected almost exclusively at more rostral territories.

Cumulatively, the observation of excitatory and inhibitory synaptic inputs onto tanycytes during this investigation emphasizes the hypothesized involvement of tanycytes in synaptic signal transmission and suggests a way of communication between tanycytes and neurons of different hypothalamic nuclei.

keywords: *tanycytes, hypothalamus, III-ventricle, synapses, synaptoid contacts, synaptic communication, neurotransmission, 3-dimensional reconstructions*

Content

Affidativ i
Abstract ii
Content iii
List of Tables v
List of Figures vi
Glossary viii
1. Introduction 1
1.1. The Hypothalamus 1
1.1.1. Hypothalamic nuclei 2
1.2. Ventricular system, cerebro-spinal-fluid and volume transmission 6
1.3. Tanycytes 9
1.3.1. Tanycyte subpopulations 11
1.3.2. A transgenic mouse model to study tanycytes 14
1.4. Tanycytes and Synapses 16
1.5. Hypothesis 18
2. Material and Methods 19
2.1. Ethics statement 19
2.2. Animals 19
2.2.1. Transgenic mice 19
2.3. Tamoxifen preparation and injection 22
2.4. Genotyping 22
2.4.1. Theoretical background of PCR 22
2.4.2. PCR protocol 23
2.5. Brain preparation for microscopic analysis: perfusion and slicing 24
2.6. Immunohistochemistry & Immunofluorescence 25
2.6.1. Theoretical background of Immunohistochemistry 25
2.6.2. Characterization of primary antibodies 25
2.6.3. Immunostaining protocol 26
2.7. Image Acquisition 29
2.8. Analyzed positions 30
2.9. Image processing and analysis 32

2.9.1. Synaptic inputs 32
2.9.2. Tanycytic processes 32
2.9.3. Synaptic inputs on tanycytic processes 32
2.9.4. Nuclei reconstruction 33
2.10. Statistical analysis 33
3. Results 35
3.1. Genotyping results 35
3.2. Distribution and interaction of neuronal inputs with tanycytes 36
3.3. Imaris reconstructions 41
3.3.1. Detected cell types along the III-ventricle's walls and floor part 41
3.3.2. Filament tracer tool is more suitable for reconstructing tanycytic processes 42
3.3.3. Image reconstruction workflow 48
3.4. Synaptic inputs on tanycytic processes 52
3.5. Differences in the amount of synaptic inputs 56
3.6. Differences between α and β tanycytes 58
3.7. Identification of tanycyte subtypes by different markers 62
3.8. Summary 66
4. Discussion 68
References 72
Appendix 79
Zusammenfassung 80

List of Tables

Table 1 | Localization of chemical synapses 16
Table 2 | Experimental mouse models used 19
Table 3 | Tamoxifen injection 22
Table 4 | List of primers used for genotyping 23
Table 5 | PCR mastermix 24
Table 6 | Thermal cycler protocol used for RAX-Cre-ER^{T2}-tdTomato genotyping 24
Table 7 | Primary antibodies 27
Table 8 | Secondary antibodies 28
Table 9 | Mouse lines, number of used animals per line, number of sections and analyzed positions 31
Table 10 | Detected cell types at position 1 to 13 located at the caudal-to- rostral expansion of the lateral walls and floor part of the hypothalamic III-ventricle 42
Table 11 | Values for reconstruction of tanycytic soma and process executed by using the 'Surface Reconstruction' tool 43
Table 12 | Number of reconstructed tanycytic processes per mouse line 48

List of Figures

Figure 1 | Sagittal view of hypothalamic nuclei 2
Figure 2 | Localization and structures of the ventricular system 7
Figure 3 | Location of hypothalamic α- and β- tanycytes lining the walls and floor part of the III-ventricle 12
Figure 4 | RAX-regulated Cre-ER^{T2}-mediated tdTomato expression 15
Figure 5| Inducible knock-out system using tamoxifen 21
Figure 6 | Theoretical localization of selected coronal mouse brain sections 30
Figure 7 | Representative overview scans of RAX-Cre-ER^{T2}-tdTomato 31
Figure 8 | Agarose gel with PCR amplicons showing heterozygous mice expressing the transgenic Cre-ER^{T2} allele (290bp) and the Wild type allele (401bp) 36
Figure 9 | Slice 1 approximate -2.30mm relative to bregma with positions 1 and 2 37
Figure 10 | Slice 2approximate -1.82mm relative to bregma with positions 3, 4, 5 and 6 38
Figure 11 | Slice 3 approximate -1.34mm relative to bregma with positions 7, 8, 9 and 10 39
Figure 12 | Slice 4 approximate -0.70mm to bregma with positions 11, 12 and 13 40
Figure 13 | Reconstructed tanycytes by using the 'Surface Reconstruction' tool 43
Figure 14 | Reconstruction of tanycytic processes using the 'Automatic Tracing' tool 44
Figure 15 | Drawing of tanycytic processes by using the 'AutoDepth' mode 45
Figure 16 | More inputs onto tanycytes remodeled by 'Surface Reconstruction' tool 46
Figure 17 | Comparison between 'Surface Reconstruction' and 'Filament Tracer' tool 47
Figure 18 | IMARIS reconstruction workflow 49
Figure 19| IMARIS reconstructions of position 1 to 13 51
Figure 20 | Nestin+ tanycytic processes receiving synaptic VGLUT2+ inputs 53
Figure 21 | Amount of reconstructed tanycytic processes, tanycytes receiving synaptic inputs and total amount of synaptic inputs in all analyzed mouse lines 54
Figure 22 | Percentage of tanycytes receiving or not receiving synaptic inputs in all analyzed mouse lines 55
Figure 23 | Differences between the amount of synaptic inputs across all positions examined alongside the walls of the hypothalamic III-ventricle 57
Figure 24 | Different tanycytic sub-populations found on slice 2 59
Figure 25 | Different tanycytic sub-populations found on slice 3 60

Figure 26 | Differences in synaptic inputs between individual subtypes found at the same rostro-caudal position 61
Figure 27 | Differences in synaptic inputs within one tanycytic subtype located at different rostro-caudal positions 62
Figure 28 | Caudal-to-rostral distribution of different tanycytic markers across the borders of the hypothalamic III-ventricle 64
Figure 29 | Distribution of RAX+ and GFAP+ tanycytes around the area of the dorsomedial and ventromedial hypothalamus (slice 2) 65
Figure 30 | Inhibitory VGAT+ inputs onto RAX+ and GFPA+ tanycytic processes at the area of the VMH (position4) 66
Figure 31 | TH+ neuronal terminals in close proximity to RAX+ tanycytic processes at the area of the 70

Glossary

ACTH	Adrenocorticotropic hormone
AgRP	Agouti-related peptide
AHN	Anterior hypothalamic nucleus
AMPA	α-amino-3-hydroxy-5-methyl-4-isoxazolepropionic acid
AN/ArcN	Arcuate nucleus
ANOVA	Analysis of variance
AVP	Arginine vasopressin
BSA	Bovine serum albumin
CART	Cocaine- and amphetamine-regulated transcript
cDNA	Complementary DNA
CNS	Central nervous system
CNTF	Ciliary neurotrophic factor
CNX43	Connexin 43
Cre	Causes Recombination
CRH	Corticotropin-releasing hormone
CSF	Cerebro-spinal-fluid
CVO	Circumventricular organ
DABCO	1,4-diazabicyclo [2.2.2] octane
DHA	Dorsal hypothalamic area
DMN/DMH	Dorsomedial hypothalamic nucleus
DNA	Deoxyribonucleic acid
E	Embryonic day
EAAT2	Excitatory amino acid transporter 2
ECFP	Enhanced cyan fluorescent protein
EDTA	Ethylenediaminetetraacetic acid
EGFP	Enhanced green fluorescent protein
EYFP	Enhanced yellow fluorescent protein
ER	Estrogen receptor
FSH	Follicle-stimulating hormone
GABA	γ-aminobutyric acid
GFP	Green fluorescent protein
GFAP	Glial fibrillary acidic protein
GhRH	Growth hormone-releasing hormone
GnRH	Gonadotropin-releasing hormone

GO	Gene ontology
GRIA2/GluA2	Glutamate ionotropic receptor AMPA type subunit 2
HFD	High fat diet
Hsp	Heat-shock protein
IHC	Immunohistochemical analysis
LH	Luteinizing hormone
LHA	Lateral hypothalamic area
LoC	Locus coeruleus
LoxP	Locus X over P1
LSCM	Laser scanning confocal microscope
M	Molarity
MB	Mammillary bodies
MCH	Melanin-concentrating hormone
mCherry	Monomeric cherry
ME	Median eminence
NA	Numerical aperture
NDS	Normal donkey serum
NGF	Nerve Growth Factor
NG2	Oligodendrocyte precursor cells, Polydendrocytes,
NMDA	N-Methyl-D-Aspartate
NPY	Neuropeptide Y
NSC	Neuronal stem cells
P	Postnatal day
PB	Phosphate buffer
PCR	Polymerase chain reaction
PeN	Periventricular nucleus
PFA	Paraformaldehyde
PHN	Posterior hypothalamic nucleus
POA	Preoptic area
POMC	Pro-opiomelanocortin
PVN	Paraventricular nucleus
RAX	Retina and anterior neural fold homeobox
RFP	Red fluorescent protein
RNA	Ribonucleic acid
ROI	Region of interest

ROSA26	Reverse orientated splice acceptor clone 26
SCN	Suprachiasmatic nucleus
Scn7a	Sodium voltage-gated channel alpha subunit 7
SEM	Standard error mean
Slc1a2	Solute carrier family 1 member 2
Slc7a11	Solute carrier family 7 member 11
Slc17a8	Solute carrier family 17 member 8
SON	Supraoptic nucleus
SSR	Site-specific recombinase system
SST	Somatostatin
Sx_c^-	System x_c^-
TAE	Tris-acetate EDTA
tdTomato	Tandem dimer tomato
TH	Tyrosine hydroxylase
TMN	Tuberomammillary nucleus
TRH	Thyrotropin-releasing hormone
TRHR1	Thyrotropin-releasing hormone receptor 1
Tris	Tris(hydroxymethyl)aminomethane
TSH	Thyroid-stimulating hormone
VGAT	Vesicular inhibitory amino acid (GABA) transporter
VGLUT1	Vesicular glutamate transporter 1
VGLUT2	Vesicular glutamate transporter 2
VGLUT3	Vesicular glutamate transporter 3
VMN/VMH	Ventromedial hypothalamic nucleus
4-OHT	4-hydroxytamoxifen (Tamoxifen)

1. Introduction

1.1. The Hypothalamus

The hypothalamus is located at the basis of the diencephalon and separated from the overlying thalamus by the hypothalamic sulcus. It resides at both sides of the brain and is divided by the III-ventricle in a symmetrical way resulting in one half of the hypothalamus extending in each brain hemisphere. The hypothalamus is considered as the main regulator of the body's homeostatic functions including energy metabolism, reproductive activity, stress and threat responses, thermoregulation and sleep-wake states. Moreover, together with the thalamus, the amygdala and hippocampus, the hypothalamus is part of the limbic system which is regarded as the emotional center of the brain. (Greenstein & Greenstein, 2000; Purves et al., 2004).

Representing only 0.4% of the total brain volume, the hypothalamus is one of the smallest brain components. Regardless of its size, it is involved in a diversity of different processes and displays a complex anatomical constitution mainly compromising of grey matter with various nuclei that control numerous homeostatic functions (Henning 2001). It integrates signals from the cerebral cortex, the amygdala and the hippocampal formation and sensory inputs from viscero- and somato-sensory pathways, chemosensory signals and hormones to create a variety of responses (Purves et al., 2004). On account of its privileged location, the hypothalamus closely links the nervous system via the infundibulum to the pituitary gland (also called hypophysis), thus exercising control over the body's endocrine system (Henning, 2001).

Usually, the hypothalamus is divided from a rostral-to-caudal direction into 3 regions with each region being further subdivided into a periventricular, a medial and a lateral zone. The anterior region is mainly involved in thermoregulation, fever, electrolyte balance, wake-sleep states, circadian rhythms and sexual behavior. The middle region of the hypothalamus is related to feeding, sexual behavior, aggression as well as various other automatic and endocrine responses. The most caudal part, the posterior region, plays an important role in the arousal system and the regulation of wakefulness as well as sleep (Sapper & Lowell, 2014). *Figure 1* displays a sagittal view of the hypothalamus and the localization of the various hypothalamic nuclei published in an article from 2015 by Elizondo-Vega et al.

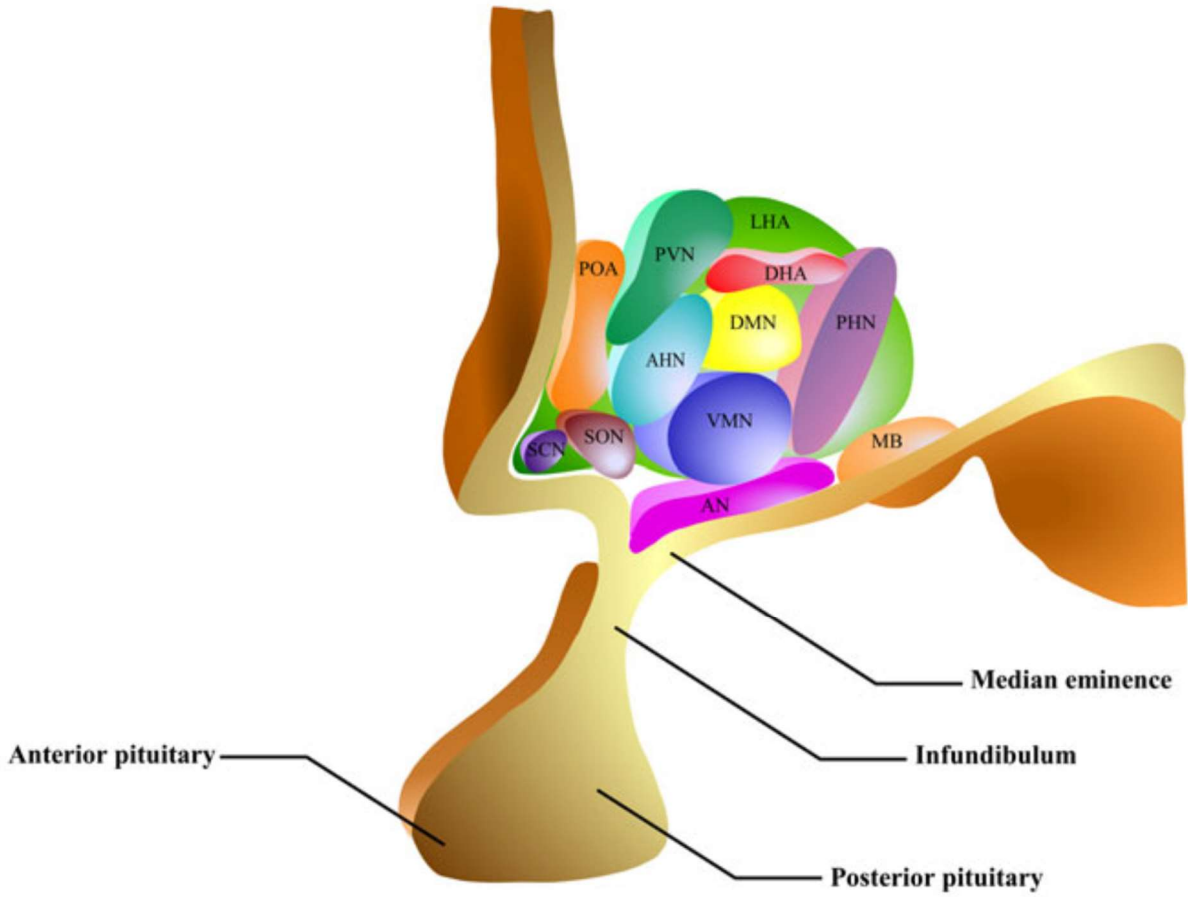

Figure 1* | *Sagittal view of hypothalamic nuclei

AHN: anterior hypothalamic nucleus, AN: arcuate nucleus, DHA: dorsal hypothalamic area, DMN: dorsomedial nucleus, LHA: lateral hypothalamic area, MB: mammillary bodies, PHN: posterior hypothalamic nucleus, POA: preoptic area, PVN: paraventricular nucleus, SCN: suprachiasmatic nucleus, SON: supraoptic nucleus, VMN: ventromedial nucleus

Reference: (Elizondo-Vega et al., 2015)

1.1.1. Hypothalamic nuclei

The next paragraphs give an overview of the complex hypothalamic anatomy describing its diverse nuclei, their location, identified neuronal cell types and some validated functions.

Supraoptic nucleus (SON)

The supraoptic nucleus is found at the medial and lateral zone of the anterior region with some nuclei extending caudally into the tuberal hypothalamic region (Felten, O'Banion, & Maida, 2016). Magnocellular neurosecretory cells produce the neurohormones arginine vasopressin (AVP) and oxytocin which are transported via axons to the fenestrated capillaries of the neurohypophysis (posterior pituitary) constituting the main connection between the central nervous system (CNS) and the endocrine system. Oxytocin is known to be involved in food

intake, maternal as well as sexual behavior and in man it is thought to influence sexual arousal and ejaculation while AVP is important for water homeostasis in the body. Other neuroactive substance like galanin and corticotropin-releasing hormone (CRH) are produced additionally (Armstrong, 2015; Hofman & Swaab, 2004).

Suprachiasmatic nucleus (SCN)

This nucleus lies in the medial zone of the anterior region and contains parvocellular neurons which are immunopositive for amongst others the neuropeptides AVP, neuropeptide Y (NPY) and neurotensin. It controls the circadian rhythm of nearly all bodily functions by a cyclical transcription-translation loop of the so-called clock genes. This mechanism is conserved in cells all over the brain and body and is controlled by the SCN. Furthermore, the SCN is involved in seasonal control of reproduction, sexual behavior and glucose homeostasis (Hofman & Swaab, 2004; Saper & Stornetta, 2015).

Paraventricular nucleus (PVN)

The PVN is localized in the periventricular and medial zone of the anterior region. Magnocellular neurosecretory cells are projecting towards the neurohypophysis to release AVP and oxytocin into the blood circulation. Parvocellular neurosecretory cells target the median eminence (ME) and are immunopositive for among others CRH, tyrosine hydroxylase (TH), γ-aminobutyric acid (GABA), galanin, growth hormone-releasing hormone (GhRH), thyrotropin-releasing hormone (TRH) and thyroid-stimulating hormone (TSH). Furthermore, nonendocrine projection neurons target caudally to the brain stem and spinal cord (Armstrong, 2015). CRH containing neurons are especially important for stress responses: projecting towards the ME they release their hormonal content into the portal blood system to innervate the adenohypophysis (anterior pituitary) to secrete adrenocorticotropic hormone (ACTH) which triggers corticosteroid release from the adrenal glands (Alpár et al., 2018).

Arcuate (infundibular) nucleus (AN, ArcN)

This horseshoe-shaped nucleus is located at the periventricular and medial zone of the tuberal region and is rich in neurotransmitters and neuropeptides. Neurons located here regulate endocrine, behavioral and metabolic mechanisms involved in feeding and reproduction activity. (Saper & Stornetta, 2015). Anorexigenic neurons containing the neurotransmitters pro-opiomelanocortin (POMC) and cocaine- and amphetamine-regulated transcript (CART) and orexigenic neurons with the neuropeptides agouti-related peptide (AgRP) and NPY are found

at the area of the ArcN which both are able to sense metabolic signals like glucose, ghrelin and leptin (Goodman & Hajihosseini, 2015). Leptin acts on ArcN-neurons in a two-sided way: on the one hand it activates anorexigenic POMC/CART-positive neurons to support weight loss and satiety and on the other hand it inhibits orexigenic AgRP/NPY-positive neurons that support food intake and weight gain (Canteras, 2012). Additionally, GhRH neurons are located here and control the secretion of growth hormones which is important for normal growth during childhood and regulates adult metabolism (Hofman & Swaab, 2004).

Ventromedial hypothalamic nucleus (VMN, VMH)

The pear-shaped VMH resides in the medial zone of the tuberal region. High numbers of somatostatin (SST) neurons are found here, additionally the presence of TRH hormone fibers and oxytocin binding in this area has been detected. Due to its connection to the basal forebrain, it is postulated that the VMH is involved in the regulation of higher cortical functions as well as behavioral responses. Furthermore, the VMH influences the female reproductive behavior, sexual orientation, gonadotropin release, aggression and feeding (Hofman & Swaab, 2004). Previous studies showed that lesions in this region result in rage and aggressive behavior (Carmichael & Braunstein, 2009).

Dorsomedial hypothalamic nucleus (DMN, DMH)

Residing in the medial zone of the tuberal region this nucleus is involved in thermoregulation of the body, blood pressure and heart rat as well as it mediates circadian rhythms of amongst others feeding behavior and sleep-wake states. On some projections expression of leptin receptors has been detected. (Saper & Stornetta, 2015). The DMH is regarded to influence appetite control as lesions in this region lead to hyperphagia which is characterized by an abnormal increase in food consumption (Carmichael & Braunstein, 2009).

Median eminence (ME)

Located in the hypothalamic tuberal region, the ME is attached to the infundibulum thus constituting a bridge between the hypothalamus and the hypophyseal gland (Felten et al., 2016). Moreover, the ME is the brain's only portal capillary system which is characterized by blood capillaries with a fenestrated endothelium that facilitates the exchange of signals between the hypothalamus and the blood circulation (Yin & Gore, 2010). Further, the ME is one out of 7 circumventricular organs (CVO) of the brain, meaning it is a structure which surrounds the cerebral ventricles. Normally, the blood-brain-barrier prevents the access of blood-born

molecules to the brain but in CVO this barrier function is incomplete on account of fenestrated capillaries (Rizzoti & Lovell-badge, 2017). Due to its location and unique features the ME represent a key intersection between the neuronal and endocrine system. One example is the release of gonadotropin-releasing hormone (GnRH): secreted into the portal blood circulation in a pulsatile manner by hypothalamic neurosecretory axon terminals in the ME, GnRH is transported to the anterior lobe of the pituitary. There, it stimulates the secretion of the gonadotrophins luteinizing hormone (LH) and follicle-stimulating hormone (FSH) which both are important regulators of sexuality and the female reproductive cycle (Prevot et al. 2010).

Posterior hypothalamic nucleus (PHN)

Found in the medial zone of the posterior region, the PHN is involved in the control of sleep and circadian rhythms, emotional expression and behavior as well as temperature regulation. Lesions in this area are associated with hypothermia which is characterized by a severe reduction in the body's temperature. It has also been shown that electrical activation of this region leads to a feeling of fear or horror (Carmichael & Braunstein, 2009).

Mammillary bodies (MB)

This structure resides in the posterior region in the medial zone of the hypothalamus and is divided into two different nuclei: a medial and a smaller lateral nucleus, but the latter harbors the largest cells in the mammillary bodies. Both nuclei show connections with the hippocampus and the anterior thalamus, structures which are associated with memory and thus this system can be influenced by the MB (Vann & Aggleton, 2004).

Tuberomammillary nucleus (TMN)

The TMN is found in the posterior region of the hypothalamus next to the mammillary bodies and represents the only source of histaminergic cells in the brain. It shows extensive projection to other hypothalamic areas as well as towards the cerebral cortex and brain stem. Histidine increases wakefulness as well as it maintains cortical arousal during emotional excitement. Importantly, histamine is one of the few neurotransmitters involved in sleep-wake processes that execute its signals via volume transmission, a concept which will be explained in chapter 1.2., and not through classic synaptic transmission. Furthermore, these neurons contain GABA, adenosine, brain natriuretic peptide, orexin and galanin. (Saper and Stornetta 2015; Schneider 2017).

Periventricular nucleus (PeN)

This nucleus forms a thin layer of cells around the walls of the III-ventricle and stretches through all hypothalamic regions. Neurons in the anteroventral part receive innervations from dopaminergic cells and further express the neuropeptide kisspeptin1 which is involved in reproduction behavior as well as GnRH secretion (Saper & Stornetta, 2015). SST expressing neurons located in this area inhibit the secretion of growth hormones (Hofman & Swaab, 2004).

Lateral hypothalamic area (LHA)

The LHA extends through all hypothalamic regions and is associated with functioning in food and water acquisition, increasing body temperature, arousal and wakefulness (Felten et al., 2016). The LHA neurons express neuropeptides orexin A and B and the melanin-concentrating hormone (MCH) which have a stimulating effect on food intake. MHC additionally plays a role in the control of sleep as well as endocrine signaling and is also encountered in the cerebro-spinal fluid (CSF). In patients suffering from schizophrenia higher levels of MHC are monitored and positively correlates with the time these patients need to fall asleep. (Swaab, 2004). Lesions in this nucleus induce anorexia and weight loss (Carmichael & Braunstein, 2009).

As already mentioned, the hypothalamus is a structure which surrounds the III-ventricle at its lateral walls and floor part. In this way, many of the various hypothalamic neurons have access to the ventricular system and the therein circulating CSF which is described in the following chapter.

1.2. Ventricular system, cerebro-spinal-fluid and volume transmission

The ventricular system of the brain consists of the 4 ventricles: (*i*) two large lateral ventricles, one in each hemisphere of the telencephalon, (*ii*) the III-ventricle located in the diencephalon, and (*iii*) the IV-ventricle located between the metencephalon and myelencephalon. The lateral ventricles are connected with the III-ventricle via two interventricular foramina of Munro and the cerebral aqueduct further links the III-ventricle to the IV-ventricle (Corbett & Haines, 2018). *Figure 2* shows the ventricular system and its location within the human brain.

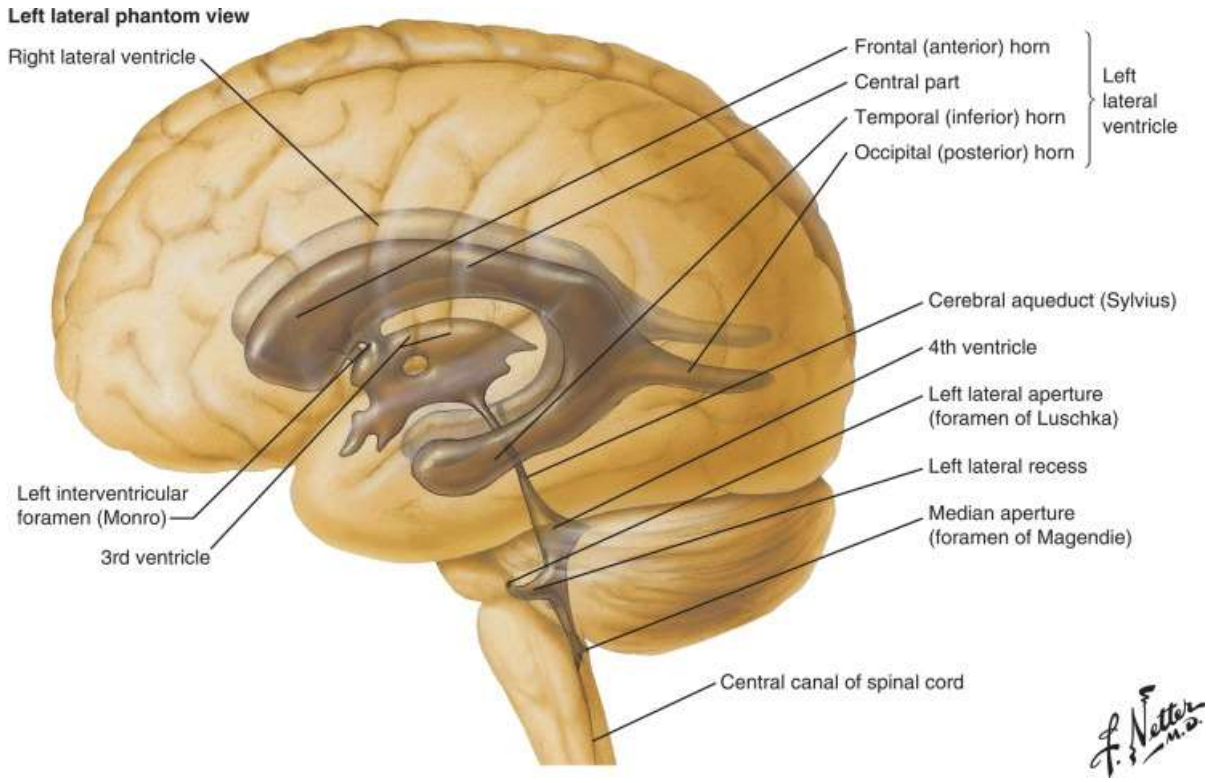

Figure 2 | Localization and structures of the ventricular system
Reference:(Felten et al., 2016)

Inside the ventricular system, the CSF is constantly circulating. This clear fluid is defined as an ultrafiltrate of plasma representing 18% of the adult human brain volume and is exchanged daily 3 to 4 times. Around 500ml of CSF are produced per day by specialized, highly vascularized structures called the choroid plexuses. These structures are found at the lateral ventricles as well as at the roof of the III- and IV-ventricle and consist of choroid epithelial cells which actively secret the CSF. There are two additional sources of water for the CSF: (*i*) there is the interstitial fluid produced by endothelial cells of the blood-brain barrier in the choroid plexuses and (*ii*) there is the complete oxidation reaction of glucose to carbon dioxide and water by parenchymal cells. After its release from the choroid plexuses, the CSF flows through all ventricles until reaching the IV-ventricle where it exits the ventricular system through two left (foramina Luschka) and one median (foramen Magendie) aperture (most of the CSF outflow occurs here) and enters the subarachnoid space. The subarachnoid space is a cavity between the arachnoid membrane and the pia mater which continuously surrounds the brain and the spinal cord. Inside this cavity, the CSF is essential for creating a buoyancy force that reduces the weight of the brain to only 45g in comparison to 1400g in air. Like this, nerves and blood capillaries located here are protected of getting damaged by the brain inside the cranial vault. Trabeculae, special tissue bridges which are attached to the arachnoid membrane, support a stable position of the brain when suspended in the CSF. After crossing the subarachnoid space,

the CSF exits through arachnoid villi which are spreading into the superior sagittal sinus as well as the venous lake of the superior sagittal sinus and is reabsorbed into the venous and lymphatic system. The majority of CSF is directly transported through the arachnoid villi in membrane bound vessels and only a minor amount passes in between these structures (Corbett & Haines, 2018; Greenstein & Greenstein, 2000; Meunier, Sawamoto, & Spassky, 2013).

The main components of the CSF are Na^+, Cl^- and HCO_3^-, but the concentration of the individual ions is steadily changing as the CSF travels from its production sites to its exit points. Additionally, a variety of different proteins are present in the CSF but at a much lower amount than in the blood (15-45mg per 100ml). Different secretion and reabsorption patterns along the walls of the ventricles and subarachnoid space lead to concentration differences of proteins as the CSF flows through this system. Furthermore, different substrates like trophic factors and nutrients are found (Greenstein & Greenstein, 2000).

Various substances are present in the CSF which are circulating through the ventricular system. Advanced mass spectrometry analysis, which have been performed during the last years, identified some of these substances as biologically active proteins, distinct peptides and neurotransmitters. They are derived from different sources: some are secreted directly by neurons or glial cells contacting the ventricular walls, others are transported from the blood into the CSF or a few are even produced by cells residing in the CSF. In this way, the CSF represents a medium which allows long-distance signal transduction and further leads to a cross-talk between remote brain regions (Rodríguez, Guerra, Peruzzo, & Blázquez, 2019). This mechanism is called volume transmission and constitutes a communication pathway additionally to classical wiring signaling. The concept of volume transmission is determined as a form of signal transduction occurring within the extracellular fluid of the brain, like e.g. the CSF, in contrast to wiring transmission which is described as the communication between neuronal or glial cells that are physically connected by defined structures like synapse or gap junctions (Agnati, Zolli, Strömberg, & Fuxe, 1995).

In 2018, an excellent study showed that CRH-releasing neurons located in the hypothalamus target ependymal cells lining the walls of the III-ventricle and stimulate the release of ciliary neurotrophic factor (CNTF) into the ventricular system. CNTF is transported via the CSF to its specific target receptors on norepinephrinergic neurons of the Locus coeruleus (LoC) which borders the passage from the cerebral aqueduct into to the IV-ventricle (Alpár et al., 2018). This mechanism represents a way to convert synaptic excitation through volume transmission via the CSF into neuromodulation of target cells remote from the sites of ligand production and release.

The constant flow of the CSF is maintained, besides others, by the movement of cilia found on cuboid ependymocytes lining the walls of all ventricles. These cells form an ependymal epithelium and further are important to establish a barrier between the CSF and the brain parenchyma (Corbett & Haines, 2018). At the walls and floor part of the III-ventricle, another cell type is found and of particular interest: the tanycyte. These cells contact the III-ventricle with their soma and additionally show long radial processes projecting into the hypothalamic brain parenchyma (Meunier, Sawamoto, and Spassky 2013). Their morphology, location and some of their diverse functions are described in detail in the next chapter.

1.3. Tanycytes

The term 'tanycyte'(greek *ταν*ύ*ς* (tanus) meaning 'stretched' or 'elongated') was introduced in the year 1954 by Ernst Horstmann, a German doctor and researcher. Horstmann was the first person describing these elongated bipolar ependymoglial cells lining the lateral walls and basis of the hypothalamic III-ventricle he detected while studying the brain of cartilaginous fish. So far, tanycytes have been detected exclusively at the borders of the III-ventricle at the area of the tuberal region of the hypothalamus where the DMH, VMH, ArcN and ME are located (Prevot et al., 2018; Robins et al., 2013), nonetheless, there are some publications speculating about the existence of tanycytes bordering the IV-ventricle (Feng, Wiggins, & von Bartheld, 2011). The tanycytes' most prominent morphologic feature is their long radial process which is projecting deeply into the brain parenchyma where it establishes contact with hypothalamic-hypophyseal portal capillaries while their cylindrical cell bodies reside at the borders of the III-ventricular walls facing the CSF (Prevot et al. 2018).

Tanycytes start to arise at the very end of embryonic development around embryonic day (E) 17 to E19 in mice at similar regions where hypothalamic neurons were produced some days earlier (Goodman & Hajihosseini, 2015; Miranda-Angulo et al., 2015). A previous study showed that the transcription factor retina and anterior neural fold homeobox transcription factor (RAX) is exclusively expressed in tanycytes and essential for correct tanycytic differentiation. Tanycytes proceed to be generated until the first or second postnatal week but are only considered as fully mature when they reach one month of life. (Miranda-Angulo et al., 2015). Moreover, tanycytes continue to proliferate postnatally but within age this capacity seems to diminish and even the total number of tanycytes drops by around 30% at later stages of life. It has been postulated further, that aged tanycytes adapt phagocytic abilities to degrade decaying neurons. (Goodman & Hajihosseini, 2015).

In contrast to the neighboring ependymal cells, tanycytes are not multiciliated but, depending on their location, they are biciliated or just display only a primary cilium extending into the CSF. At the borders of the III-ventricle, tanycytic cell bodies are connected by tight junction proteins, mainly occludins and claudins, and form a compact boundary (Langlet et al., 2013). One study published by Mullier et al. in the year 2010 detected differences in local diffusion barriers at the III-ventricular walls and claimed that a distinct expression of tight junction proteins in tanycytes could be responsible for this phenomenon: an unorganized expression of occludins in tanycytes found at the area of the ArcN enables free and uncontrolled diffusion of molecules towards the CSF, meanwhile the diffusion barriers between ArcN and both ME and VMH are still maintained. Beside tight junctions, gap junction proteins are expressed in tanycytes as well. Gap junctions are specialized intracellular channels localized between cells that enable small molecules to pass through its central pore which is regarded as a mechanism of communication between different cells. Previous immunohistochemical studies showed that tanycytes are closely linked to each other as well as to other glial cells via connexin 43 (CNX43). Furthermore, CNX43 enables the establishment of a 'panglial network' that connects tanycytes, astrocytes and oligodendrocytes. Additionally, is has been postulated that CNX43-linked tanycytes might display similar intracellular compositions allowing them to behave like one unit (Recabal et al., 2018; Szilvásy-Szabó et al., 2017).

Due to their unique morphology and advantageous location tanycytes emerge to be key regulators of some of the main metabolic and endocrine functions of the hypothalamus and are regarded as important modulators of the exchange of metabolic hormones and other biologically active substances between the blood and the CSF (Prevot et al. 2018). For example, is has been shown, that tanycytes regulate the secretion of GnRH into the blood circulation at the area of the ME. During the female menstrual cycle tanycytic end-feet totally engulf GnRH secretary axon terminals which inhibits their neurohaemal contact to fenestrated blood capillaries but during the preovulatory surge a reorganization of their end-feet happens leading to the formation of a direct access of GnRH terminals to ME blood vessels (Prevot et al. 2010). Furthermore, a study published in 2017 by Müller-Fielitz et al. dealing with the role of tanycytes in hormone detection revealed another astonishing feature of tanycytes: axons of TRH producing paraventricular neurons project towards the ME where they secrete their hormonal content into the portal capillary system which stimulates TSH release from the hypophyseal gland. At the area of the ME, TRH axon terminals contact β-tanycyte processes and activate TRH receptor 1 (TRHR1) expressed on tanycytes. This provokes an increase of intracellular Ca^{2+} levels which triggers activation of the $G\alpha_{q/11}$ proteins, leading to an enlargement of

tanycytic end-feet that cover portal blood vessels and activation of TRH-degrading enzyme, two mechanism inhibiting TRH release into the pituitary. In this way tanycytes regulate the access of blood-born molecules from the periphery to the brain and influence the hypothalamic-hypophyseal-axis. Moreover, there are several publications describing tanycytic transport function of small bioactive molecules. For instance Balland et al. claimed that blood-born leptin is taken up by tanycytic processes reaching towards the area of the ME and transported into the CSF of the III-ventricle from where it is shuttled to tanycytes at the ArcN. Due to different barrier properties of these tanycytes leptin can pass freely into the ArcN from where it could spread out further to other hypothalamic regions by paracellular diffusion Another striking feature of tanycytes is that they are equipped with a gluco-sensing machinery similar to the one of insulin producing pancreatic β cells and thus are capable of sensing glucose in the brain (Raikwar et al., 2018). Besides transport and chemo-sensing capability, another, not yet fully understood, ability of tanycytes is that they possess neuronal stem cell (NSC) properties which contributes to the establishment of a neurogenetic niche in the postnatal and adult hypothalamus (Maggi, Zasso, & Conti, 2015). A study performed in 2012 by Lee et al. demonstrated that early post-natally β2-tanycytes, expressing the NSC marker Nestin, are the most proliferative subpopulation of tanycytes and give rise to newborn cells which have been identified as functionally active neurons in mice. Moreover, β2-tanycytes remain neurogenic in young animals. Additionally, hypothalamic neurogenesis was increased in adult animals when they were fed with high fat diet.

1.3.1. Tanycyte subpopulations

Historically, tanycytes are classified into 4 different subtypes, namely into α1-, α2-, β1- and β2-tanycytes based on their dorsal-to-ventral location at the walls of the III-ventricle as well as on histochemical aspects. Even though this separation exists there are no strict borders among the subtypes. Instead, transition zones are observed within tanycytic subtypes as well as between α1-tanycytes and dorsally adjacent ependymocyte territories. Furthermore, it is still not fully understood how and when this terminal differentiation of α- and β-tanycytes takes place (Goodman & Hajihosseini, 2015). *Figure 3* demonstrates where the different tanycytic subtypes are detected alongside the III-ventricular walls, the white bars indicate hypothalamic nuclei expected at these sites.

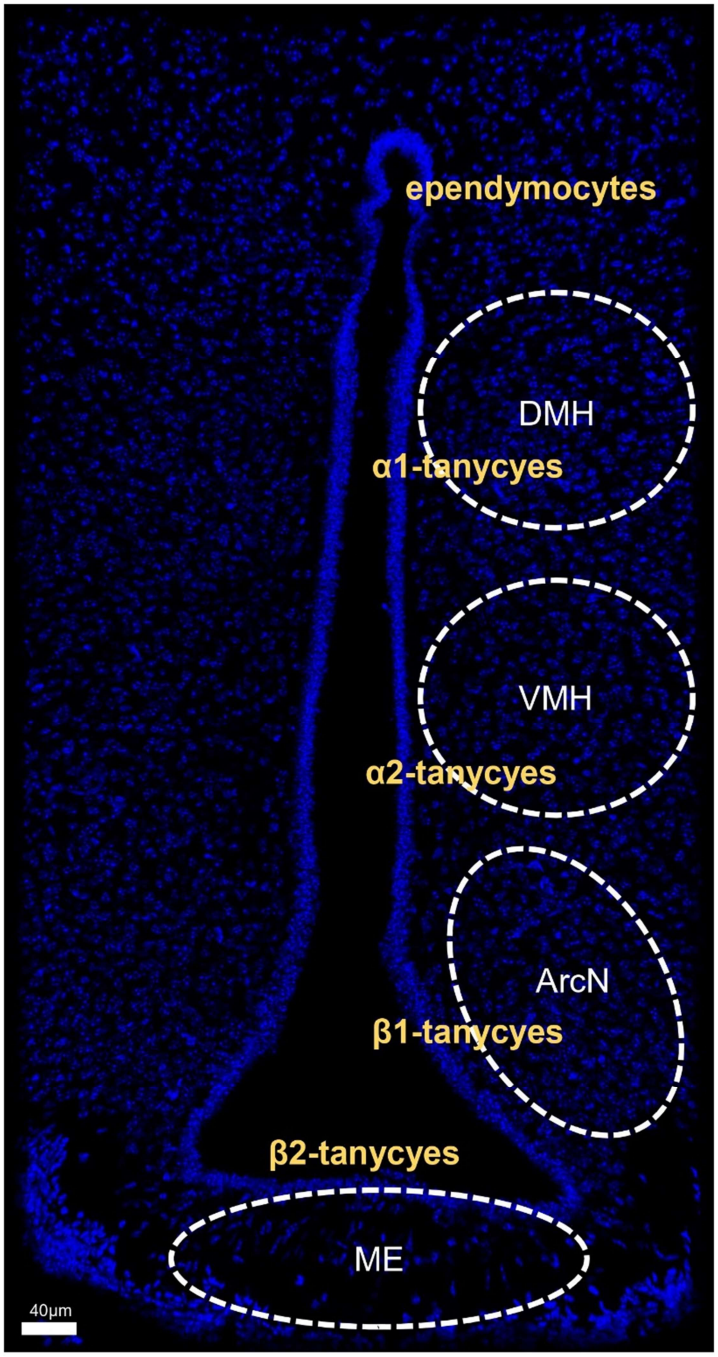

Figure 3 | Location of hypothalamic α- and β- tanycytes lining the walls and floor part of the III-ventricle
DMH: dorsomedial hypothalamic nucleus, VMH: ventromedial hypothalamic nucleus, ArcN: arcuate nucleus, ME: median eminence
Cell nuclei are labeled with Hoechst (blue)
Scale bar=40µm

In a review published in 2019 Rodriguez et al. give a detailed description of the 4 tanycytic subtypes regarding their location, morphological features of their cell bodies and processes as well as some functions. These characteristics should be summarized in the following paragraphs:

α1-tanycytes

They are found at the walls of infundibular recess and line the hypothalamic VMN and parts of the DMN. Their cell body has a cylindric shape and some display two nonmotile cilia. Their processes project laterally into the DMN, dorsally and lateroventrally into the VMN. Process are contacting blood capillaries either through two or more terminals touching the capillary basement membrane or through en-passant contacts established by the process. α1-tanycytes are equipped with endo- and transcytosis machinery but their cargos are still unknown.

α2-tanycytes

Their processes emerge into the area of the ArcN and like the α1-tanycytes they are equipped with a cylindrical soma showing one or two nonmotile cilia. They have lateroventral trajectories which contact blood capillaries located at the ArcN. Dendrites have been found in close proximity to the tanycytic soma and initial part of the process.

β1-tanycytes

They are located at the lateral extensions of the infundibular recess, also having a cylindrical cell body and some show one primary cilia. Their lateroventral trajectories emerge towards the brain's limiting membrane near portal capillaries of the ME as well as the ventromedial parts of the ArcN. It has been shown that β1-tanycytes are probably involved in lipid synthesis and that they possess a machinery for endo- and transcytosis as well as a well-established transport system along the basal processes which might has a secretory activity.

β2-tanycytes

They are detected at the area of the ME and demonstrate straight trajectories with heavy ramification at the most distal part of the process. These processes extend towards the medioexternal region of the ME where they establish contacts with portal capillaries of the hypophyseal system. They are suggested to be involved in transcytosis and secretion and are possibly able to secrete peptides or proteins stored in secretory granules.

Although this division is broadly accepted and referenced by various publications one should take note that due to recent studies dealing with tanycyte physiology as well as their genetic profiles this older classification may no longer be adequate and should be updated and revised taking these findings into consideration (Chen et al., 2017).

1.3.2. A transgenic mouse model to study tanycytes

RAX

The already mentioned RAX gene encodes for the paired-typed homeodomain-containing transcription factor and its expression starts during early embryogenesis in the neural plate and later in the retina, the hypothalamus and the pineal gland of multiple vertebrates, including humans and mice (Orquera et al., 2017). It is essential for the correct dorsoventral patterning of the developing medial hypothalamus between E8.0 and E8.5. Inactivation of RAX at this stage leads to a loss of gene expression profile typically for the dorsomedial hypothalamic area, such as POMC and SST, and shifts to a expression of genes which are specific for more ventral areas (Orquera et al., 2017). Additionally, an underdeveloped hypothalamic neuroepithelium as well as a disturbed neurogenesis can be observed.

Deletion of RAX at E9.5 does not affect the development of the hypothalamus but the differentiation and function of tanycytes located in the hypothalamic area around the III-ventricle is notably impaired (Orquera et al., 2017; Salvatierra et al., 2014). Under normal conditions, in the hypothalamus, RAX is expressed selectively in tanycytes lining the III-ventricular walls and it is crucial for correct tanycytic differentiation as well as for CSF-hypothalamus barrier function. (Miranda-Angulo et al., 2015). By E16.5, RAX expression is exclusively detected along the walls and floor part of the III-ventricle and missing form all other hypothalamic areas. Just a few days after, at the very end of embryogenesis, around E19 tanycytes start to arise at exactly this region. Their generation lasts until the first or even the second postnatal week. They are considered as fully mature, in a morphological and functional aspect, during the first month after birth. Nevertheless, it should be noted that the maturation time differs amongst tanycytic subtypes: α2 tanycytes reach their terminal morphology around the first week whereas in more dorsally located α1 the maturation process takes longer (Miranda-Angulo et al., 2015).

Mapping of RAX mRNA expression in the adult hypothalamus, around postnatal day (P) 40, showed clear restriction to cells lining the walls and the floor part of the III-ventricle in the ventral hypothalamic area, resembling the distribution of tanycytes (Miranda-Angulo et al., 2015). Considering these findings, RAX is a perfect marker for hypothalamic tanycytes.

RAX-Cre-ER^{T2}-tdTomato mouse line

In the year 2014 Pak et al. successfully generated the first RAX-Cre-ER^{T2}-tdTomato mouse line. As a first step, they inserted a 4-hydroxytamoxifen-inducible (4-OHT, Tamoxifen) Cre recombinase (Cre-ER^{T2}) cassette downstream of the initiation methionine of the endogenous

RAX gene. Next, these mice were crossed to the Cre-dependent ROSA26-CAG-lox-stop-lox-tdTomato (Ai9) line, which expresses the tdTomato reporter gene under the control of the CAG promoter, following a transcriptional stop cassette flanked by two loxP sites. After intraperitoneal injection of tamoxifen, the offspring showed restricted tdTomato in hypothalamic tanycytes. Furthermore, tdTomato labeling correlated with the expression of Sox2 and Vimentin, which are both considered as reliable tanycytic markers. In ependymocytes located at the most dorsal part of the III-ventricle, no tdTomato signal was observed. A schematic representation is illustrated in *Figure 4*. For more information about the generation of transgenic mouse strains, see paragraph 2.2.1.

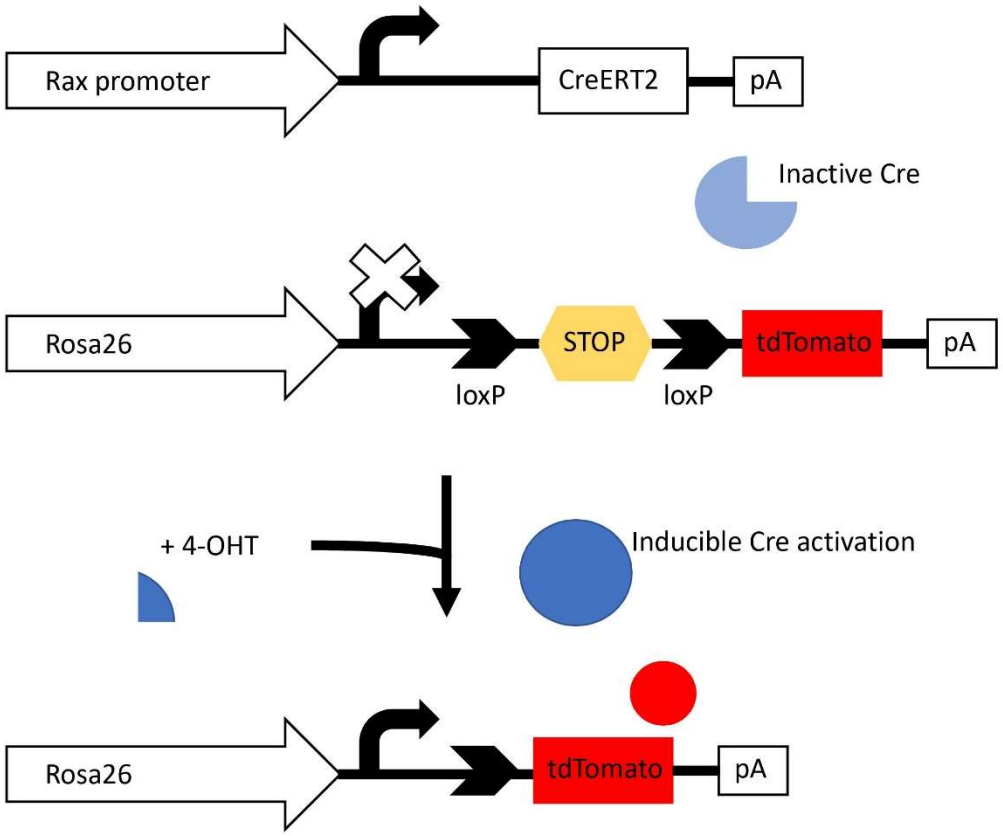

Figure 4 | RAX-regulated Cre-ER^{T2}-mediated tdTomato expression
Poly(A) tail (pA), estrogen receptor T2 (ER^{T2}), Tamoxifen (4-OHT)
Adapted from Pak et al., 2014

Moreover, Pak et al. evaluated the RAX-Cre-ER^{T2} phenotype, concluded it to be morphologically normal, and reported no ectopic Cre-activation/tdTomato expression.
Due to restricted Cre activity in tanycytes, prospective studies can use this mouse line to specifically label tanycytes for their analysis.

1.4. Tanycytes and Synapses

The way how neurons interact with each other and transfer information occurs via synaptic signal transmission. 10^{14} synaptic connections are estimated to exist in the human brain building a highly organized network of communication across the entire central nervous system (Alberts et al., 2015). This network is established by two types of synapse: electrical or chemical.

The electrical synapse is formed by gap junctions which almost continuously connect the pre- and postsynaptic cell, the gap in between the two cells constructing the synapse is just around 3.5nm wide. The presynaptic cell transduces an electrical current which leads to a change in the membrane potential of the postsynaptic cell and further results in depolarization of the cell. Because this form of signal transmission relies exclusively on an ionic current it occurs very fast and with almost no delay, which is the main advantage of the electrical synapse (Greenstein & Greenstein, 2000). In case of the chemical synapse, the signal transduction depends on small chemical substances called neurotransmitters which are packed in membrane-coated vesicles and stored at the nerve terminal of a presynaptic cell. These vesicles fuse with the cell membrane to release the neurotransmitters into the synaptic cleft, which is a round around 20nm wide. This short distance allows the neurotransmitter to rapidly diffuse across the synaptic cleft to reach the postsynaptic cell. Here, the neurotransmitter binds to its specific receptor and provokes an electrical change in the postsynaptic cells. After its release the neurotransmitter molecules are either degraded by specialized enzymes or up taken by the presynaptic or neighboring cells. The quick removal of neurotransmitters out of the synaptic gap is essential for a precise signaling mechanism because it prevents them to influence other adjacent neurons as well as it empties the cleft before new neurotransmitters are secreted by the presynaptic cell. Like this, signal transmission at the chemical synapse is more accurate and wide-ranging compared to the electrical synapse (Alberts et al., 2015; Greenstein & Greenstein, 2000). Several localization-types of chemical synapses exist which are classified based on the different cellular structures that form the synapse (see *Table 1*).

Table 1 | Localization of chemical synapses *(Greenstein & Greenstein, 2000)*

	Presynaptic structure	**Postsynaptic structure**
Axosomatic	Axon	Cell body
Axodendritic	Axon	Dendrite
Dendrodentritic	Dendrite	Dendrite
Axoaxonic	Axon	Axon

For decades researchers associated only neurons to communicated via synaptic transmission but over the years it became evident that synaptic interactions exist between neurons and glia cells too. Glia of the brain can be divided into 7 main subtypes: astrocytes, oligodendrocytes, oligodendrocyte precursor cells (NG2), microglia, radial glia cells, tanycytes and pituicytes (Clasadonte & Prevot, 2017). The star-shaped, highly abundant astrocytes are able to detect, take up and release neurotransmitters like glutamate and GABA, thus interacting with neurons via a so-called tripartite synapse. It has been shown that astrocytes are equipped with neurotransmitter receptors as well as transporters like the vesicular glutamate transports VGLUT1, VGLUT2 and VGLUT3. Another glia cell type, the oligodendrocyte, also establishes synaptic communication with neurons. Oligodendrocytes, which are essential for rapid electrical signal transduction along axons by enwrapping them with myelin sheaths, have been detected to be immunopositive for several neurotransmitter receptors, like AMPA and NMDA type of glutamate receptor. Furthermore, NG2 cells that generate oligodendrocytes over their entire life span, have been implicated to be involved in synapse formation with neurons (Clasadonte & Prevot, 2017; Gundersen, Storm-Mathisen, & Bergersen, 2015).

One of the oldest studies dealing with the existence of a synaptical connection between tanycytes and neurons was published in 1967 by Wittkowski. He found numerous synaptical contacts between neurosecretory axons and tanycytic processes in the outer layer of the ME of the guinea pig and discussed transport, sensory and especially secretory functions executed by tanycytes. In the year 1973, Güldner and Wolff also postulated the existence of what they named ‘neurono-glial synaptoid contacts’ on tanycytic processes in the ME of the rat. They performed 3-dimensional reconstructions of electron micrographs and observed a random distribution of presynaptic formations onto the surface of the tanycytic processes, only the apical part of the cell body showed less contacts. Overall, they estimated a total number of 100-200 synaptoid contacts per cell. However, the origin of the axons contacting tanycytic processes was obscure as well as the influence of these synaptoid contacts on the postsynaptic cells remained unknown. Some years later in 1979, Scott and Paull claimed that nerve terminals detected in close proximity to the cell membrane of tanycytic processes in the ME of the rat could be a potential way of communication between cells. They observed axons harboring small, clear microvesicles as well as less frequent larger dense core vesicles which both suggest a functional ending or an ‘en passant synapse’ onto tanycytic processes. Even though none of these publications specified the tanycytic subtype getting in contact with neurons one can conclude that all of them dealt with β-tanycytes due to the analyzed positions.

A very recent review published in 2019 by Rodríguez et al. reconsidered this topic. They examined the ultrastructure of α1-tanycytes but only identified 5 synaptoid contacts in 12 analyzed tanycytic processes. Furthermore, they emphasized how little is known about these neuronal inputs and suggested to perform 3-dimensional reconstruction of tanycytic processes with axonal contacts to reveal if and where these neuronal inputs are present.

1.5. Hypothesis

As described in the last paragraphs evidence is rising that tanycytes participate in synaptic communication with neurons in the hypothalamus. Due to their privileged position alongside the boarders of the III-ventricle they have access to the CSF with their cell bodies as well as their long processes target deep into the hypothalamic brain parenchyma where a variety of nuclei are located. The mechanisms described by Alpár et al. in 2018 that CRH-releasing neurons target ependymal cells lining the walls of the III-ventricle to induce the secretion of CNTF into the brain's aqueductal system, and its transport via the CSF to specific target receptors on neurons of the locus coeruleus could exist in tanycytes too. Therefore, we hypothesized that tanycytes do transduce neuronal electrochemical signaling to volume transmission via the CSF to influence long distance neuronal activity of regions close to the ventricular system. The following study represents one aspect of the formulated research questions and especially was performed to detected and further quantify the amount of synaptic inputs of several classes of neurons converging to tanycytes in different and topographically established regions around the hypothalamic III-ventricle.

2. Material and Methods

2.1. Ethics statement

All mice used in this study were maintained and sacrificed according to protocols approved by the ethical review board of the Medical University of Vienna (BMWFW-66.009/0277-WF/V/3b/2017, Tierversuchsgesetz 2012, BGBI, Nr. 114/2012). All experiments were conducted in accordance to the European Convention for the Protection of Vertebrate Animals used for the experimental and other scientific purpose (86/609/EEC). Perfusion was performed under deep isoflurane anesthesia and all efforts were made to minimize the animal's suffering as well as the number of used animals for the performed experiments.

2.2. Animals

Male mice ranging from P60 to P90 from strains listed in *Figure 2* were used for the experiments.

Table 2 | Experimental mouse models used

Mouse Line	n
C57BL/6J (Wild type)	5
RAX-Cre-ER^{T2}-tdTomato	3
CRH-Cre-tdTomato	2

Mice were kept under a controlled light cycle (12 hours light / 12 hours dark) at standard conditions and were provided with standard laboratory chow and water *ad libitum*. Mice were housed as maximal two animals per cage and their general health was checked weekly. All transgenic mouse lines were established on a C57BL/6J background.

2.2.1. Transgenic mice

The term "transgenic mouse" refers to a mouse, which has a genetically manipulated genome meaning that foreign DNA was introduced into the mouse's germ line. Inserting this extrinsic DNA into the mouse genome can be achieved by using different techniques: (1) retroviral infection of mouse embryos, (2) pronuclear-microinjection into one-cell mouse embryos, and (3) targeted manipulation of mouse embryonic stem cells at desired loci by introducing loss or again of function mutation. (Kumar et al., 2009). Since the development of the first transgenic mouse lines until today these technologies have evolved rapidly and nowadays the creation of

transgenic, knock-out, conditional knock-out and knock-in mouse lines is possible offering nearly unlimited alternatives to study gene functions in development and under normal physiological conditions as well as in disease. Further, molecular mechanisms of genes, gene products and their interaction with one another can be unveiled using genetically engineered mouse lines (Cho, Haruyama, & Kulkarni, 2009; Kumar et al., 2009).

Conditional knock-out

The conditional knock-out technique offers tissue-specific control and leads to a knock-out of a gene of interest only in a particular tissue or cell-type which is absolutely necessary if the deletion of the gene in the whole organism would be lethal to the animal. Site-specific Recombinase systems (SSRs) are used for this purpose, the Cre-loxP system is one of them. This system is derived from the bacteriophage P1 and is using an enzyme, the Cre recombinase (Causes Recombination), which is capable of specifically identifying a 34bp DNA sequence, called the loxP (Locus X over P1) site. After Cre recognizes the loxP sites it catalyzes the exact homologous exchange (recombination) between them, without gaining or losing any additional nucleotides. Based on the orientation of the loxP sites, this system is used to perform deletions, inversion and exchange of DNA sequences.

To create a conditional knock-out mouse line, two loxP sites, orientated in the same direction, are introduced into the genome of the animal and are flanking any gene of interest which should be targeted. The tissue specific cut is further achieved by crossing these mice with a mouse line carrying the Cre recombinases inserted downstream of a tissue-specific promoter. (Zhang et al., 2012)

Stage specific conditional knock-out

Using exogenous chemicals such as tamoxifen or 4-hydroxytamoxifen one can specifically induce the expression of Cre recombinase and create a way to knock out genes in a time-specific manner. In this approach, Cre recombinase is fused to an engineered from of the ligand binding domain of the Estrogen Receptor (ER), resulting in a Cre-ER^T protein. This protein now only binds to the synthetic ligand tamoxifen or 4-hydroxytamoxifen rather than its natural ligand 17β-estradiol. At the beginning, without tamoxifen, Cre-ER^T is found in the cytoplasm, bound to heat-shock proteins (Hsp) like Hsp90. By applying tamoxifen, Hsp90 dislocates and exposes the nuclear localization signal on the ER, which promotes moving of Cre-ER^T into the cell nucleus. Here, it recognizes the loxP sites and cuts out the gene of interest located in between. (Zhang et al., 2012). A schematic representation of this mechanism is shown in *Figure 5*.

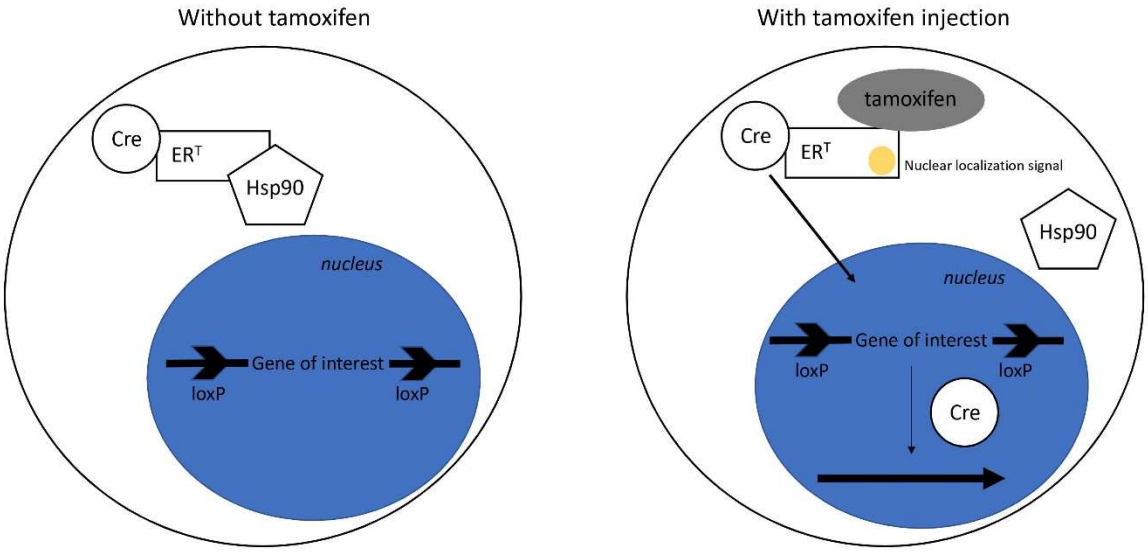

Figure 5| Inducible knock-out system using tamoxifen
Estrogen receptor T (ER^T), heat-shock protein 90 (Hsp90)

Conditional reporter models

Besides the described conditional knock-out models, the Cre-loxP system is also a suitable tool for the generation of conditional reporter animal models. Here, a STOP cassette, flanked by two loxP sites, is inserted downstream of a ubiquitous promoter and prevents the transcription of a fluorescent reporter gene. Breeding with a line carrying the Cre recombinase fused to the modified ER under the control of a tissue specific promoter results in offspring, which has the STOP codon deleted in Cre-expressing tissue and shows a fluorescent signal pattern guided by the Cre-promoter.

Examples for established fluorescent reporter genes are GFP (Green Fluorescent Protein) and its variants EGFP (Enhanced Green), EYFP (Enhanced Yellow) or ECFP (Enhanced Cyan), RFP (Red Fluorescent Protein), mCherry (Monomeric Cherry), tdTomato (Tandem Dimer Tomato), etc (Li et al., 2018). A commonly used locus for the insertion of the reporter gene is the ROSA26 (Revers Orientated Splice Acceptor, Clone 26) locus. No sever effects for the animal if the gene is lost, a high transcriptional activity, and an ubiquitous expression profile make ROSA26 a preferred locus of insertion of transgenes without interfering with fertility or viability of the organism. Often the synthetic CAG promoter is inserted as well in order to enhance expression activity at the ROSA26 locus. (Jackson Laboratory Webpage, Li et al., 2017).

2.3. Tamoxifen preparation and injection

Tamoxifen injection solution was prepared by adding corn oil (Sigma Aldrich) to Tamoxifen >99% (Sigma Aldrich) to obtain a 20mg/ml suspension. The solution was heated for approximately one hour at 50°C while shaking until tamoxifen was dissolved completely. Before injecting the animals, the solution was warmed in the water bath for one hour at 37°C. Mice at P60 were injected intraperitoneally with 0.15mg of 20mg/ml Tamoxifen per g of body weight of the animal for three consecutive days and sacrificed one week after the last injection. *Table 3* lists the body weight of animals which were injected and the exact amount of tamoxifen used.

Table 3 | Tamoxifen injection

Animal	Body weight	20mg/ml Tamoxifen injected
Rax-Cre-ER^{T2}-tdTom #1	26g	195µl
Rax-Cre-ER^{T2}-tdTom #2	27g	202.5µl
Rax-Cre-ER^{T2}-tdTom #3	29g	217.5µl

2.4. Genotyping

For genotyping, the genomic mouse DNA was extracted from mice ear clip biopsies collected with new razor blades for each animal to avoid cross-contamination.

Each ear clip was incubated in 600µl of 50M NaOH solution, heated for 10 min at 95°C while shaking and cooled down for 1min on ice. Next, 50µl of 1M TRIS-HCl (pH 8.0) was added and the solution was vortexed for 10sec. The DNA was pulse-spinned at maximum speed and kept on ice until further usage and later stored at -20°C.

To determine the presence of the inserted Cre-ER^{T2} allele in the transgenic RAX-Cre-ER^{T2}-tdTomato mice a Polymerase Chain Reaction (PCR) was performed.

2.4.1. Theoretical background of PCR

First invented in 1990 by Mullis, the polymerase chain reaction (PCR) is one of the most widely used techniques in today's field of molecular biology. It is suitable for disease diagnose, genomic studies, pathogen detection and forensic analysis. The PCR reaction catalyzes an amplification of a specific DNA fragment of a double-stranded template DNA. The needed components to successfully perform this amplification are: a template DNA, a forward and a revers primer, nucleotides and a DNA polymerase. Primers are short fragments of DNA with a

sequence complementary to a sequence of interest on the provided template DNA. They mark the binding site for the polymerase where amplification should start. Using the given nucleotides, the polymerase creates single-stranded complementary DNA fragments (cDNA) resembling the template DNA sequence of interest. A test tube containing all the components is placed in a thermal cycler and further undergoes repeated cycles of different applied temperature. First, high temperatures lead to separation of the double-stranded DNA (denaturation step). Second, the specific binding of primers to the region of interest, which should be amplified, happens on the single-stranded DNA during the application of lower temperatures (annealing step). As a last step, temperature is increased again to allow the DNA polymerase to recognize the primers and start amplifying this specific region (extension step). Each cycle doubles the number of copied DNA fragments leading to an amplification of the region of interest that is now detectable by gel-electrophoresis which enables the separation of DNA fragments by its sizes (Garibya & Avashia, 2014).

2.4.2. PCR protocol

Primers to identify the RAX-Cre-ER^{T2}-tdTomato either Wild type (WT) or mutant allele were used and are listed in *Figure* 4, a PCR mix, containing the DNA polymerase, from Promega was used. The PCR mastermix as well as the thermal cycler protocol is cited in *Figure 5* and *6.* Following the amplification of the DNA, bands were visualized by a run of each amplicon on a gel composed of 1.5% Agarose dissolved in 0.1M TAE (4.8g 0.4M TRIS, 0.372 g 0.01M EDTA, 1.21 ml 0.2M CH_3COOH diluted in 1L with distilled H_2O) and GelRed 1:10000 (Biotinum). The amplicons were loaded with a 1X loading dye (Promega). After gel-electrophoresis, the DNA bands were visualized with ChemiDOC (BioRad). PCR products of 290bp in length were expected in mice which successfully inserted Cre-ER^{T2} allel and animals with the desired phenotype were selected for further experiments. Transgenic CRH-Cre-tdTomato animals were previously examined and generously donated by the lab.

Table 4 | List of primers used for genotyping

RAX-Cre-ER^{T2}-tdTomato	
Primer	Sequence
common_forward	5'- CCC TGA GGC TAA ACT TGC AG -3'
WT_reverse	5'- AGG TGT CTA GGA TGC CGT CT-3'
CRE_reverse	5'- AGG CAA ATT TTG GTG TAC GG -3'

Table 5 | PCR mastermix
Components and volumes indicated for one reaction

PCR Mastermix	
Primer common_forward	0.5µl
Primer WT_reverse	0.5µl
Primer CRE_reverse	0.5µl
PCR mix	10µl
H_2O	6.5µl
cDNA	2µl

Table 6 | Thermal cycler protocol used for RAX-Cre-ER^{T2}-tdTomato genotyping

Temperature	**Duration**	
94°C	4min	
94°C	30sec	
60°C	30sec	→repeat 35x
72°C	45sec	
72°C	4min	
10°C	infinite	

2.5. Brain preparation for microscopic analysis: perfusion and slicing

Mice were anesthetized by inhalation of isoflurane (AbbVie GmbH). Once they reached a complete anesthetic state (checked by e.g. lack of movement of tail or paw when squeezed) the mice were perfused transcardially with 0.1M phosphate buffer (PB) (77.4ml 0.1 Na_2HPO_4 and 22.6ml 0.1 M NaH_2PO_4 diluted in 1L with distilled H_2O, pH 7.4) at room temperature and subsequently with 20ml ice cold 4% paraformaldehyde (PFA) in 0.1M PB. The brains were carefully removed and kept overnight at 4°C in 4% PFA. The day after, the brains were gradually dehydrated in an increasing concentration of 10%, 20%, and 30% Sucrose in 0.1M PB while rotating at 4°C. Next, Wild type and CRH-Cre-tdTomato mice brains were cut into 50µm-thick coronal sections with a Cryostat (CryoStar Nx70, Thermo Fisher), brains of RAX-Cre-ER^{T2}-tdTomato mice were cut with a Vibratome (VT1000 S, Leica). The slices were collected free-floating in a well containing 0.1M PB with 0.02% NaN_3. Every well contained 4 brain slices that span an area of 200µm, slices for further analysis were collected from every second well to get an approximate distance of 400-500µm in between. The slices were stored at 4°C until usage.

2.6. Immunohistochemistry & Immunofluorescence

For detection of hypothalamic tanycytes located around the III-ventricle and synaptic inputs the collected brain tissues were labeled immunohistochemically with specific antibodies.

2.6.1. Theoretical background of Immunohistochemistry

Immunohistochemistry is a widely used method to localize proteins of interest in cells and tissue by using specific antibodies for detection (Goldstein & Watkins, 2008). Antibodies are serum immunoglobulins with binding specificity for particular antigens. Antibodies used for immunohistochemistry exist in in two different types: mono- or polyclonal. Monoclonal antibodies are very specific and only recognize one epitope on an antigen whereas polyclonal antibodies recognize many different epitopes. To avoid non-specific cross-reactions affinity purification of the polyclonal antibodies is essential before usage. Furthermore, there are two main techniques for immunofluorescent detection of the protein of interest: a direct and an indirect way. In the direct approach the antibody is conjugate to a fluorochrome which's fluorescence is detectable with a fluorescence microscope. In contrast, using the indirect approach a primary antibody first binds to an antigen and in a second step a secondary antibody fused to a fluorochrome detects and binds the primary antibody. In this way, it reveals the primary antibody's binding site by a fluorescent mark which can be visualized using the fluorescence microscope. Advantages of the indirect approach are: a higher sensitivity because the signal amplification occurs when several secondary antibodies bind to one single antibody; it is easier to conduct and very specific secondary antibodies are commercially available (Ausubel et al., 2003; Goldstein & Watkins, 2008). In this study, only the indirect detection approach was used to reveal prim. antibody binding sites.

2.6.2. Characterization of primary antibodies

Vimentin

Vimentin is classified as a type-III intermediate filament protein and predominantly detected in mesenchymal cells, like fibroblasts. It plays a crucial role in cell motility, cell shape and resistance to mechanical forces (Challa & Stefanovic, 2011). Additionally, Vimentin is also a reliable marker for glial cells including tanycytes located at the walls of the III-ventricle (Bolborea & Dale, 2013; Lee et al., 2012; Rodríguez et al., 2005).

Nestin

Nestin is a large type-VI intermediate filament protein, expressed in all precursor cells of the CNS and considered as a neural stem cell marker. A wide range of previous studies postulated Nestin expression in hypothalamic tanycytes (Bolborea & Dale, 2013; Lee et al., 2012; Rodríguez et al., 2005).

GFAP

The Glial Fibrillary Acidic Protein (GFAP) is a member of the type-III intermediate protein family. It is a broadly used marker, mainly to label astrocytes (Hofmann et al., 2017). There are some recent publication showing a subpopulation of tanycytes labeled positively for GFAP (Robins et al., 2013).

VGAT

The Vesicular GABA Transporter (VGAT) has an important function in the uptake and storage of the inhibitory neurotransmitter GABA into synaptic vesicles before they are released into the synaptic cleft. It is located presynaptically at the nerve endings of GABAergic and glycinergic neurons in the brain as well as in the spinal cord (Chaudhry et al., 1998).

VGLUT2

Similar to VGAT, the Vesicular Glutamate Transporter (VGLUT) is involved in transporting a neurotransmitter, in this case the excitatory neurotransmitter glutamate, into synaptic vesicles for release into the synaptic cleft where it triggers a response in the postsynaptic cell (Yin et al., 2015).

All antibodies were used successfully by members of the lab in previous immunohistochemical experiments investigating hypothalamic sections from mice and their specificity has been demonstrated.

2.6.3. Immunostaining protocol

Free-floating coronal brain slices (50µm) were washed in 0.1M PB a few times for 10 minutes on an orbital shaker. Afterwards, non-specific antigen binding was prevented by incubating the sections in a blocking solution composed of 0.3% Triton X in 0.1M PB (PB-Triton), 2% bovine serum albumin (BSA) and 5% normal donkey serum (NDS) for 2 hours at room temperature while shaking. Following the blocking step, different combinations of primary antibodies diluted in 0.3% PB-triton, 0.1% BSA, 2% NDS, and 0.02% NaN_3 were applied to the sections

for three-to-four days on an orbital shaker at 4°C. Primary antibodies used in the experiments are listed below (*Figure 7*).

Table 7 | Primary antibodies

Antibody	Host species Clonality	Manufacturer/Company Catalogue Number Lot	Dilution
Tanycyte markers			
GFAP	Guinea pig Polyclonal	Synaptic Systems Cat. No.: 173-004	1:1000
Nestin	Mouse Monoclonal	Merck/Millipore, Sigma Aldrich Cat. No.: MAB353 Lot: 2987440 and 3108484	1:400 and 1:200
Vimentin	Goat Polyclonal	Sigma Aldrich Cat. No.: V4630 Lot: 015M4845V	1:200
Vesicular transporter markers			
VGAT	Rabbit Polyclonal	Synaptic Systems Cat. No.: 131-003 Lot: 131003/25	1:250
VGLUT2	Rabbit Polyclonal	Synaptic Systems Cat. No.: 135-403	1:800
other			
TH	Rabbit Polyclonal	Merck Millipore Cat. -No.: AB152	1:100 and 1:300

After primary antibody incubation, the slices were rinsed several times to overnight in 0.1M PB at 4°C on an orbital shaker. Next, species-specific fluorophore-conjugated secondary antibodies were used to hybridize for 2 hours at room temperature while shaking to reveal primary antibody binding. Secondary antibodies were diluted at 1:300 in a solution composed of 0.03% PB-triton, 2% BSA, and cell nuclei were counterstained with Hoechst 33,342 1:10000. A detailed list of secondary antibodies used in the experiments is shown in *Figure 8* in the supplementary.

Table 8 | Secondary antibodies

Antibody	Company Catalogue Number Batch/Lot	Dilution	Mass
Alexa Fluor® 488 AffiniPure Donkey Anti-Goat IgG (H+L)	Jackson ImmunoResearch Cat. No.: 705-545-147 Lot: 131699	1:300	0.5mg
Alexa Fluor® 488 AffiniPure Donkey Anti-Guinea Pig IgG (H+L)	Jackson ImmunoResearch Cat. No.: 706-545-148 Lot: 134611	1:300	0.5mg
Alexa Fluor® 488 AffiniPure Donkey Anti-Mouse IgG (H+L)	Jackson ImmunoResearch Cat. No.: 715-545-151 Lot: 127820	1:300	0.5mg
Alexa Fluor® 488 AffiniPure Donkey Anti-Rabbit IgG (H+L)	Jackson ImmunoResearch Cat. No.: 711-545-152 Lot: 132876	1:300	0.5mg
Cy™3 AffiniPure Donkey Anti-Goat IgG (H+L)	Jackson ImmunoResearch Cat. No.: 705-165-147 Lot: 134527	1:300	0.5mg
Cy™3 AffiniPure Donkey Anti-Guinea Pig IgG (H+L)	Jackson ImmunoResearch Cat. No.: 706-165-148 Lot: 115370	1:300	0.5mg
Cy™3 AffiniPure Donkey Anti-Rabbit IgG (H+L)	Alexa Fluor Jackson ImmunoResearch Cat. No.: 711-165-152 Lot: 139288	1:300	0.5mg
Alexa Fluor® 647 AffiniPure Donkey Anti-Goat IgG (H+L)	Jackson ImmunoResearch Cat. No.: 705-605-147 Lot: Lot: 103972	1:300	0.5mg
Alexa Fluor® 647 AffiniPure Donkey Anti-Guinea Pig IgG (H+L)	Jackson ImmunoResearch Cat. No.: 706-605-148 116734	1:300	0.5mg
Alexa Fluor® 647 AffiniPure Donkey Anti-Mouse IgG (H+L)	Jackson ImmunoResearch Cat. No.: 715-605-151 Lot: 131502	1:300	0.5mg
Alexa Fluor® 647 AffiniPure Donkey Anti-Rabbit IgG (H+L)	Jackson ImmunoResearch Cat. No.: 711-605-152 Lot: 127614	1:300	0.5mg

Antibody	Company Catalogue Number Batch/Lot	Dilution	Mass
DyLight™ 405 AffiniPure F(ab')₂ Fragment Donkey Anti-Rabbit IgG (H+L)	Jackson ImmunoResearch Cat. No.: 711-476-152 Lot: 137441	1:300	0.5mg
Hoechst 33,342	Thermo Fischer Cat. No.: H1399	1:10000	

After exposure to the secondary antibody solution the slices were washed in 0.1M PB several times to overnight at 4°C on an orbital shaker. As a last step the sections were mounted with a solution containing 2.4g Mowiol 488 reagent (Sigma Aldrich), 6g glycerol analytical grade, 12ml 0.2M TRIS buffer pH 8.0, 6ml MilliQ water and 2.5% w/v DABCO (Sigma Aldrich) on glass slides (Economy HistoFrost) and kept at 4°C until imaging.

2.7. Image Acquisition

52 immunohistochemically stained brain sections from 10 animals were used for microscopic analysis. With an inverted LSM880 laser-scanning confocal microscope (LSCM) from Zeiss these sections were evaluated by acquiring micrographs of 13 regions of interest (ROI) along the III-ventricle. The microscope was equipped with a motorized stage and the Zen software (Zeiss, Version 2). Micrographs consisting of tile-scan images and z-stacks of the ROI were acquired with an oil immersion 63x objective (Plan-Apochromate 63x/1.40 Oil). Before starting the acquisition, the pinhole width was adapted and optimized for combinations of more than one recorded channel to be as similar as possible and set between to 142-143µm. The scanning frequency was put between 8 and 9 seconds and average scanning to 2 lines. The microscopic digital zoom was set to 1.2 at 63x primary magnification. 40 to 50 planes were recorded for each z-stacks over 40-50 µm (thickness of optical section) with a step size of 1 µm. The detection of emission spectra for the fluorescent dyes was set as follows: Alexa Fluor 488 (490-530nm), Cy3 (560-610nm), Alexa Fluor 647 (640-700nm), tdTomato (560-600nm), and Hoechst (420-450nm). The Laser intensity was manually adjusted for every section to avoid artefacts and reduce background noise. Additionally, overview scans of each brain section were executed with an 20x or 40x water immersion objective (Plan-Apochromate 20x/1.40, Plan-Apochromate 40x/1.40).

2.8. Analyzed positions

Previous mapping and characterization studies of tanycytes showed that within the hypothalamus, tanycyte cell bodies are localized in the central and posterior parts of the hypothalamic parenchyma (Robins et al., 2013). Consequently, the stereotaxic coordinates of examined sections where chosen in a way to cover exactly these regions.

Briefly recalled, 50µm thick coronal slices of mouse brains were derived either with a Cryostat (CryoStar Nx70, Thermo Fisher) or a Vibratome (VT1000 S, Leica) and collected free-floating in a well containing 0.1M PB with 0.02% NaN_3. Every well contained 4 slices that span an area of 200µm. The slices which were further analyzed were collected from every second well to have an approximate distance of 400-500µm between them.

In total 4 coronal brain sections for each animal from 3 different mouse lines were analyzed leading to an overall of 52 examined sections. Starting with the most caudal slice 1 at approximate -2.30mm relative to bregma, followed by slice 2 at bregma -1.82mm, slice 3 at bregma -1.34mm, and the last as well as most rostral slice 4 at bregma -0.70mm. A theoretical representation of sections taken into considerations is shown in *Figure* 6 as well as within the appendix.

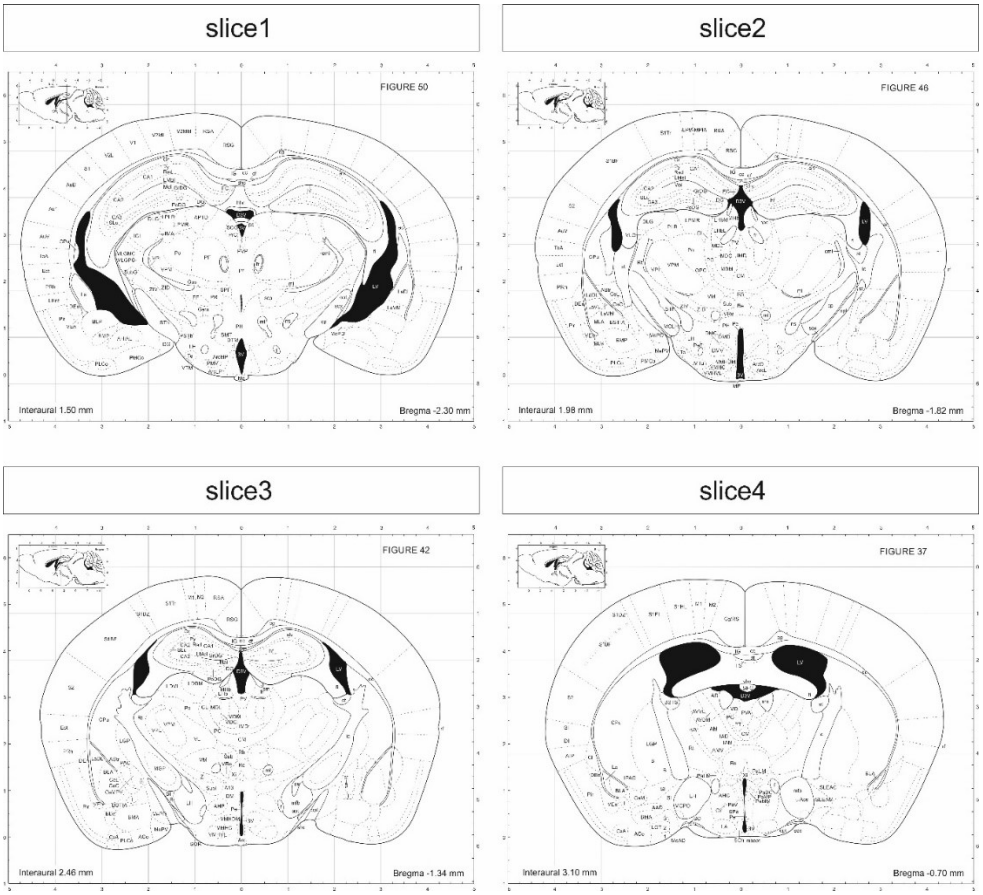

Figure 6 | Theoretical localization of selected coronal mouse brain sections
Reference: The Mouse Brain in Stereotaxic Coordinates, Franklin 1997

The following *Figure 7* demonstrates representative overview scans of all 4 sections examined. Additional overview scans of all animals used for this study can be found in the appendix.

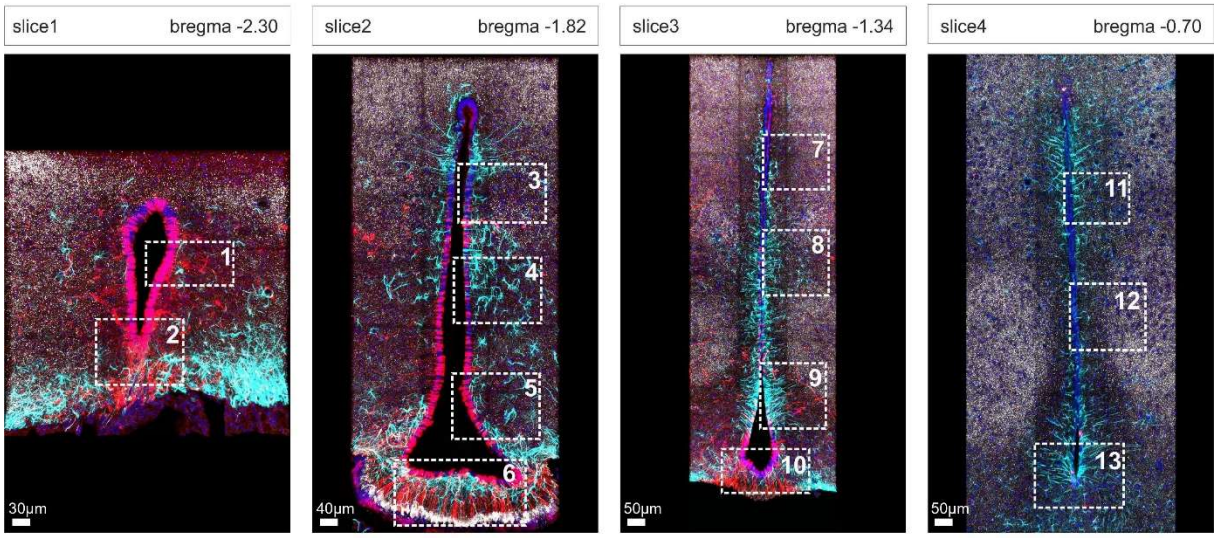

Figure 7 | Representative overview scans of RAX-Cre-ER^{T2}-tdTomato
Sections show clear and distinguishable signals and sparse background
Further analyzed positions are labeled from 1 to 13 and are marked with white bars
RAX (red), GFAP (cyan), VGLUT2 (white), Hoechst (blue)
Scale bars=30µm, 40µm and 50µm

To visually quantify neuronal innervations onto tanycytes, 63x confocal z-stack images of the 13 positions spanning the areas depicted in *Figure 7* were recorded. Based on findings of recent studies which identified separated territories for ependymocytes, α- and β-tanycytes. (Goodman & Hajihosseini, 2015; Maggi et al., 2015), each position was selected in a sense to map all the different tanycytic subtypes and ependymocytes respectively. This approach led to a total number of 676 examined positions within all animals used. Different sections but from the same 3 RAX-Cre-ER^{T2}-tdTomato mice were used for both VGLUT2 as well as VGAT staining resulting in a total number of 24 analyzed slices and 312 positions within the RAX-Cre-ER^{T2}-tdTomato sections (see *Table 9*).

Table 9 | Mouse lines, number of used animals per line, number of sections and analyzed positions

Mouse line	n animals	n slices	n positions (n slices * 13)
Wild type	5	20	260
RAX-Cre-ER^{T2}-tdTomato	3	24	312
CRH-Cre-tdTomato	2	8	104
	10	**52**	**676**

2.9. Image processing and analysis

All z-stack images were quantified using the IMARIS software (Version 9.0.2, BitPlane). Images were manually processed (i.e.: adjustments of brightness and contrast) and z-stacks were merged by the software.

2.9.1. Synaptic inputs

The 'Spot Detection' tool creates point-like structures based on a selected signal of the image and was used for 3-dimensional quantification of either the VGLUT2, VGAT or CRH signal in the different mouse lines examined. The background subtraction tool was applied to every image. As staining, illumination and photon detection affect the quality of confocal images this tool uses a Gaussian filter (sigma=object diameter / 2, to define the background at each voxel) to smooth the image and reduce noise homogeneously without introducing artefacts. For the channels which recorded the input signals, the filter width was manually set to 1µm, meaning that structures smaller than this filter were removed. The filtered image was then automatically subtracted from the original and was used for subsequent analysis. The xy- as well as the z-diameter of detected spots was set to 1µm. Further manual adjustments were executed to avoid detection errors due to excess or lack of detected signal which otherwise would result in over- or under-sampling.

2.9.2. Tanycytic processes

To analyze and quantify tanycytic processes the 'Surface Reconstruction' as well as the 'Filament Tracer' tool were used. For both methods the reconstructions were performed on the Vimentin, Nestin, RAX and GFAP signal which are considered as markers for tanycytes located in the hypothalamic area along the walls of the III-ventricle. Measurements of length, diameter and volume of individual processes were taken automatically by the software. Advantages and disadvantages of both methods are explained detailly in paragraph 3.3.2.

2.9.3. Synaptic inputs on tanycytic processes

Using the 'Distance Calculation' tool previously detected spots were further characterized as being afar or closer than 0.8µm to the reconstructed tanycytic processes. The resolution of a LSCM for a 60x NA 1.4 object lens is normally indicated as a theoretical maximum resolution of ~0.2µm regarding the xy-plane (=lateral resolution), in the z-plane (=vertical resolution) it is slightly reduced to ~0.5µm (Paddock, 2000). In our case, more than one channel was

recorded, so the pinhole width had to be adapted to be as similar as possible for all channels before starting the image acquisition process. This led to an un-unitary numerical aperture (NA) which further resulted in a reduced working resolution. Even though the synaptic gap at a chemical synapse is only spanning a distance of around 0.02µm (Greenstein & Greenstein, 2000) it was not possible to record these small details and therefore the threshold of considering a reconstructed spot as a 'synaptic input' was set to be closer than 0.8µm to the tanycytic process. Spots which fulfilled the criterion to be closer than 0.8µm to the process were considered as synaptic inputs on tanycytic processes. For calculating the distance between spots and filaments, the 'Absolute Distance' mode was chosen, meaning that the distance was measured ranging from the center of the spot to the edge of the reconstructed filament.

2.9.4. Nuclei reconstruction

As a last step, nuclei of cells lining the walls of the III-ventricle with their soma were recreated using the 'Surface Reconstruction' tool again. First, the diameter of cell nuclei was examined manually for every image using the 'slicing view' and ranged between 4 to 6 µm. By enabling the 'split touching objects/region growing' mode separation of individual nuclei was possible. This tool allows the separation of touching objects even though they were identified initially as a single one. First, so-called 'seed points' had to be defined. As the reconstruction process continued a region started to grow around these seed points until a certain diameter was reached and the growing ended. Depending on the previously determined diameter of the nuclei the threshold for the growing region was set according to this diameter leading to the reconstruction of single nuclei along the ventricular walls. Subsequently an approximate estimation of the number of cells exposed to the CSF was possible.

2.10. Statistical analysis

The data were analyzed with GraphPad PRISM (Version 8.1.0) and values are presented as mean and ± standard error mean (SEM). Data were examined for normality by using the Kolmogorov-Smirnov test and equality of variances using the Barlett's test or Levene's test respectively. If the data were considered as parametric then significant differences were tested by using a non-repeated one- and two-way ANOVA followed by post-hoc tests.

A one-way ANOVA with the 13 different positions taken into consideration alongside the III-ventricle as the independent factor was used to analyze differences in amounts of synaptic inputs (meaning VGLUT2+, VGAT+ or CRH+ inputs) onto tanycytic processes.

A two-way ANOVA was used to compare differences in the regional amount of inputs on different tanycytic subtypes located on two different positions alongside the III-ventricle. In this case the independent factors are the individual tanycyte subtypes and the slice taken into consideration. As post-hoc tests Tukey and Bonferroni multiple comparison were used.
The threshold for significant differences was considered as $p < 0.05$. The number of analyzed animals (n) and p values are indicated in the figure legends.

3. Results

Over the past years evidence is growing that tanycytes might play a crucial role in the communication with neurons located in the hypothalamic parenchyma adjacent to the III-ventricle and possibly tanycytes are capable of responding to neuronal synaptic innervations. Bordering the III-ventricle with their soma, tanycytes are additionally equipped with a long process emerging into the surrounding brain parenchyma where important hypothalamic structures are located, namely the DMH, VMH, ArcN as well as the ME which lies adjacent to the infundibulum, the main link between the CNS and the endocrine system of the brain, the pituitary gland (hypophysis). This unique location offers tanycytes a privileged access to the CSF as well as to blood capillaries which they contact through their radial processes.

Publications from the 60ies and 70ies showed first indications of the existence of synaptoid contacts between axons of unknown origin and tanycytic processes (Wittkowski 1967; Güldner and Wolff 1973; Scott and Paull 1979). Moreover, a recent study performed by members of our lab demonstrated that neurons target ependymocytes located at the borders of the III-ventricle and induce the release of CNTF into the CSF (Alpár et al. 2018). Due to the reason that tanycytes occupy similar territories as ependymocytes and are also considered as ependymal cells we hypothesized that this mechanism could exist in tanycytes too.

In this study I wanted to investigate if tanycytes do get synaptic inputs from different classes of neurons and detailly analyze the distribution of neuronal innervations onto tanycytes along the rostro-caudal extension of the hypothalamic III-ventricle.

3.1. Genotyping results

To study neuronal innervations onto tanycytes, I used a transgenic mouse line that expresses an inducible Cre recombinase under the control, in adult animals, of the tanycytic-specific RAX gene promoter, namely the RAX-Cre-ER^{T2} line (Pak et al., 2014). To visualize tanycytes, I took advantage of the Cre-loxP recombination system by crossing the RAX-Cre-ER^{T2} mouse line with a Cre-dependent loxP-tdTomato reporter mouse line, namely Ai9(RCL-tdT) or tdTomato. Due to the specific and tamoxifen inducible Cre activity in tanycytes, the recombined mouse line drive tdTomato expression exclusively in tanycytes. For more details concerning transgenic mice and production, see paragraph 2.2.1.

In order to determine the presence of the inserted Cre-ER^{T2} allele in the RAX-Cre-ER^{T2}-tdTomato derived mice, I genotyped genomic mouse DNA from ear clip biopsies. The following *Figure 8* shows an agarose gel with PCR amplicons that represent the amplified Cre-

ER^{T2} allele at 290bp and the Wild type allele at 401bp of transgenic animals used in the experiments. For details concerning the genotyping protocol I used, see paragraph 2.4.

For the purpose of this thesis, I used heterozygous RAX-Cre-$ER^{T2\,(+/-)}$ mice, that showed both 401bp and 290bp amplicons. The RAX-Cre-$ER^{T2\,(+/-)}$ mice were crossed with an homozygous tdTomato reporter line and I used the resulting RAX-Cre-$ER^{T2\,(+/-)}$-tdTomato offspring for all experiments conducted in this study.

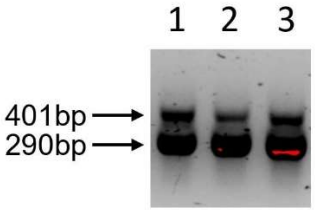

Figure 8 | Agarose gel with PCR amplicons showing heterozygous mice expressing the transgenic Cre-ER^{T2} allele (290bp) and the Wild type allele (401bp)

3.2. Distribution and interaction of neuronal inputs with tanycytes

In order to analyze how the neuronal inputs are distributed and interact with tanycytes along the rostro-caudal axis of the hypothalamic III-ventricle, I performed an immunohistochemical (IHC) and immunofluorescence (IF) analysis. To do this, I immunolabeled the RAX-Cre-ER^{T2}-tdTomato mouse brain sections for: *i)* glutamatergic presynaptic terminal with an antibody against the vesicular glutamate transporter 2 (VGLUT2); *ii)* GABAergic presynaptic terminals by immunohybridizing inhibitory neurons vesicles with the vesicular inhibitory aminoacid transporter (VGAT); *iii)* ependymal cell population consisting of both ependymocytes and tanycytes by using a Nestin-directed antibody; *iv)* tanycytes by the endogenous expression of tdTomato driven by the RAX promoter from the RAX-Cre-ER^{T2}-tdTomato mouse line; *v)* tanycytes and astrocytes with the glial fibrillary acidic protein (GFAP); *vi)* and the corticotropin-releasing hormone (CRH). To map the distribution of the neuronal inputs onto tanycytes in the considered rostro-caudal distribution, I selected brain sections that span most of the hypothalamic III-ventricle that correspond to a distance relative to Bregma: slice 1, -2.30mm; slice 2, -1.82mm, slice 3. -1.34mm; slice 4, -0.70mm.

The following *Figures 9, 10, 11* and *12* show 20x and 40x overview scans of 4 immunohistochemically stained RAX-Cre-ER^{T2}-tdTomato mouse brain sections as well as their theoretical localization and stereotaxic coordinates (Franklin, 1997) within the brain. To gain

a more detailed high-spatial resolution, I acquired and analyzed confocal micrographs with an oil immersion 63x objective in different positions that are depicted in *Figures 9, 10, 11* and *12*.

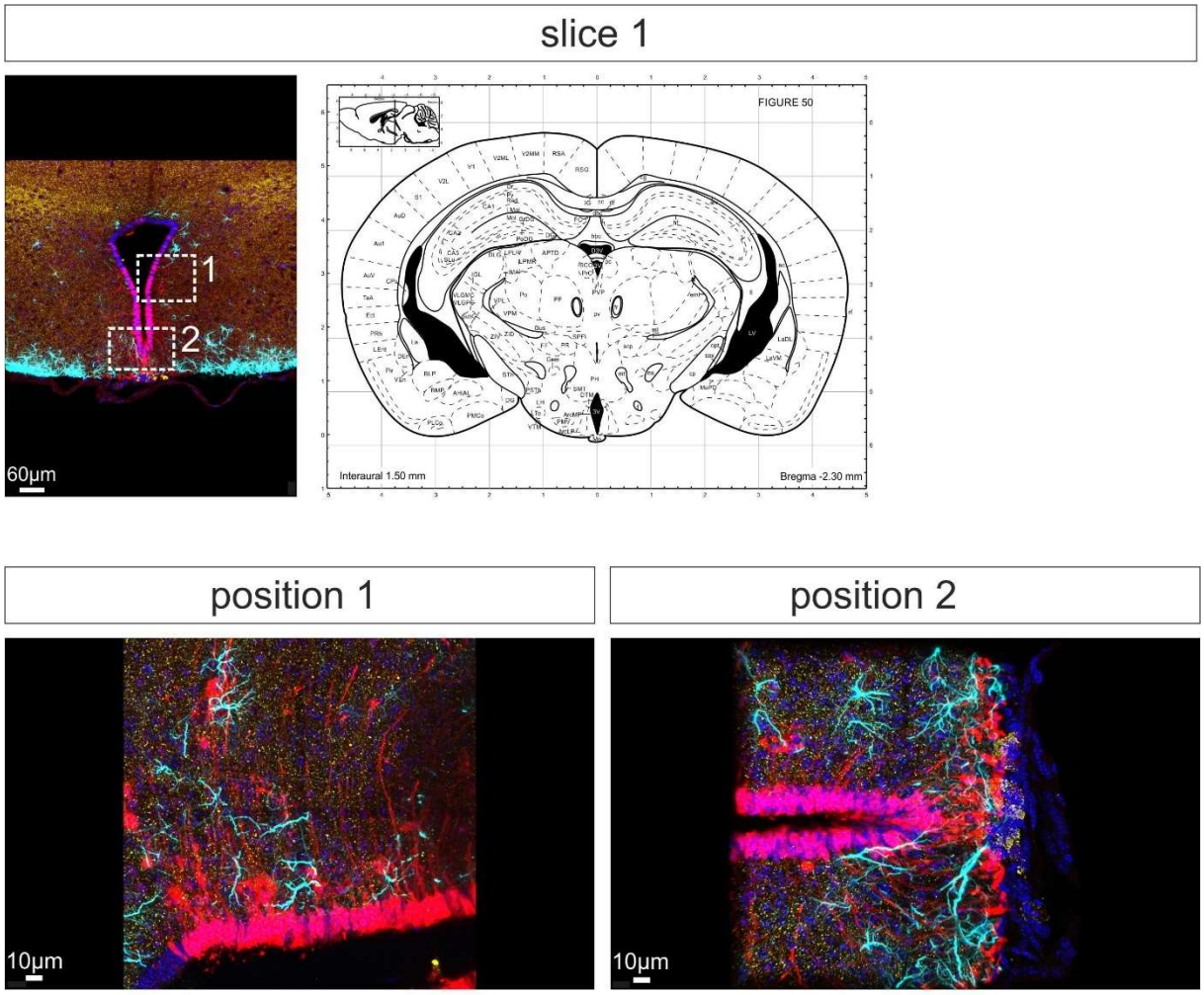

Figure 9 | Slice 1 approximate -2.30mm relative to bregma with positions 1 and 2
RAX (red), GFAP (cyan), VGAT (yellow) and Hoechst (blue)
Scale bar for 40x overview scan=60µm
Scale bar for 63x scans of positions 1 and 2=10µm

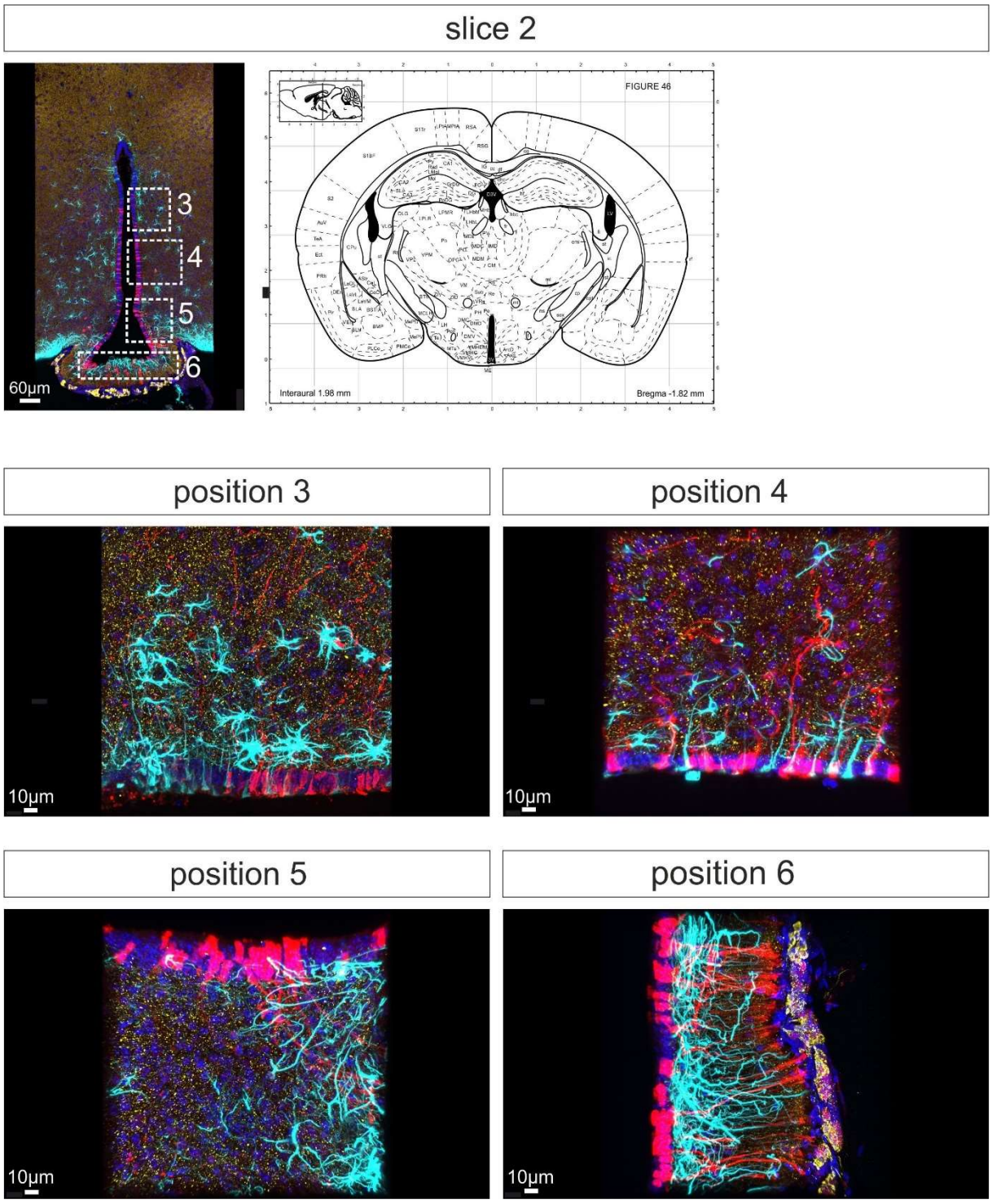

Figure 10 | Slice 2approximate -1.82mm relative to bregma with positions 3, 4, 5 and 6
RAX (red), GFAP (cyan), VGAT (yellow) and Hoechst (blue)
Scale bar for 40x overview scan=60µm
Scale bar for 63x scans of positions 3 to 6=10µm

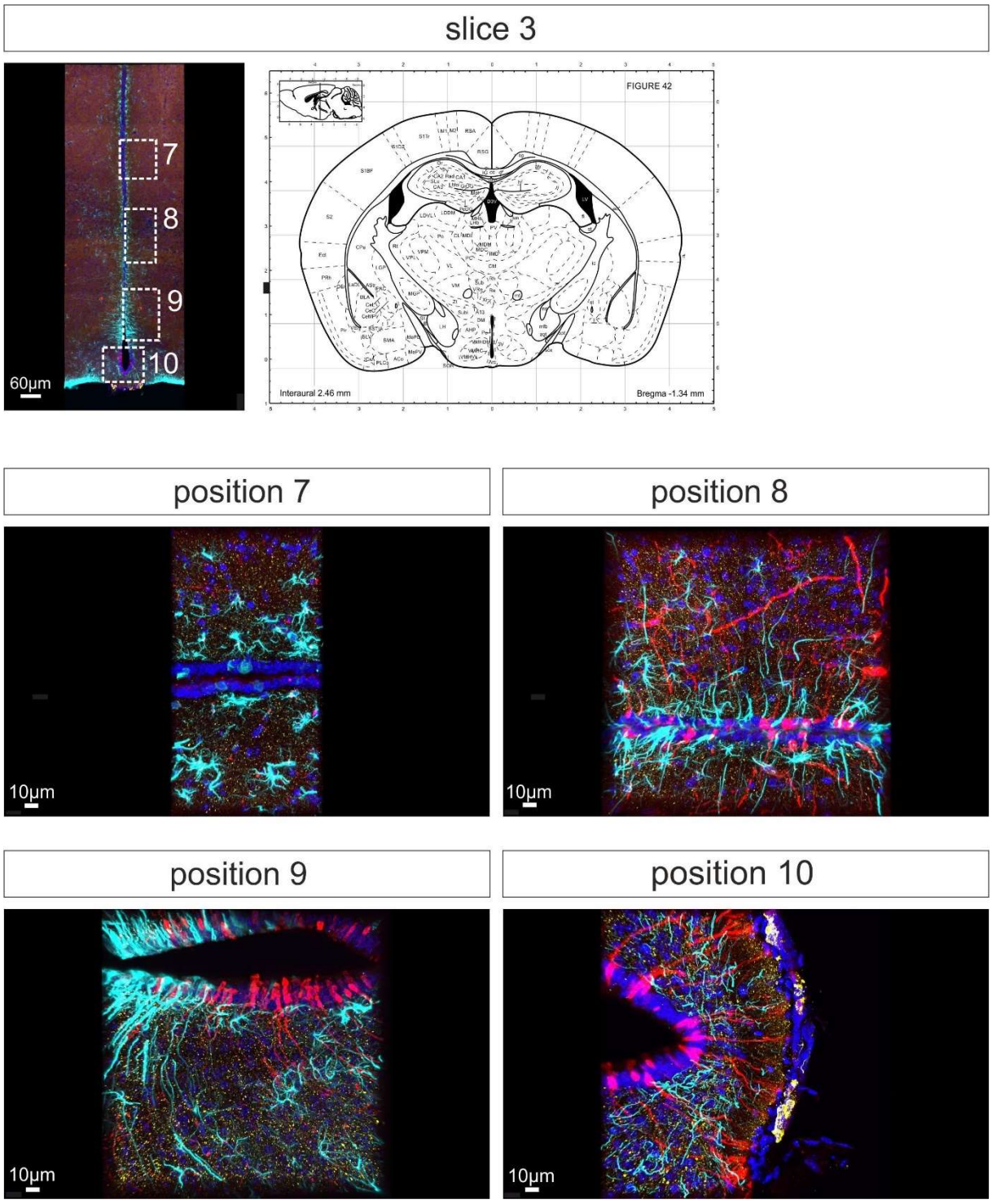

Figure 11 | Slice 3 approximate -1.34mm relative to bregma with positions 7, 8, 9 and 10
RAX (red), GFAP (cyan), VGAT (yellow) and Hoechst (blue)
Scale bar for 40x overview scan=60µm
Scale bar for 63x scans of positions 7 to 10=10µm

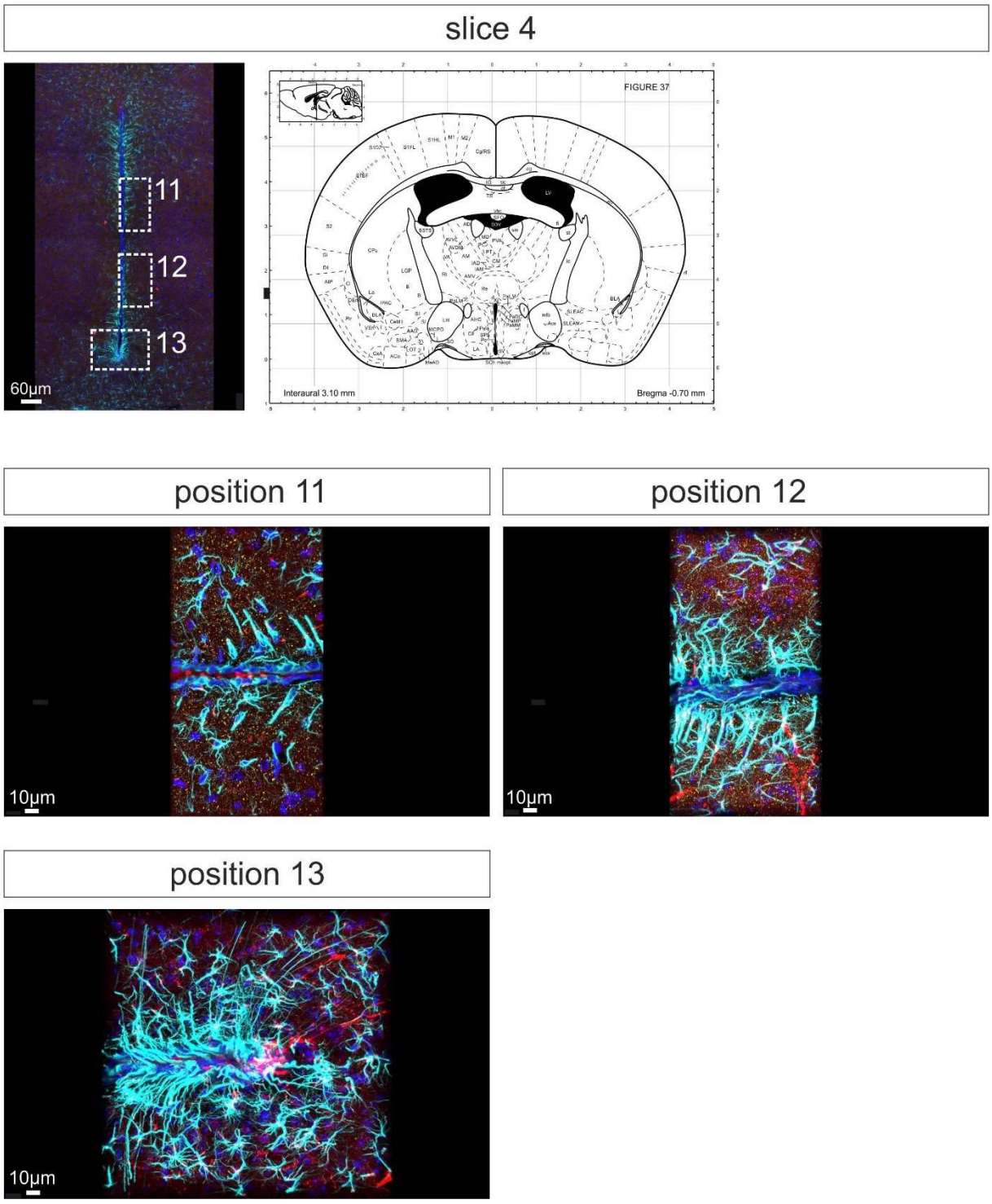

Figure 12 | Slice 4 approximate -0.70mm to bregma with positions 11, 12 and 13
RAX (red), GFAP (cyan), VGAT (yellow) and Hoechst (blue)
Scale bar for 20x overview scan=60µm
Scale bar for 63x scans of positions 11 to 13=10µm

3.3. Imaris reconstructions

Subsequently, all confocal 63x micrographs were uploaded into the IMARIS program (Version 9.0.2, Bitplane) to display 3-dimensional images of the acquired z-stacks. For every image, I recorded between 40 to 50 planes with a step size of 1µm spanning total width of 40 to 50 µm (=optical section).

My overall aim was to develop and optimize a protocol for a reliable 3-dimensional reconstruction of tanycytic processes arising from tanycytic cell bodies located at the caudal-to-rostral extensions of the lateral walls of the III-ventricle and further the detection of the existence of synaptic inputs onto these processes. Briefly recapitulated, by using the 'Surface Reconstruction' or the 'Filament Tracer' tool I performed the reconstruction of processes based on either the Vimentin, Nestin, RAX or GFAP signal which are all considered as tanycyte markers (Bolborea and Dale 2013; Lee et al. 2012; Robins et al. 2013, Rodríguez et al. 2005). To locate synaptic inputs, I first used the 'Spot Detection' tool to create point-like structures based on the VGLUT2, VGAT or CRH signal which I regarded as synaptic markers in the different mouse lines examined. I set the diameter of the detected spots to 1µm in the xy- as well as in the z-plane. Then, I applied the 'Distance Calculation' tool to characterize these detected spots as being afar or closer than 0.8µm to the remodeled tanycytic process. I considered spots which fulfilled the criterion to be closer than 0.8µm to the process as 'synaptic inputs'. For more details about image processing, see paragraph 2.9.

3.3.1. Detected cell types along the III-ventricle's walls and floor part

Before starting with the reconstruction of processes and synaptic inputs, it was necessary to reveal the cells' identity in order to reliably distinguish between tanycytes and ependymocytes. Based on previously described morphological features, I identified the hypothalamic periventricular ependymal cells. Tanycytes are equipped with an elongated radial process emerging into the hypothalamic brain parenchyma while their cell bodies are bordering the walls of the III-ventricle. In contrast to tanycytes, ependymocytes display a cuboidal shape with multiple apical beating cilia that contributes to the CSF flow. (Clasadonte & Prevot, 2017; Prevot et al., 2018). The dorso-to-ventral distribution of ependymocytes and tanycytes differs. Ependymocytes reside at the dorsal parts of the III-ventricular wall, whereas tanycytes start to arise at more ventral positions around the VMH as well as parts of the DMH and continue ventrally to the border of III-ventricle floor, where the ME is located. Nevertheless, one should keep in mind that this division shows no strict borders but instead transition zones are observable (Rodriguez at al. 2019). *Table 10* summarizes the analyzed cell types across the III-

ventricle in all evaluated mouse lines. Tanycytes were found at the expected positions, consistent with previous studies describing the location of hypothalamic tanycytes (Prevot et al., 2018; Robins et al., 2013). Based on these results I precisely separated the analysis of tanycytes and ependymocytes.

Table 10 | Detected cell types at position 1 to 13 located at the caudal-to- rostral expansion of the lateral walls and floor part of the hypothalamic III-ventricle
Tanycytes (T), ependymocytes (E)
Wild type (WT), RAX-Cre-ER^{T2}-tdTomato (RAX), CRH-Cre-tdTomato (CRH)

Positions along the hypothalamic borders of the III-ventricle													
Slice	1		2				3				4		
Bregma	-2.30mm		-1.82mm				-1.34mm				-0.70mm		
Position	1	2	3	4	5	6	7	8	9	10	11	12	13
WT	E+T	T	E+T	E+T	E+T	T	E+T	E+T	E+T	E+T	E+T	E+T	E+T
RAX	T	T	T	T	T	T	E+T	T	T	T	E	E+T	E+T
CRH	T	T	E	T	T	T	E	E+T	E+T	T	T	T	T

3.3.2. Filament tracer tool is more suitable for reconstructing tanycytic processes

In order to quantify and map neuronal inputs onto tanycytes, as a first step I used IMARIS to delineate tanycytic processes from confocal acquired micrographs. To do this, I reconstructed tanycytic processes from brain sections immunolabeled with Nestin, Vimentin and GFAP and from a mouse model that drive tdTomato expression under the RAX promoter control from the RAX-Cre-ER^{T2} transgenic mouse (Pak et al., 2014).

To successfully achieve this goal, I tested two different methods provided by the IMARIS software, namely the ‘Surface Reconstruction’ and the ‘Filament Tracer’ tool.

The ‘Surface Reconstruction’ creates a 3-dimensional representation of a specific signal selected in the data set, leading to the visualization of structures labeled by this signal. Additional parameters like signal thresholding and smoothness of the reconstructed object were manually adjusted to truthfully reproduce tanycytic processes. The ‘Surface Reconstruction’ tool showed one major drawback: due to the dense arrangement of tanycytes along the ventricular walls no separation of individual processes was possible, and the reconstruction resulted in one big connected object, rendering the analysis not precise enough for the goal of this study. Moreover, the rough surface of the object conducted a surface expansion which in turn led to higher amounts of detected spots resulting in an oversampling of the synaptic inputs (see *Figure 16*). In all the reconstructions I aimed to recreate the tanycytic cell bodies and

processes separately in order to determine differences between the amounts of inputs at the area I classified as ‘soma’ in contrast to ‘process’. The following *Figure 13* illustrates an exemplary reconstruction executed by using the ‘Surface Reconstruction’ tool. Additionally, *Tables 11* lists the values for volume of the reconstructed structures and the number of detected spots closer than 0.8µm to the processes which are considered as ‘synaptic inputs'. For interested readers, values for all reconstructions performed with the ‘Surface Reconstruction’ tool can be found in the appendix.

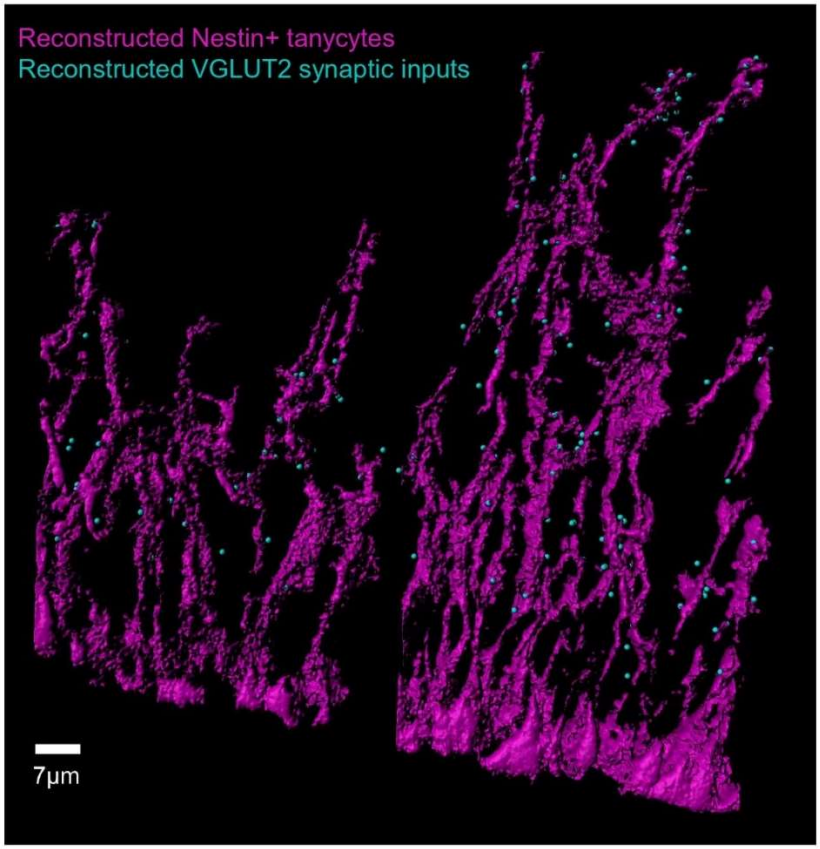

Figure 13 | Reconstructed tanycytes by using the 'Surface Reconstruction' tool
Reconstructed Nestin+ tanycytic process (magenta) and synaptic VGLUT2 input (cyan)
Scale bar=7µm

Table 11 | Values for reconstruction of tanycytic soma and process executed by using the ‘Surface Reconstruction’ tool

Cell Type	Reconstructed structure	Volume in µm³	Spots < 0.8µm close to process considered as synaptic inputs
Tanycytes	*Soma*	2940	0
		3501.675	11
	Process	6838.445	101
		4908.025	211

The second tool I tested to visualize tanycytic processes was the 'Filament Tracer'. This method offers the possibility to segment, track, edit, draw, display and measure filaments in the confocal z-stack. Like the 'Surface Reconstruction' tool, it generates a 3-dimensional depiction based on a selected signal (RAX, Nestin, Vimentin or GFAP). The major difference to the 'Surface Reconstruction' is that the 'Filament Tracer' qualifies these objects as 'Filaments' if length and average thickness meet with the respective criteria (for filaments). There are different options to perform the tracing: either automatically, semi-automatically or manually. First, I tested the 'Automatic Tracing' mode but it displayed too many and too narrow filaments, which did not result in a realistic representation of tanycytic processes (see *Figure 14*). Another issue was that due to overlapping processes the program frequently assigned them as one single filament with several branches which actually does not correspond to the real structure.

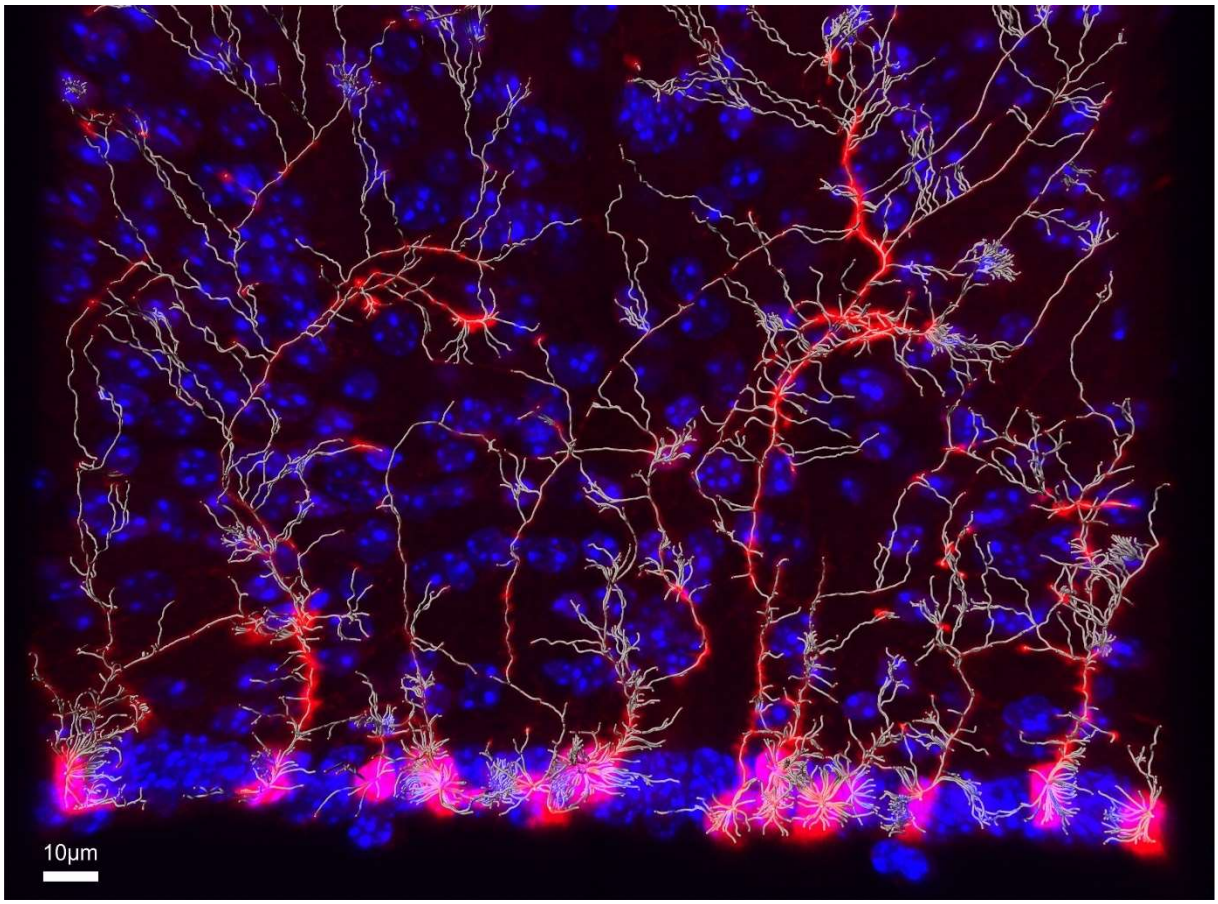

Figure 14 | Reconstruction of tanycytic processes using the 'Automatic Tracing' tool
RAX (red) and Hoechst (blue)
Reconstructed RAX+ tanycytic process (grey)
Scale bar=10µm

For this reason, I opted to draw the processes in a semi-automatical ('AutoDepth') or manual ('Manual') way. Both modes allow precise and concordant manual drawing of 3-dimensional

filaments directly onto the selected signal which provides a visual reference/template for the person drawing. Drawing is executed in the xy-plane, while the z-planes can be adjusted manually by the drawer using the computers mouse cursor ('Manual') or is changed automatically by the program itself ('AutoDepth'). The two methods yield to homogenous recreations of tanycytic processes. *Figure 15* shows an image of tanycytic processes arising from the ventricular walls with the mouse cursor executing the reconstruction in yellow (*A*), one 3-dimensionally reconstructed processes again depicted in yellow (*B*) and the final image after remodeling all tanycytic processes (*C*).

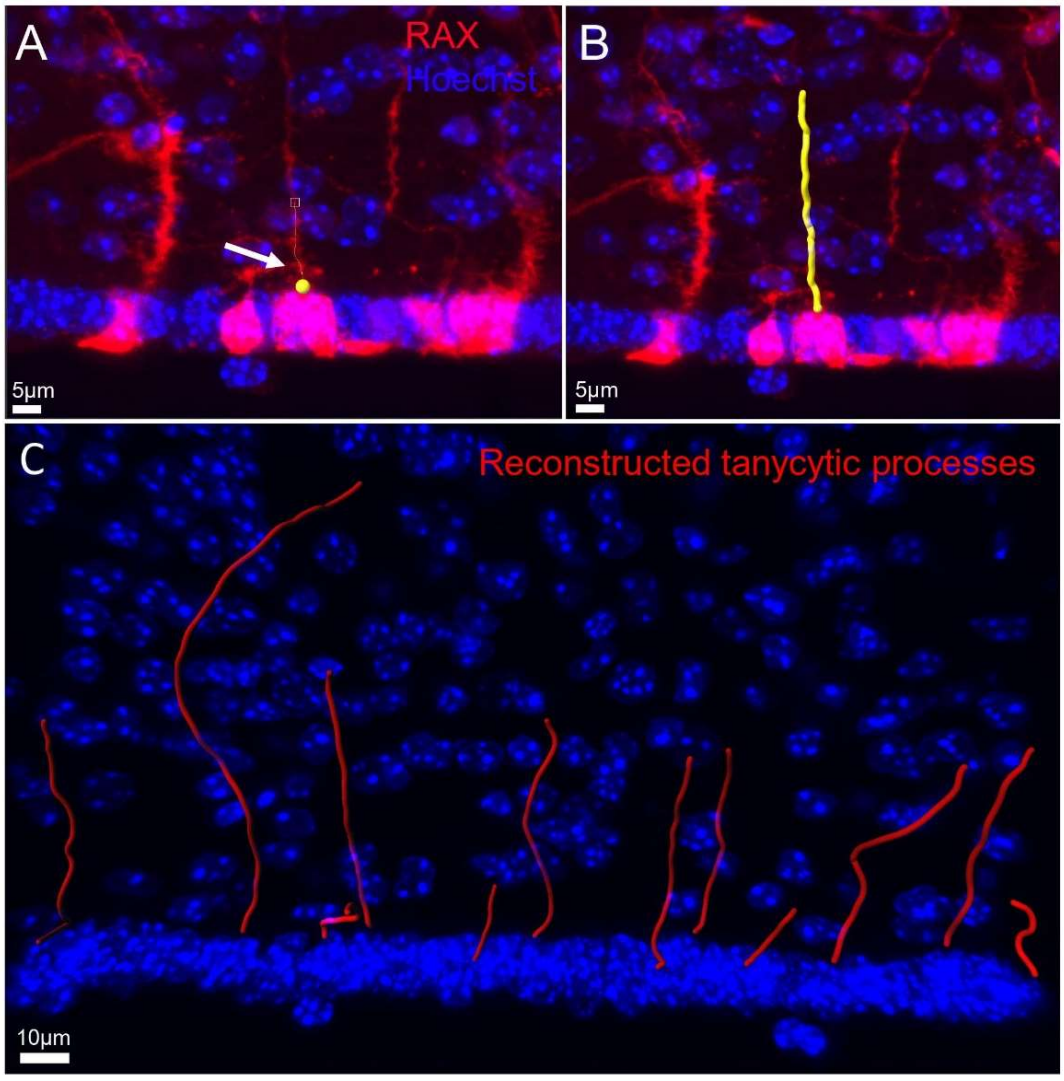

Figure 15 | Drawing of tanycytic processes by using the 'AutoDepth' mode
RAX (red) and Hoechst (blue)
A) mouse cursor tracing the tanycytic process; B) 3-dimensionally remodeled process, reconstructed RAX+ tanycytic process (yellow); C) final image after reconstruction of all processes at this position, reconstructed RAX+ tanycytic process (red)

As already mentioned, the detection of synaptic inputs onto tanycytic process which have been reconstructed by using the 'Surface Reconstruction' tool resulted in higher amounts of inputs compared to less numbers of synaptic inputs onto processes remodeled by applying the 'Filament Tracer'. The reason for this phenomenon lies within the harsh and rough exterior of processes conducted by the 'Surface Reconstruction' which in turn results in a surface expansion which likely causes an oversampling of neuronal inputs. This is prevented by the usage of the 'Filament Tracer' as it allows drawing of a smooth and even filament which reproduces a reliable reflection of the tanycytic process und further a more realistic amount of detected inputs. *Figure 16* shows two positions alongside the ventricular walls which have been remodeled by using the 'Surface Reconstruction'(*A, C*) as well as the 'Filament Tracer' tool (*B, D*), the detected amounts of inputs (n) closer than 0.8µg to the edge of the reconstructed surfaces are indicated and show higher numbers of synaptic inputs onto tanycytic processes reconstructed by using 'Surface Reconstruction' at both positions.

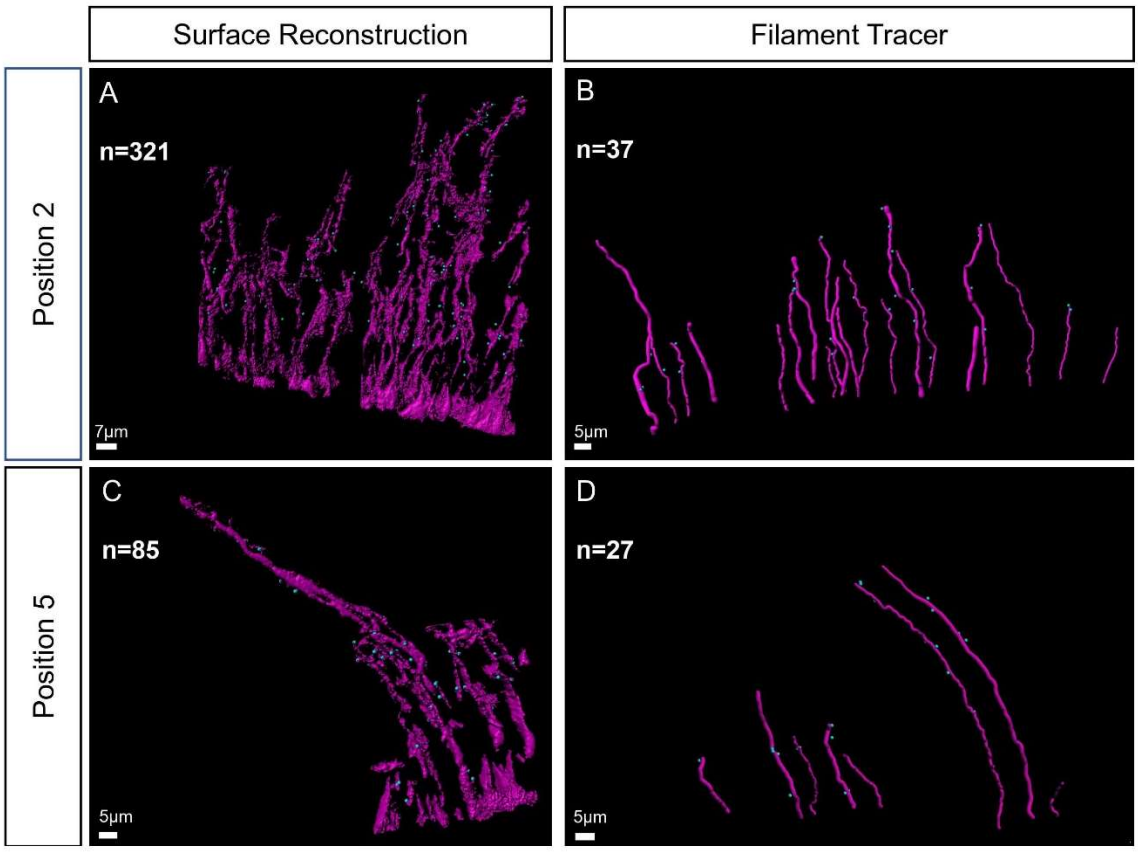

Figure 16 | More inputs onto tanycytes remodeled by 'Surface Reconstruction' tool
Remodeled tanycytic processes (magenta), synaptic VGLUT2+ inputs (cyan)
n=amount of synaptic inputs
A) tanycytic processes at position 2 remodeled with 'Surface Reconstruction'; B) tanycytic processes at position 2 remodeled with 'Filament Tracer'; C) tanycytic processes at position 5 remodeled with 'Surface Reconstruction'; D) tanycytic processes at position 5 remodeled with 'Filament Tracer'
Scale bars=7µm and 5µmF

All the different aspects of the two tools taken into consideration, I concluded, that using the 'AutoDepth' and 'Manual drawing' mode provided by the 'Filament Tracer' resulted in the most realistic morphological representation of the tanycytic filament needed for my analysis. A comparison of tanycytic processes once reconstructed with the 'Surface Reconstruction' and once with the 'Filament Tracer' tool is shown in *Figure 17.* This confrontation unambiguously demonstrates the described advantages of the 'Filament Tracer' which I selected as the method of choice for all subsequent reconstructions.

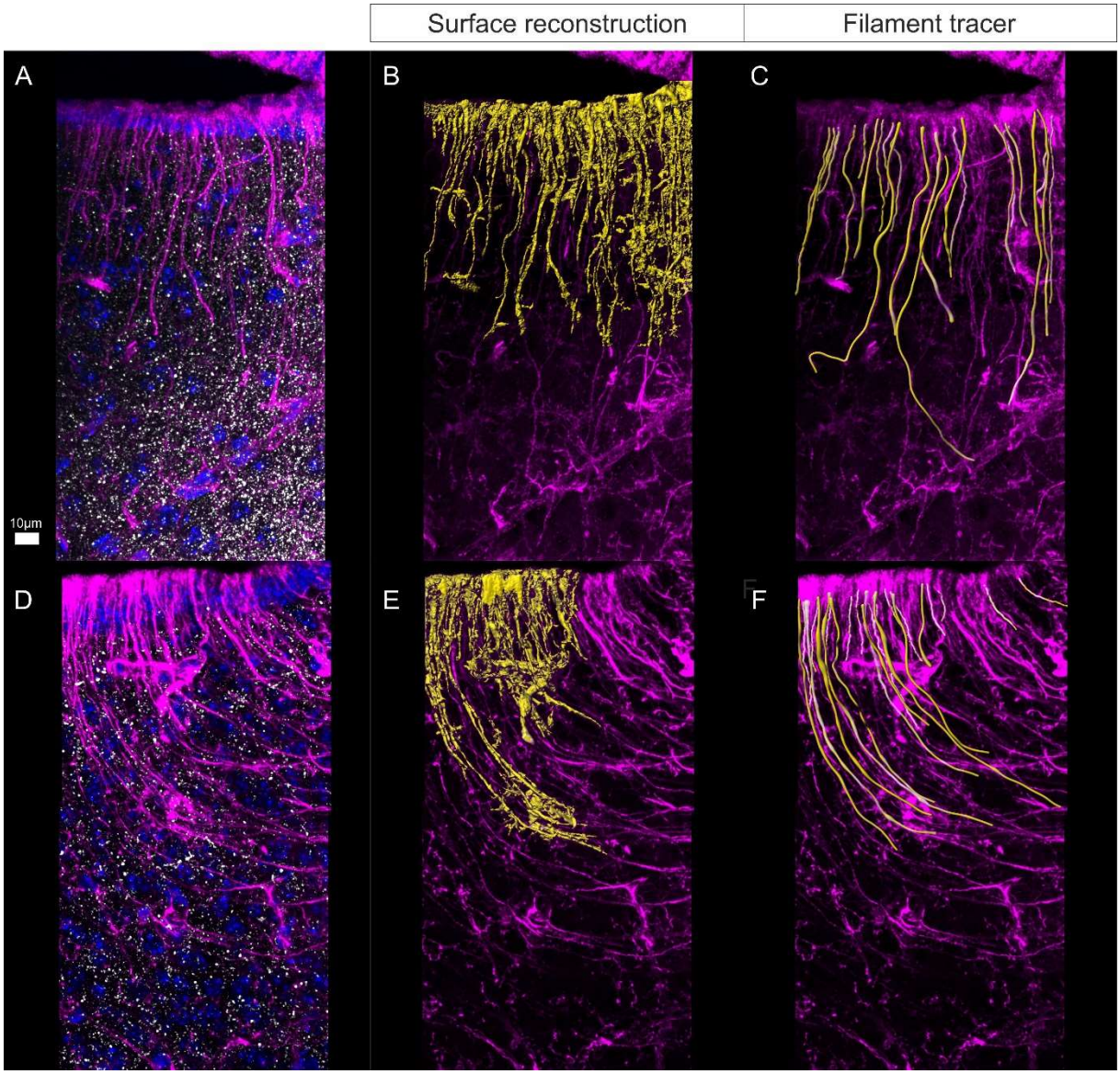

Figure 17 | Comparison between 'Surface Reconstruction' and 'Filament Tracer' tool
Nestin (magenta), VGLUT2 (white) and Hoechst (blue)
Reconstructed Nestin+ tanycytic process (yellow)
A) and D) confocal 63x micrographs of tanycytes facing the CSF inside the III-ventricle; B) and E) reconstructions of tanycytic processes performed with 'Surface Reconstruction'; C) and F) reconstruction of tanycytic processes performed with 'Filament Tracer'
Scale bar=10µm

3.3.3. Image reconstruction workflow

After establishing an adequate and reliable way to reconstruct tanycytic processes by using the 'Filament Tracer', I developed a straight-forward image processing pipeline which was applied to all the confocal z-stacks of the 13 regions of interest. *Figure 18* illustrates the entire reconstruction process that is described in the following paragraph:

As a first step, I uploaded the confocal image into the IMARIS software. Then, I applied small adjustments to the image (contrast, brightness, background subtraction). Next, I detected and reconstructed spots based on the different signals VGLUT2, VGAT or CRH by using the 'Spot Detection' tool. (see paragraph 2.9.1.). Subsequently, I performed reconstructions of tanycytic processes, based on different signals depending on which tanycyte marker was used: either Nestin, Vimentin, RAX or GFAP. Then, I detected spots in close proximity to tanycytic processes by calculation the distance of spots to processes with the 'Find spots close to filaments' tool and assigned spots found closer than 0.8µm as 'synaptic inputs on tanycyte processes' (see paragraph 2.9.3.) As a last step, I reconstructed cell nuclei lining the ventricular walls by using the 'Surface Reconstruction' tool to get an approximate estimation of the number of cells found at this position (see paragraph 2.9.4.) Collectively, these steps result in the final picture, that I considered for further analysis. I applied this protocol to all confocal micrographs and in this way, I reconstructed and analyzed a total number of 2318 tanycyte processes (see *Table 12*).

Table 12 | Number of reconstructed tanycytic processes per mouse line

Mouse line	Number of reconstructed tanycytic processes
Wild type	644
RAX-Cre-ER^{T2}-tdTomato	1375
CRH-Cre-tdTomato	299
	2318

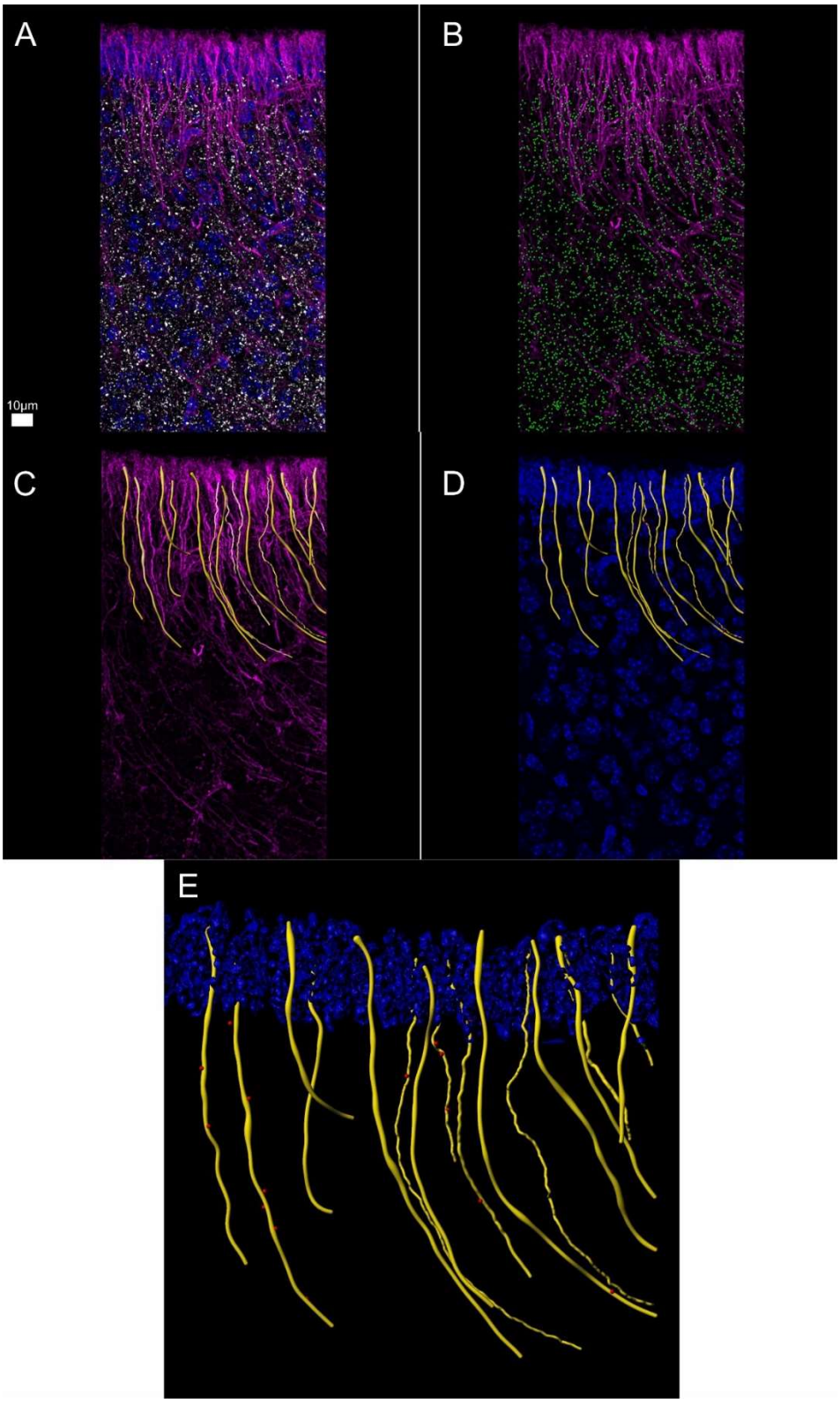

Figure 18 | IMARIS reconstruction workflow

Nestin (magenta), VGLUT2 (white) and Hoechst (blue)

Reconstructed Nestin+ tanycytic process (yellow), VGLUT2+ spots (green), synaptic VGLUT2+ inputs <0.8µm to tanycytic process (red) and Hoechst (blue)

A) 63x confocal micrograph image, B) reconstructed VGLUT2 punctae by using 'Spot Detection' tool, C) reconstructed Nestin+ tanycytic processes by using 'Filament Tracer' tool, D) VGLUT2 punctae <0.8µm to tancytic processes detected by using 'Distance Calculation' tool, E) final image

Scale bar=10µm

The following gallery (*Figure 19*) demonstrates an overview of all positions analyzed with reconstructions performed for tanycytic processes and detected synaptic inputs. Used markers for tanycytes, synaptic inputs and cell bodies as well as scale bars are annotated.

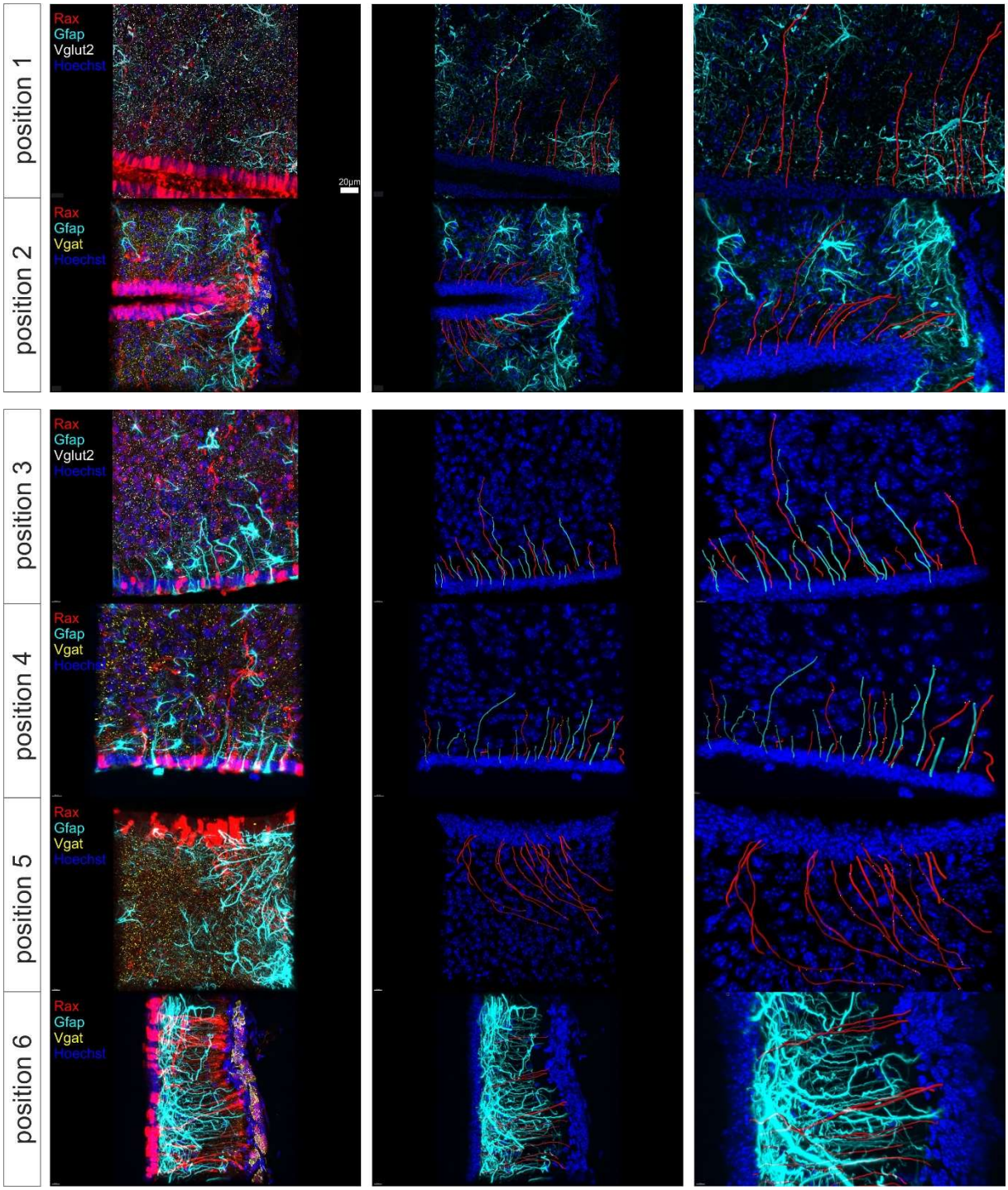

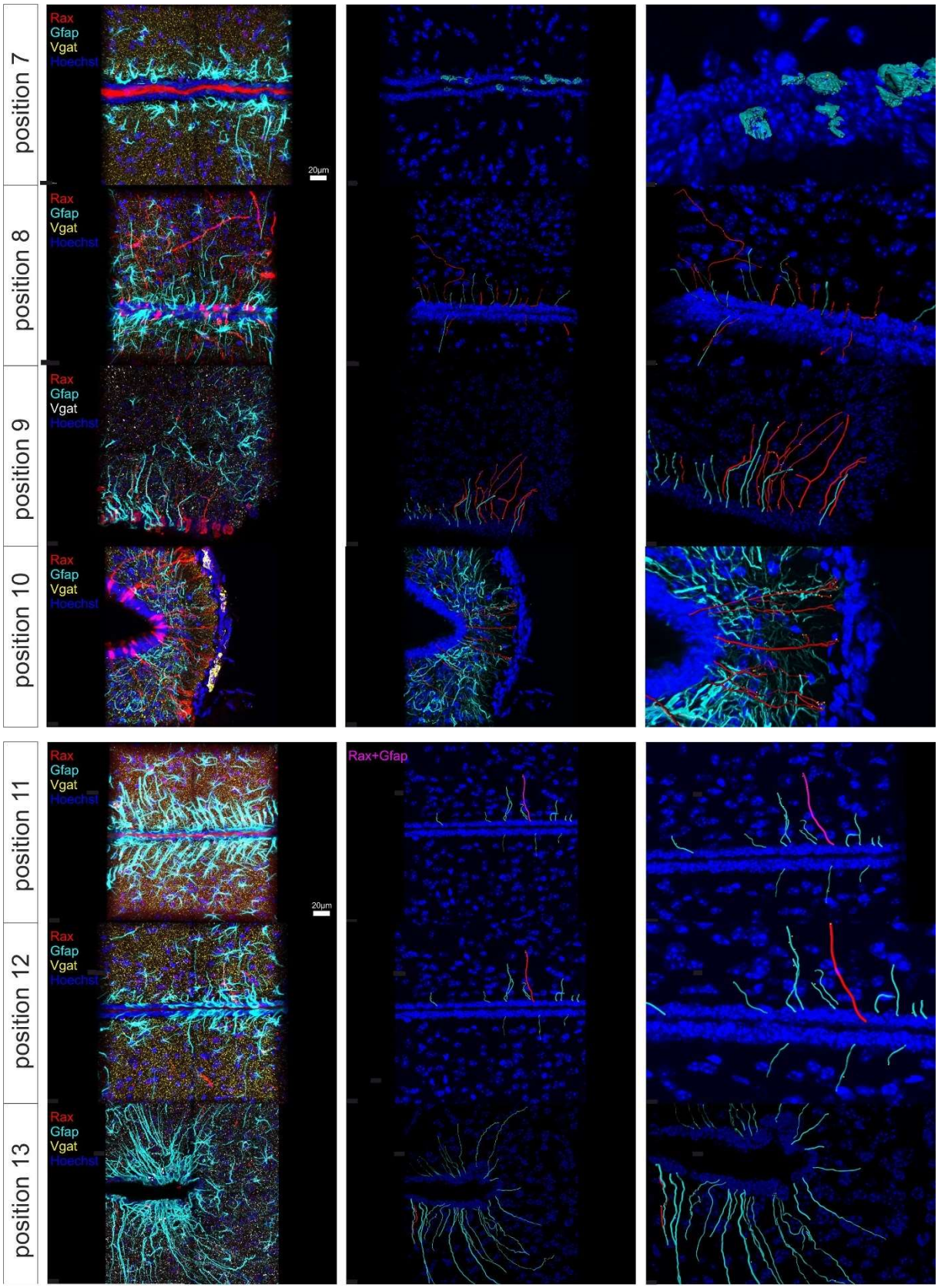

Figure 19| IMARIS reconstructions of position 1 to 13

Used markers and colors are indicated on every image: RAX and GFAP to identify tanycytes, VGLUT2 and VGAT to identify excitatory and inhibitory synaptic inputs, Hoechst to identify cell nuclei
Scale bar=20µm

3.4. Synaptic inputs on tanycytic processes

After I developed a straightforward and reliable reconstruction protocol for tanycytic processes I applied it to shed light on our main research question: do tanycytes get synaptic inputs form neurons in the hypothalamic area of the III-ventricle? And if so, to reveal their distribution pattern with the final aim to portray neuronal inputs onto tanycytic processes along the extension of the III-ventricle. Inspired by a study performed in 2018 by Alpár and colleagues who unambiguously demonstrated that ependymocytes lining the walls of the III-ventricle are targeted by hypothalamic CRH-releasing neurons to induce the liberation of CNTF into the ventricular system, I hypothesized that this mechanism could exist between neurons and hypothalamic tanycytes too. Moreover, after a profound literature research, I found evidence of so-called 'synaptoid-contacts' between tanycytic process and neuronal axons of unknown origin primarily in the area of the ME (Wittkowski 1967, Güldner and Wolff 1973, Scott and Paull 1979) which further encouraged me to study this type of cellular interactions.

In this study, I analyzed several positions on mouse hypothalamic sections immunolabeled for the presynaptic markers VGLUT2, VGAT and CRH (using the CRH-Cre-tdTomato mouse line) as well as immunolabeled for Nestin, Vimentin, GFAP which are established markers for tanycytes. Further, I used the transgenic mouse model RAX-Cre-ER^{T2}-tdTomato which drives tdTomato expression in hypothalamic tanycytes (Pak et al. 2014).

After 3-dimensional reconstruction of both synaptic inputs and tanycytes, I determined and measured if tanycytic processes receiving synaptic inputs by counting inputs in close proximity to the processes across all positions considered. The selected positions cover the extension of the hypothalamic III-ventricle form a caudal-to-rostral orientation, see paragraph 3.2. They correspond to the main regions of the hypothalamus where some important nuclei are located executing a wide range of different functions (for more details see paragraph 1.1. as well as paragraph 1.3.).

In short summary, as a first step I identified and distinguished between hypothalamic tanycytes and ependymocytes based on morphological features and their location alongside the ventricular walls. Next, I acquired 63x confocal micrographs and executed 3-dimensional reconstruction of tanycytic processes by using the 'AutoDepth' respectively the 'Manual' mode of the 'Filament Tracer' tool provided by IMARIS. Both modes result in a concordant and realistic representation of tanycytic processes that I further analyzed. I detected different synaptic signals, namely VGLUT2, VGAT, and CRH and remodeled them as 3-dimensional spots. Then, I examined their distance to tanycytic processes and finally annotated them as

'synaptic inputs' if they fit the criterion to be located closer than 0.8µm to the tanycytic process (*Figure 20*).

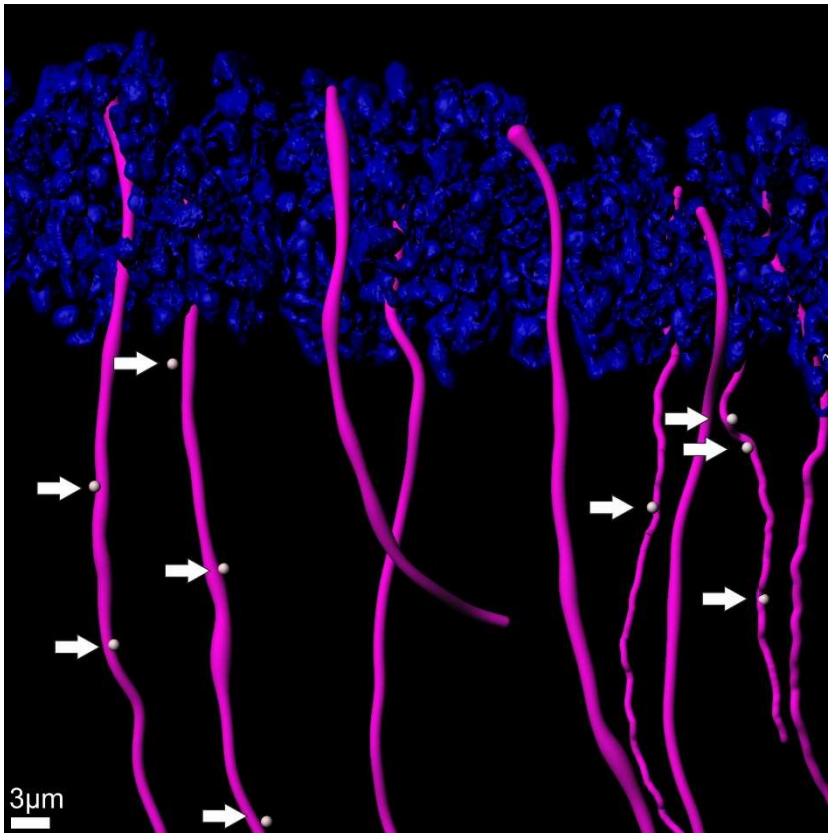

Figure 20 | Nestin+ tanycytic processes receiving synaptic VGLUT2+ inputs
Reconstructed Nestin+ tanycytic processes (magenta), reconstructed VGLUT2+ inputs (white), reconstructed cell nuclei (blue)
Arrows point towards synaptic inputs onto tanycytes
Scale bar=3µm

My observations clearly showed that at all investigated positions alongside the hypothalamic III-ventricle tanycytic processes receive VGLUT2, VGAT and CRH synaptic inputs from adjacent neurons located in the hypothalamic brain parenchyma (*Figure 21*). In all positions considered, I noticed that only a subset of reconstructed tanycytes receive neuronal inputs (*Figure 22*). Moreover, there is a slight trend observable that the number of synaptic inputs onto tanycytic processes is higher in caudal regions around the area of the DMH, VMH, ArcN and parts of the ME compared to more rostral regions of the ArcN and ME. Positions considered as 'caudal' ranging from 1 to 6 correspond to a theoretical localization of -2.30mm and -1.82mm relative to Bregma whereas positions regarded as 'rostral' ranging from position 7 to 13 correspond to a theoretical localization of -1.34mm and -0.70mm relative to Bregma. Subsequently, I quantified the amount of synaptic inputs at the considered positions.

Figure 21 presents values as means and ± standard error means (SEM) for analyzed and quantified absolute numbers of the total amount of reconstructed tanycytic processes (black bar), the amount of tanycytes receiving synaptic inputs (red bar) and the total amount of synaptic inputs (blue bar) observed at all positions considered the walls of the III-ventricle. *Figure 21* (*A*) shows values for VGLUT2+ inputs onto Nestin+ tanycytes in Wild type animals, (*B*) values of VGLUT2+ inputs onto RAX+ as well as GFAP+ tanycytes in RAX-Cre-ER^{T2}-tdTomato animals, (*C*) values of VGAT+ inputs onto RAX+ as well as GFAP+ tanycytes in RAX-Cre-ER^{T2}-tdTomato animals and (*D*) values of CRH+ inputs onto Vimentin+ tanycytes in CRH-Cre-tdTomato animals.

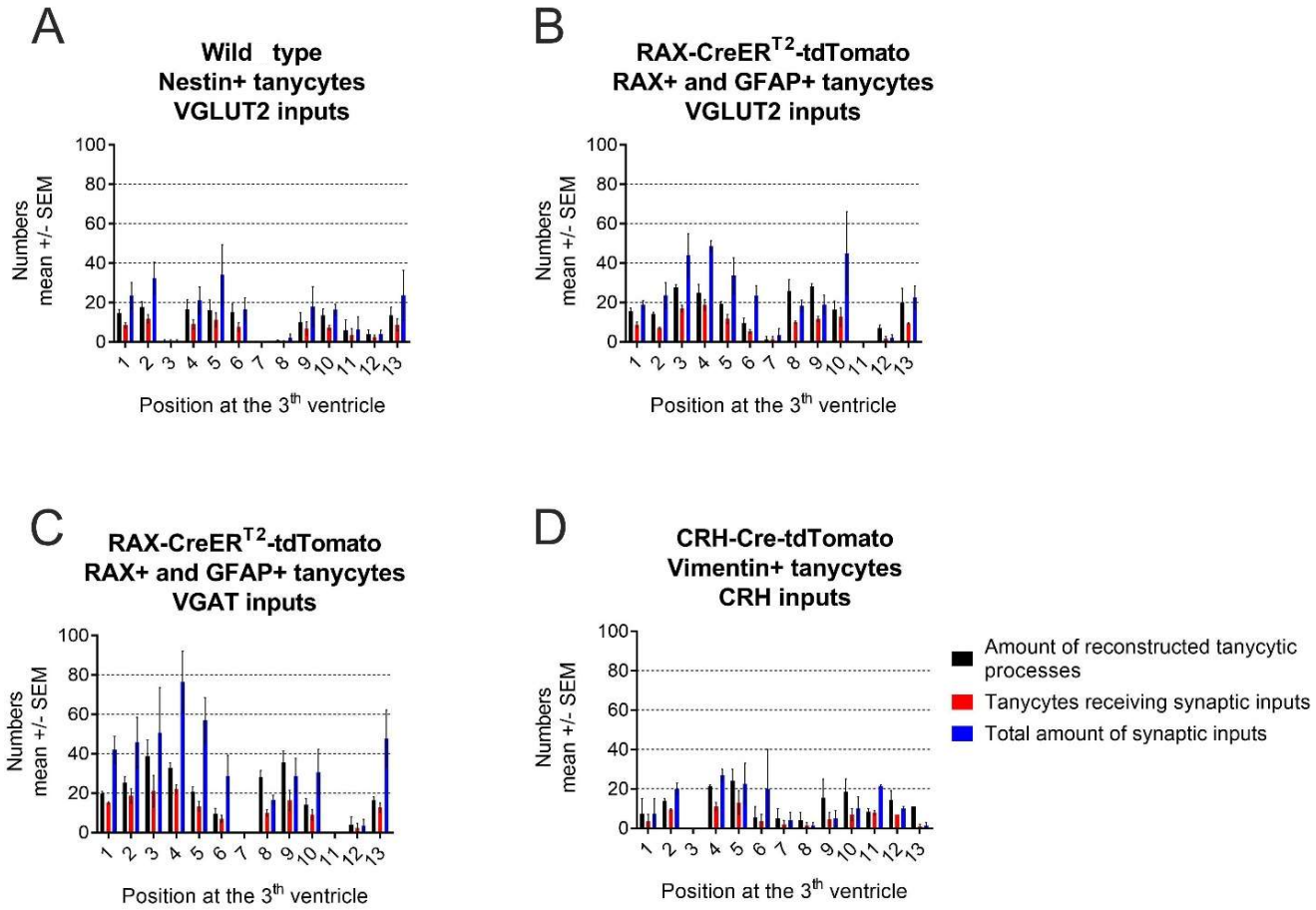

Figure 21 | Amount of reconstructed tanycytic processes, tanycytes receiving synaptic inputs and total amount of synaptic inputs in all analyzed mouse lines

Values presented as means and SEM

A) VGLUT2+ inputs on Nestin+ tanycytes in Wild type animals B) VGLUT2+ inputs onto RAX+ and GFAP+ tanycytes in RAX-Cre-ER^{T2}-tdTomato animals, C) VGAT+ inputs onto RAX+ and GFAP+ tanycytes in RAX-Cre-ER^{T2}-tdTomato animals, C) CRH+ inputs onto Vimentin+ tanycytes in CRH-Cre-tdTomato animals

It is of importance to note, that not all but only a fraction of tanycytes receive synaptic inputs. I saw that this is true for all considered positions alongside the walls of the III-ventricle as well as for all investigated synaptic inputs. This finding is graphically demonstrated in *Figure 22*

which displays the amount of tanycytes receiving synaptic inputs in comparison to tanycytes not receiving synaptic inputs at a given positions analyzed. *Figure 22* (*A*) shows the % of Nestin+ tanycytes receiving or not receiving VGLUT2+ inputs in Wild type animals, (*B*) the % of RAX+ and GFAP+ tanycytes receiving or not receiving VGLUT2+ inputs in RAX-Cre-ER^{T2}-tdTomato animals, (*C*) the % of RAX+ and GFAP+ tanycytes receiving or not receiving VGAT+ inputs in RAX-Cre-ER^{T2}-tdTomato animals and (*D*) the % of Vimentin+ tanycytes receiving or not receiving CRH+ inputs in CRH-Cre-tdTomato animals.

All examined positions from 1 to 13 are indicated on the x-axis of the graph, blue and grey columns demonstrate the percentage of tanycytes with or without synaptic inputs which were calculated by the following formula:

$$\frac{\text{tanycytes receiving / not receiving synaptic inputs}}{\text{total amount of reconstructed tanycytes}} * 100$$

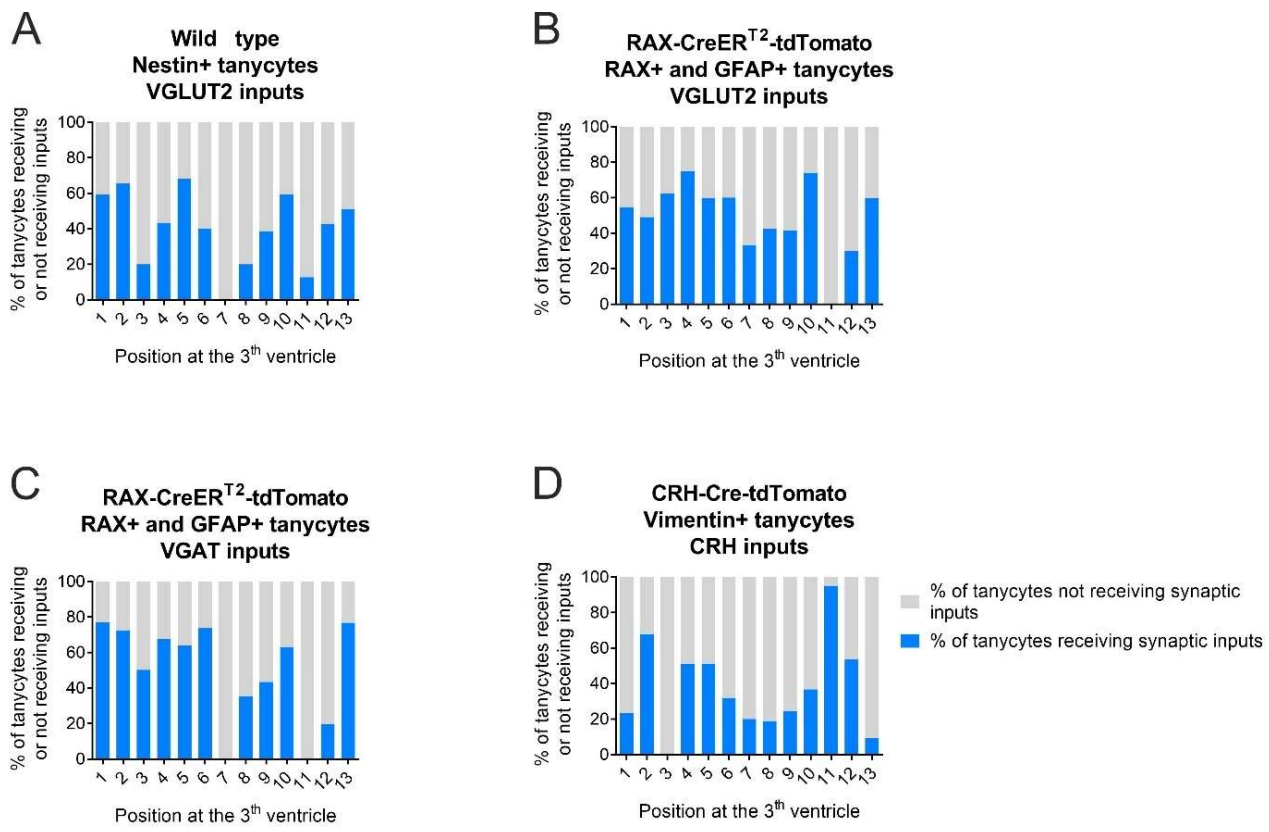

Figure 22 | Percentage of tanycytes receiving or not receiving synaptic inputs in all analyzed mouse lines

Values presented as means in percentages

A) % of Nestin+ tanycytes receiving or not receiving VGLUT2+ inputs in Wild type animals, B) % of RAX+ and GFAP+ tanycytes receiving or not receiving VGLUT2+ inputs in RAX-Cre-ER^{T2}-tdTomato animals, C) % of RAX+ and GFAP+ tanycytes receiving or not receiving VGAT+ inputs in RAX-Cre-ER^{T2}-tdTomato animals, D) % of Vimentin+ tanycytes receiving or not receiving CRH+ inputs in CRH-Cre-tdTomato animals

To conclude, I showed the first 3-dimensional reconstruction of tanycytes located at the borders of the hypothalamic III-ventricle. I confirmed immunohistochemically that tanycytes are contacted by neuronal terminals and may receive synaptic innervations. Moreover, there might be a different rostro-caudal distribution of neuronal inputs onto tanycytes along the hypothalamic III-ventricle. Intriguingly, I detected that not all tanycytes are targeted by neurons but only a fraction of the detected and reconstructed tanycytes got synaptic inputs. Interested readers can peruse the appendix for data used for compilation of the graphs shown in *Figure 21* and *Figure 22*.

3.5. Differences in the amount of synaptic inputs

There are some previous publications that describe synaptoid contacts between neurons and tanycytes (Güldner & Wolff, 1973; Scott & Paull, 1979; Wittkowski, 1967), however none of these studies reported the type of neurons contributing to this specialized type of synapses. After having optimized an imaging analysis pipeline to visualize and reliably quantify synaptoid contacts, I explored how this particular type of innervation distributes throughout all the territories occupied by tanycytes that border the hypothalamic III-ventricle. To do this, I collected all the data from the different tanycytic filament reconstructions and spot analysis from distinct neuronal termination that were 0.8µm closer to the tanycytic basal process and applied a multiparametric test, a one-way ANOVA, to determine whether the amount of neuronal inputs varies throughout the positions herein analyzed. In addition, I used, whenever there was a significant difference, a Tukey's multiple comparison post-hoc test to precisely determine at which positions the amount of inputs onto tanycytes is significant. Interestingly, I found that both excitatory and inhibitory inputs show significantly different numbers across the positions in both Wild type animals and transgenic RAX-Cre-ER^{T2}-tdTomato mice (*Figure 23*). Despite this, the differences detected need to be assessed critically because in some dorsal positions considered for the analysis (positions 7, 11 and 12) the majority of cells found were ependymocytes. For the purpose of this study, I did not consider this other type of contact, which was described earlier by our lab (Alpár et al., 2018). More importantly, the post-hoc analysis I performed highlighted a non-significant trend to increased amounts of neuronal inputs at position 3, 4 and 5 which anatomically correspond to the area of the VMH and ArcN of the hypothalamus. However, expansion of the sample size will be required to get results that are more representative.

Figure 23 shows results from the one-way ANOVA analysis and the applied post-hoc test to investigated differences between (*A*) VGLUT2+ inputs on Nestin+ tanycytes of Wild type

animals, (*B*) VGLUT2+ inputs on RAX+ and GFAP+ tanycytes of RAX-Cre-ER^{T2}-tdTomato animals, (*C*) VGAT+ inputs on RAX+ and GFAP+ tanycytes of RAX-Cre-ER^{T2}-tdTomato animals, (*D*) CRH+ inputs on Vimentin+ tanycytes of CRH-Cre-tdTomato animals. Values are shown as bar-graphs in *Figure 23* and are presented as means and SEM. *p*-values are indicated and significant differences between individual positions are marked with an Asterix.

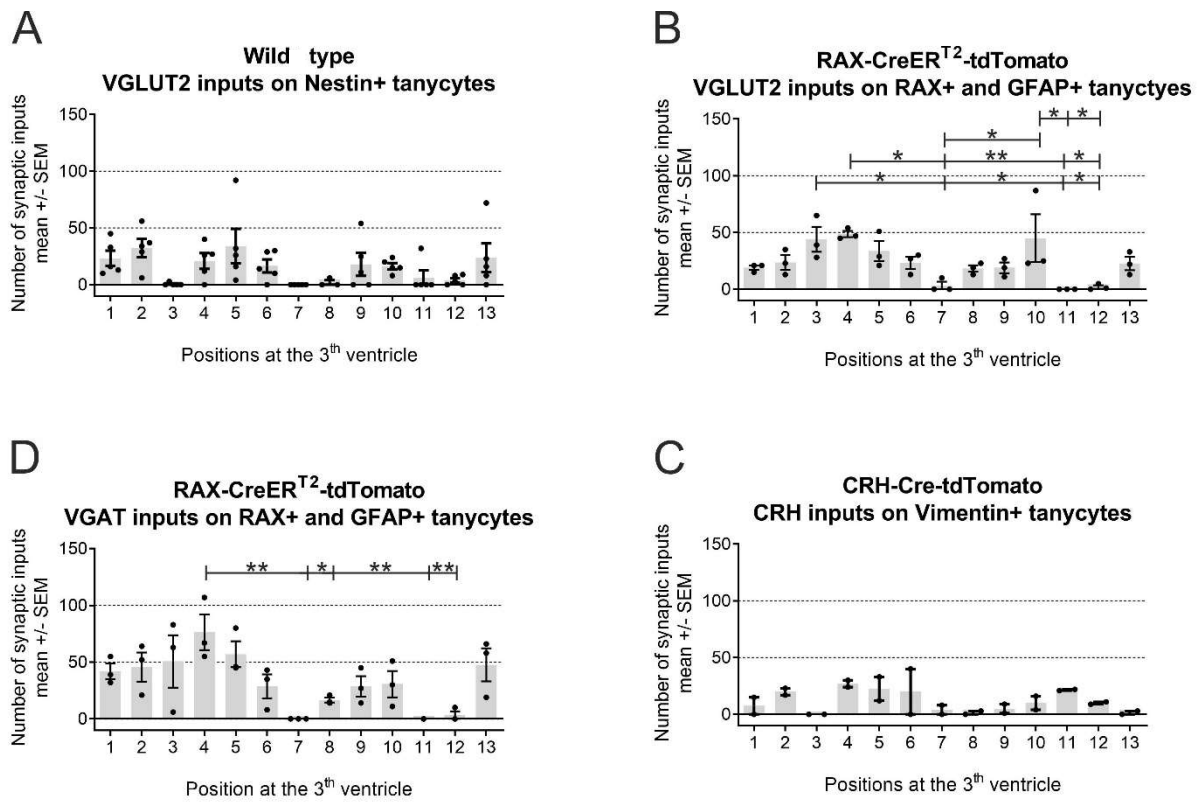

Figure 23 | Differences between the amount of synaptic inputs across all positions examined alongside the walls of the hypothalamic III-ventricle

*Values presented as means and SEM, * $p < 0.05$, ** $p < 0.01$*

Results of ANOVA analysis and post-hoc Turkey's multiple comparison test of differences between A) VGLUT2+ inputs on Nestin+ tanycytes of Wild type animals, B) VGLUT2+ inputs on RAX+ and GFAP+ tanycytes of RAX-CreER^{T2}-tdTomato animals, C) VGAT+ inputs on RAX+ and GFAP+ tanycytes of RAX-CreER^{T2}-tdTomato animals, D) CRH+ inputs on Vimentin+ tanycytes of CRH-Cre-tdTomato animals

To conclude, there are significant differences in the amount of neuronal inputs depending on the location of tanycytes alongside the hypothalamic III-ventricular walls with higher amounts of inputs in caudal regions of the hypothalamus compared to more rostral areas.

Results from the ANOVA analysis and post-hoc tests with exact values can be found in the appendix.

3.6. Differences between α and β tanycytes

Traditionally tanycytes are classified into 4 different subtypes dependent on their dorso-to-ventral location across the hypothalamic III-ventricle: the α1-, the α2-, the β1- and the β2-tanycytes. α1-tanycytes are found at the walls of the infundibular recess and line the VMH and parts of the DMH. α2-tanycytes reside at the area of the ArcN where some of their processes contact blood capillaries. β1-tanycytes are located at the lateral extensions of the infundibular recess, their processes emerge towards the brain's limiting membrane in proximity to portal capillaries of the ME as well as the ventromedial parts of the ArcN. β2-tanycytes can be detected at the area of the ME and their trajectories extend towards its medioexternal region where they establish contacts with portal capillaries and show heavy ramification of their end-feet (Rodríguez et al., 2019). Although this classification is broadly accepted, a strict separation of tanycytic subtypes is not possible due to observed transition zones where the individual subtypes share te territories as well as between α1-tanycytes and more dorsally located ependymal cells. Current investigations still aim to determine when and how differentiation between these subtypes occurs.

After detecting and measuring synaptic inputs across the entire population of tanycytes found alongside the hypothalamic borders of the III-ventricle I aimed to differentiate between individual subtypes to further examined if there are any differences in the amount of synaptic inputs on α- compared to β- tanycytes. Therefore, I used the reconstructed 63x confocal images, identified the territories occupied by the individual subtypes and categorized the reconstructed tanycytes into 3 groups based on their location: α1-, α2/β1- and β2- tanycytes. As already mentioned, strict boundaries between the subtypes are absent. Thus, I joined the α2- and β1-tanycytes into one single group. Furthermore, I excluded the most rostral respectively the most caudal slice and only considered slice 2 (*Figure 24, C*) and slice 3 (*Figure 25, C*), because these slices, in the hypothalamic region, correspond to the level of the DMH, VMH, ArcN and the ME which have also been considered in previous publications that differentiated between α- and β- tanycytes (Goodman and Hajihosseini 2015; Rodriguez at al. 2019). *Figure 24* and 25 depict 40x overview scans of slice 2 at bregma -1.82mm and slice 3 at bregma -1.43mm (*C*), the slices' theoretical location in the mouse brain (*A*) as well as hypothalamic structures found at this level alongside of the III-ventricle (*B*) (Franklin, 1997).

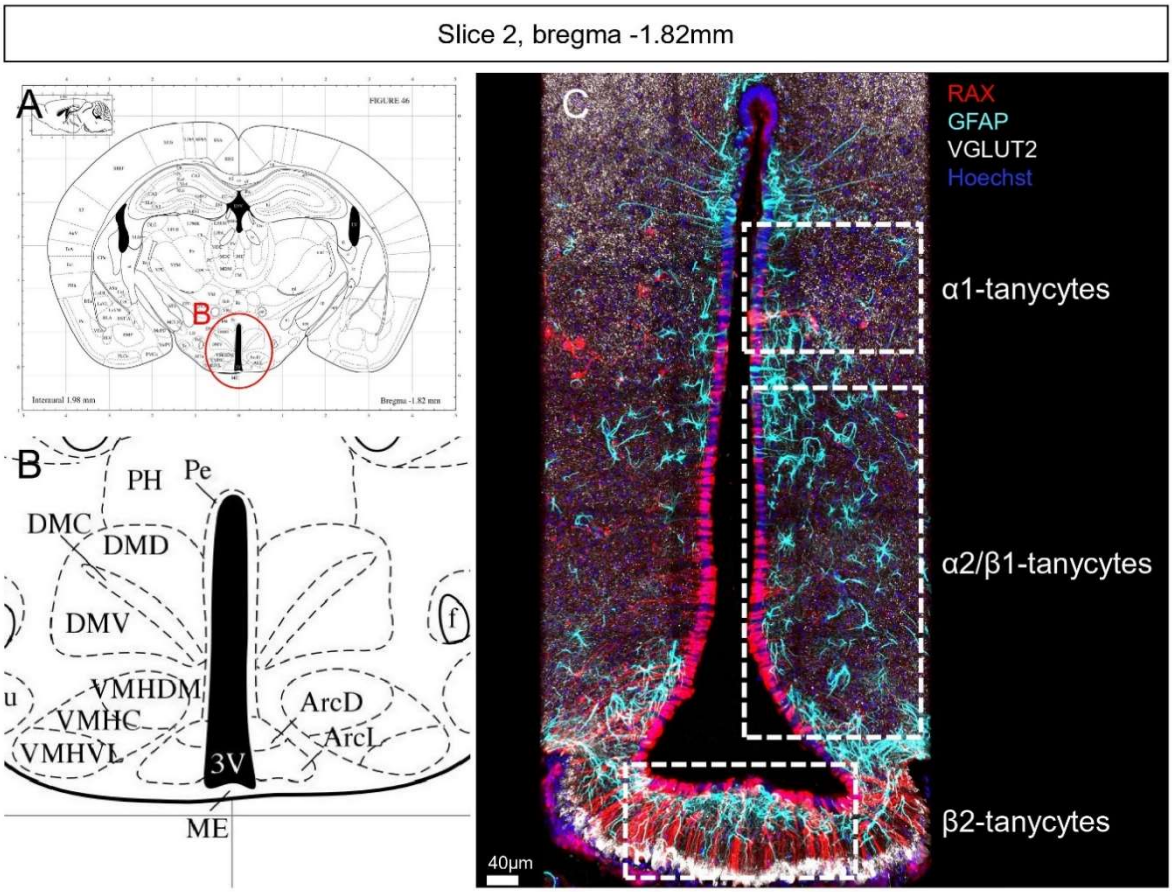

Figure 24 | Different tanycytic sub-populations found on slice 2

RAX (red), GFAP (cyan), VGLUT2 (white), Hoechst (blue)

A) theoretical localization of slice 2 in the mouse brain; B) theoretical locations of hypothalamic structures around the III-ventricle; C) 40x overview scan of slice 2, regions of analyzed sub-populations marked with bars Scale Bar=40µm

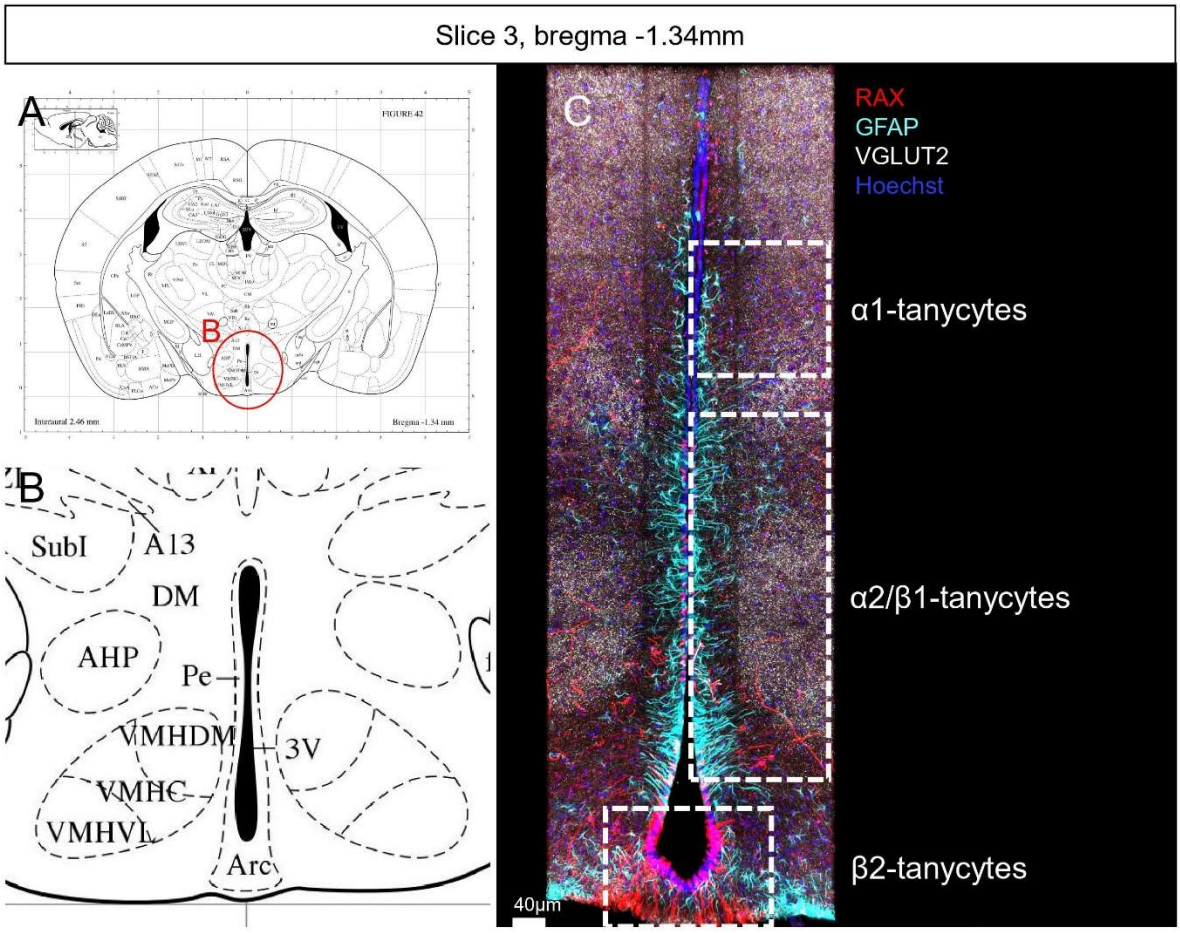

Figure 25 | Different tanycytic sub-populations found on slice 3

RAX (red), GFAP (cyan), VGLUT2 (white), Hoechst (blue)

A) theoretical localization of slice 2 in the mouse brain; B) theoretical locations of hypothalamic structures around the III-ventricle; C) 40x overview scan of slice 3, regions of analyzed sub-populations marked with bars Scale Bar=40µm

I performed a two-way ANOVA analysis to investigated differences between the 3 defined sub-populations detected on the same rostro-to-caudal location (same slice) as well as a multiple t-tests to uncover divergences between the same sub-population but detected on a different rostro-caudal position (different slice).

I uncovered, that there was no significant difference within the amount of excitatory VGLUT2+ synaptic inputs between α1-, α2/β1- and β2- tanycytes found at the same position alongside the rostro-to-caudal extension of the III-ventricle. In contrast, I observed a significate difference in the distribution of the inhibitory VGAT+ synaptic between α1- and β2- tanycytes with higher amounts of inputs onto α1-tanycytes compared to β2- tanycytes.

The results from the two-way ANOVA analysis and the post-hoc test applied are shown in *Figure 26* for either VGLUT2 (*A*) as well as for VGAT+ inputs (*B*). Values are presented as means and SEM, *p*-values are indicated and significant differences between individual positions are marked with an Asterix.

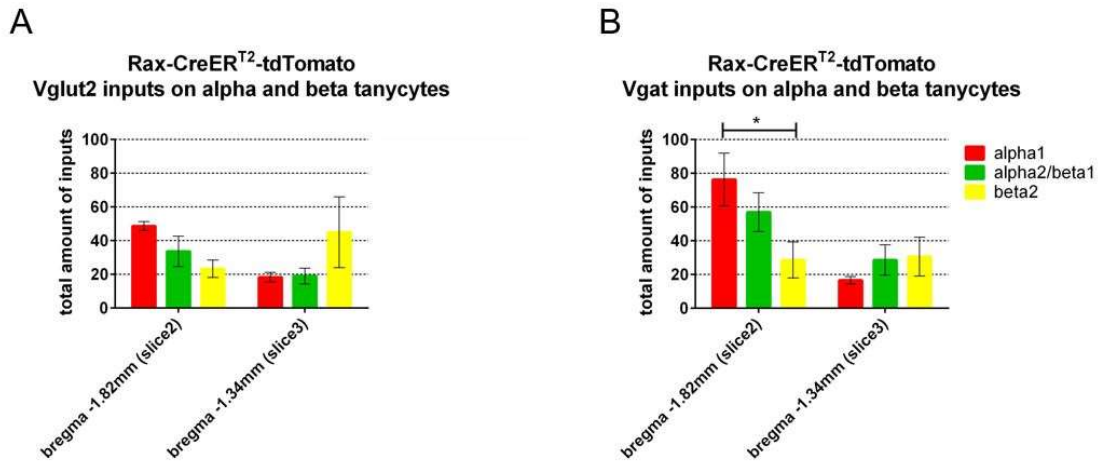

Figure 26 | Differences in synaptic inputs between individual subtypes found at the same rostro-caudal position

*Values presented as means and SEM, * $p < 0.05$*

A) Differences in VGLUT2+ inputs between tanycytic subtypes found at the same slice; B) Differences in VGAT+ inputs between tanycytic subtypes found at the same

Subsequently, I analyzed the amount of neuronal inputs within the same subtype but on a different rostro-caudal position. I found a significant difference in the excitatory inputs amongst α1- tanycytes with higher numbers of inputs onto α1- tanycytes found at the region of the ME compared to more rostrally located cells. Respecting α2/β1- and β2- tanycytes I detected no significant difference.

Figure 27 represents conclusions from multiple t-test analysis regarding VGLUT2 (*A*) and VGAT+ inputs (*B*). The values are presented as means and SEM, *p*-values are indicated and significant differences between individual positions are marked with an Asterix.

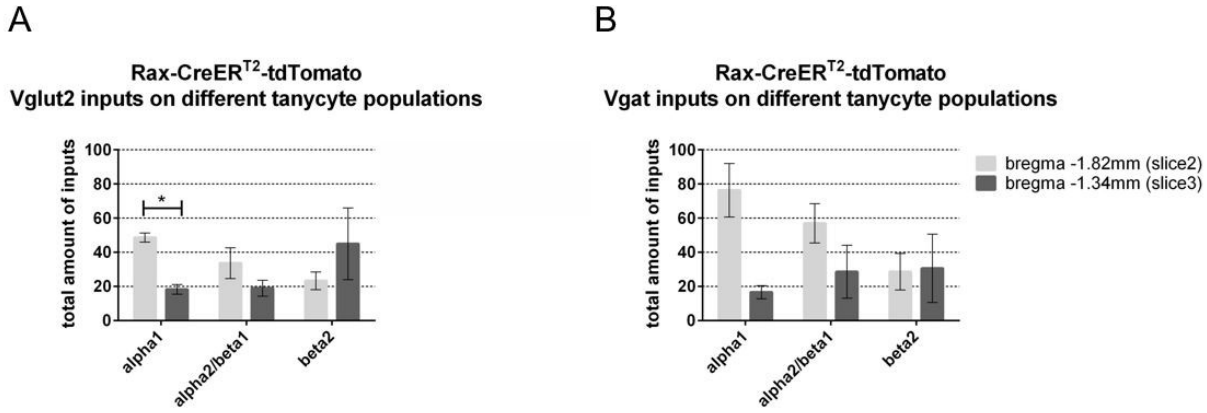

Figure 27 | Differences in synaptic inputs within one tanycytic subtype located at different rostro-caudal positions

*Values presented as means and SEM, * $p < 0.05$*

A) Differences in VGLUT2+ inputs between the same tanycytic subtypes found at the different slices; B) Differences in VGAT+ inputs between the same tanycytic subtypes found at the different slices

To be sure that the differences I detected were not biased by an uneven amount of reconstructed tanycytes at different positions I compared the total amounts of detected tanycytes amongst all positions considered for the analysis and found that there were no significant differences in numbers of detected cells.

To conclude, amounts of neuronal inputs significantly differ between α- and β- tanycytes arising at the lateral walls of the hypothalamic III-ventricle at the level of the ME and the ArcN. α1-tanycytes receive more excitatory synaptic inputs at caudal regions than α1- tanycytes at more rostral regions whereas inhibitory inputs occur cumulatively at ventrally located α1-tanycyte compared to more dorsally based β2- tanycytes.

3.7. Identification of tanycyte subtypes by different markers

In my experiments I applied various markers for immunolabeling of hypothalamic mouse sections to identify tanycytes located at the borders of the III-ventricle, namely Nestin, Vimentin and GFAP which all have been described as tanycytic markers (Bolborea & Dale, 2013; Lee et al., 2012; Robins et al., 2013; Rodríguez et al., 2005). For detailed description of antibodies used, see paragraph 2.6.2. Additionally, to further detected hypothalamic tanycyte, I used a tamoxifen-inducible RAX-Cre-ER^{T2}-tdTomato mouse model which drives tdTomato

expression specifically in tanycytes (Pak et al., 2014). Although all of these tanycyte-specific markers are well described in literature, their caudal-to-rostral distribution remains rather unclear considering that the majority of previous studies almost exclusively dealt with tanycytes located at the area of the ME and only monitored their dorso-to-ventral allocation. One study performed in 2017 by Mirzadeh et al. clearly identified the caudal-to-rostral hypothalamic territories occupied by tanycytes along the walls of the III-ventricle but only examined labeling of tanycytic processes by Nestin, Vimentin and GFAP and did not describe how single markers are distributed in a caudal-rostral orientation.

In my approach I considered the whole hypothalamic area of the III-ventricle such as it was possible to study characteristics of tanycytes distinguishable by their rostro-to-caudal location and further investigate if the tanycytic-markers I used in my experiments (Nestin, Vimentin, RAX and GFAP) are distributed equally or if there are any differences in their abundance across the entire tanycyte population which could emphasize the speculation of the existence of different tanycytic subpopulations. Some previous publications already postulated the existence of tanycytic subpopulations which do not correspond to classic separation into α- and β-tanycytes (Chen et al., 2017, Prevot at al. 2018). Moreover, I investigated if distinct subpopulations receive different amounts of synaptic inputs of excitatory and inhibitory neurons.

Consequently, I used reconstructed 63x confocal micrographs of position 1 to 13 and counted tanycytes labelled by the distinct markers, I annotated a tanycyte as being positive for a marker if cell soma and processes were showing the signal. I observed tanycytes being abundantly positive for Nestin at all investigated positions meaning that Nestin+ tanycytes are present across the whole caudal-to-rostral extension of the hypothalamic III-ventricle. This applies for Vimentin+ tanycytes as well, although there were invariably less cells detected due to a worse fluorescent signal. In contrast to Nestin and Vimentin, RAX signal showed a different distribution pattern. I detected the majority of RAX+ tanycytes at more caudal positions which correspond to the hypothalamic areas of the DMH and VMH, the ArcN as well as the ME (positions ranging from 1 to 10). In contrast, GFAP+ tanycytes are located exactly oppositional meaning that at the rostral regions of the ArcN and the ME, I detected almost no RAX+ but mainly GFAP+ tanycytes. I further observed differences in the dorso-to-ventral patterning of RAX+ and GFAP+ tanycytes especially at level of the ArcN: RAX+ tanycytes were residing at the ventral parts of the III-ventricular walls whereas GFAP+ tanycytes were detected more dorsally.

The following *Figure 28* shows a quantified distribution of RAX+, Nestin+, Vimentin+ and GFAP+ tanycytes along the walls of the hypothalamic III-ventricle. The bar-graphs represent values as means and SEM, exact data can be found attached in the appendix. On the x-axis the different positions are blotted starting with the most caudal position 1 and ranging until the most rostral position 13.

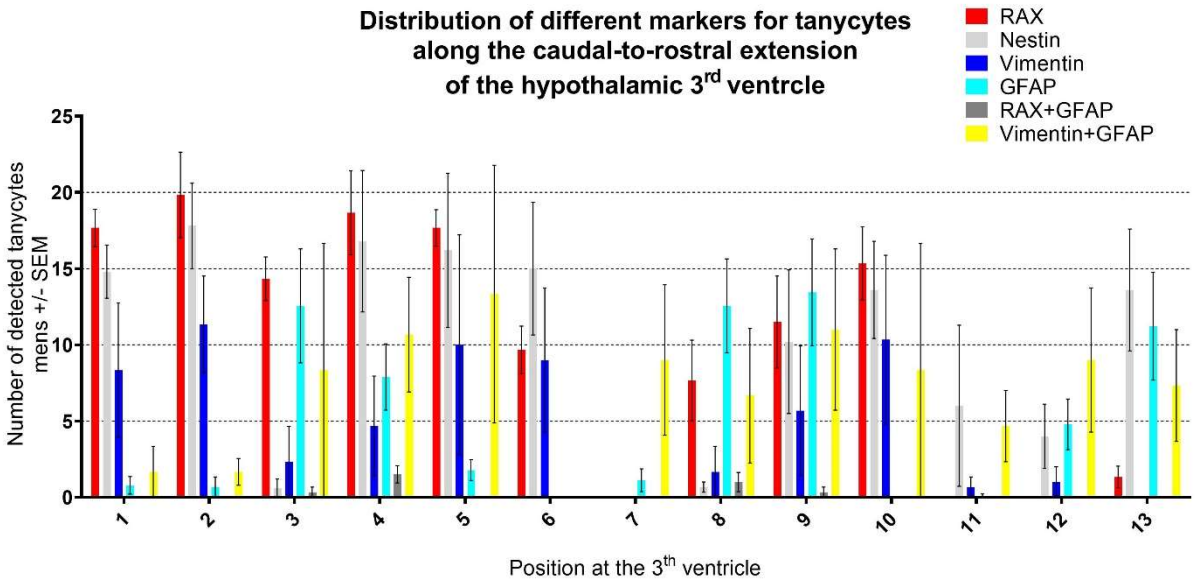

Figure 28 | Caudal-to-rostral distribution of different tanycytic markers across the borders of the hypothalamic III-ventricle
Values presented as means and SEM

Figure 29 gives an overview about the opposing distribution of RAX+ and GFAP+ tanycytes along the caudal-to-rostral extension of the III-ventricle.

Due to the 'Filament Tracer' tool provided by IMARIS, the precise reconstruction of individual RAX+ and GFAP+ tanycytic processes was possible even though they are tightly intertwined at the borders of the III-ventricle. (*A*) portrays a 40x overview scan of slice 2 approximate -1.82mm relative to bregma corresponding to the level of the DMH, VMH and ArcN, the white bar marks position 3. Here, the antagonistic location of ventral RAX+ tanycytes (red) and dorsal GFAP+ tanycytes (cyan) is demonstrated unambiguously. Although GFAP signal is visible at the ventral part of the ventricle these cells were not classified as tanycytes because they lack radial processes emerging into the hypothalamic parenchyma as well as their cell bodies are not residing at the ventricular borders facing the CSF. Due to their star-shaped morphology an astrocytic identity is suspected. Additionally, a small cohort of tanycytes showing both RAX and GFAP signal. (*B*) presents the distribution of tanycytes at a certain position being either RAX+/GFAP-, RAX-/GFAP+ or RAX+/GFAP+, values are shown in percentages. Starting

with the most caudal position where RAX+ tanycytes are detected exclusively RAX expression declines continuously towards more rostral locations where GFAP expression is detected more abundantly. Exact values used to constitute the graph can be found within the appendix. A table showing the orientation on slices and positions considered in this analysis is shown in (*C*).

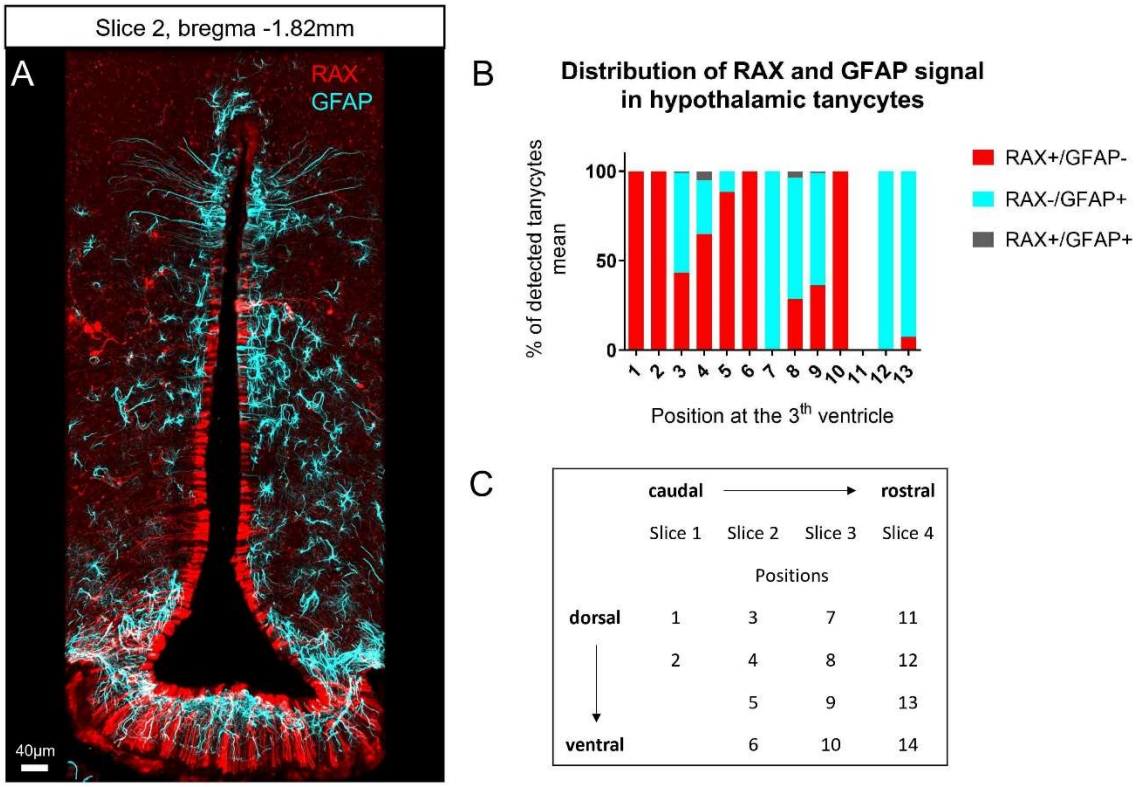

Figure 29 | Distribution of RAX+ and GFAP+ tanycytes around the area of the dorsomedial and ventromedial hypothalamus (slice 2)

RAX (red), GFAP (cyan)

Values are presented as means

A) 40x overview scan of slice 2, -1,82mm relative to bregma, Scale bar=40µm; B) % of detected tanycytes at position 1 to 13 being either RAX+/GFAP-, RAX-/GFAP+ or RAX+/GFAP; C) orientation on slices and positions considered in this analysis

Figure 30 (*A*) displays a 63x micrographs of tanycytes labeled by different markers at the area of the VMH (position 4). (*B*) shows the same hypothalamic location but with 3-dimensional reconstructions of RAX+ and GFAP+ tanycytes performed by using IMARIS. At this region RAX+ and GFAP+ subpopulations share the same territory and are tightly packed next to each other at the borders of the III-ventricle. Separation of individual processes corresponding to either RAX or GFAP signal was only possible by using the 'AutoDepth' mode of the 'Filament Tracer' tool provided by IMARIS. After the reconstruction and input detection, I applied a one-way ANOVA analysis and detected non-significant less inputs in GFAP+ tanycytes compared to RAX+ tanycytes. A possible explanation for this could be, that overall less GFAP+ tanycytes

were detected which biased the result. An increased sample size would be necessary to further monitor this observation.

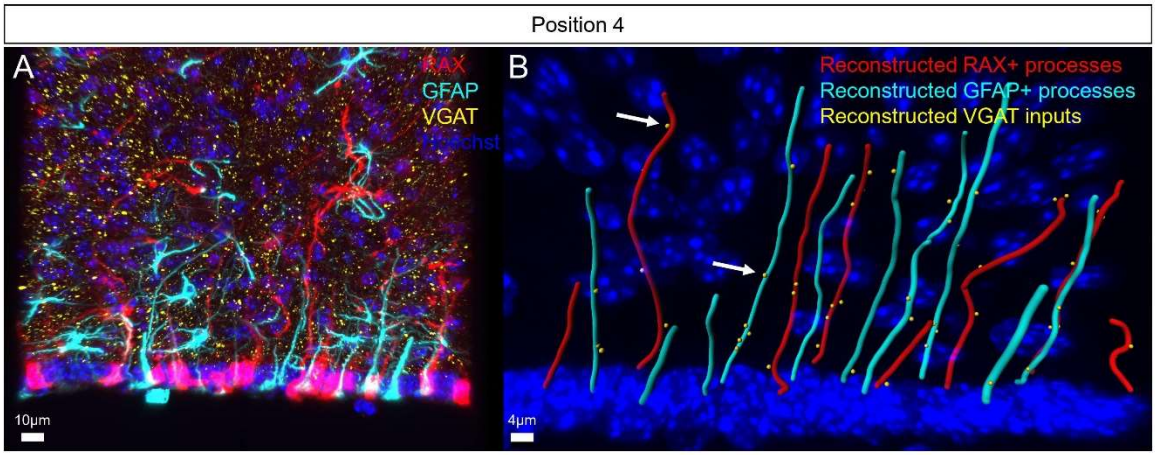

Figure 30 | Inhibitory VGAT+ inputs onto RAX+ and GFPA+ tanycytic processes at the area of the VMH (position4)

RAX (red), GFAP (cyan), VGAT (yellow), Hoechst (blue
Reconstructed RAX+ processes (red), reconstructed GFAP+ process (cyan), reconstructed VGAT+ inputs closer than <0.8µm to tanycytic processes (yellow)
Arrows point towards inhibitory neuronal VGAT input
A) 63x confocal z-stack image, B) reconstructions of tanycytic processes and synaptic inputs
Scale bars=10µm and 4µm

In conclusion, the findings of this analysis reveal that tanycytes can be distinguished by different markers which could point towards the existence of various tanycytic sub-populations which might be able to exhibit distinct functions necessary for a variety of signaling pathways.

3.8. Summary

The presented study constitutes the first 3-dimensional reconstruction of tanycytes located at the borders of the rostro-caudal extension of the III-ventricle. I established a suitable reconstruction pipeline by using the 'Filament Tracer' tool provided by IMARIS leading to a realistic and reliable reconstitution of tanycytic processes.

Moreover, I confirmed my hypothesis that hypothalamic tanycytes receive synaptic inputs from adjacent neurons. At all positions alongside the III-ventricular walls that I investigated, tanycytes get synaptic innervations from both excitatory as well as inhibitory neurons with a slight overall trend towards higher amounts of inputs at caudal regions where some main hypothalamic nuclei can be found like the DMH, the VMH, the ArcN and the ME. Interestingly, my results demonstrate that not all tanycytes get inputs but only a fraction of the total amount of reconstructed and analyzed cells are targeted by neurons.

Concerning inhibitory VGAT+ inputs, I detected higher amounts onto α1- compared to β2-tanycytes. Regarding excitatory VGLUT2+ inputs, I observed higher amounts onto α1-tanycytes located at caudal regions of the ME compared to more rostrally located α1-tanycytes. Due to the use of different markers to locate tanycytic territories at the borders of the III-ventricle I revealed that RAX+ tanycytes reside at more caudal hypothalamic areas whereas the more rostral regions are almost exclusively occupied by GFAP+ tanycytes. This finding points towards the existence of different, so far undescribed subpopulations and emphasized the need of a renewal of the classic separation of tanycytes into α- and β-tanycytic subtypes.

4. Discussion

Collectively, my study is a quantitative demonstration revealing that tanycytes receiving synaptic inputs from adjacent neurons in the hypothalamic area of the III-ventricle. The effect of these synaptic contacts could be similar to a mechanism described by Alpár et al. in 2018. Ependymocytes lining the border of the III-ventricle receive VGLUT2+ innervations from CRH releasing neurons which induces CNTF liberation by ependymocytes into the CSF. As ependymocytes and tanycytes share similar or even overlapping territories at the III-ventricular walls, the speculation about the same mechanism existing in tanycytes is tempting. Measuring membrane potentials of tanycytes by using patch-clamp electrophysiology could be one attempt to investigate this hypothesis further.

The involvement of tanycytes in synaptic signal transmission becomes further apparent by considering the results of two RNA-seq studies published in 2017. Campbell et al. performed a Drop-seq analysis exploring the gene expression profile of over 20 000 single cells from and around the hypothalamic ArcN and ME area in mice and detected more than 30 different non-neuronal cell populations with specific markers for individual cell types including tanycytes. Enriched gene transcripts in α1-tanycytes are amongst others the solute carrier family 1 member 2 (*Slc1a2*) and solute carrier family 17 member 18 (*Slc17a8*), both executing important functions in synaptic signaling. *Slc1a2* encodes a membrane-bound transporter protein, also known as the excitatory amino acid transporter 2 (EAAT2), which removes glutamate form the extracellular space to terminate excitatory signal transmission, avoid hyperexcitability of synapses and inhibit excitotoxicity (Takahashi, Foster, & Lin, 2015). *Slc17a8* encodes the vesicular glutamate transporter 3 (VGLUT3) which promotes glutamate uptake by synaptic vesicles before its release into the synaptic gap showing similar transport characteristics as two other isoforms of glutamate transporters, VGLUT1 and VGLUT2 (Takamori et al., 2002). Regarding α2-tanycytes, a high level of transcripts of the solute carrier family 7 member 11 (*Slc7a11*) was detected. SLC7a11 is part of the heteromeric amino acid antiporter system x_c^- (Sx_c^-) which controls the exchange of extracellular cystine and intracellular glutamate. Within the brain, glutamate efflux serves as a non-vesicular excitatory signaling mechanism contributing to synaptic organization, neurotransmitter release and other CNS processes. (Bridges, Natale, & Patel, 2012). Amongst enriched β1-tanycyte transcripts the glutamate ionotropic receptor AMPA type subunit 2 (*Gria2*) was detected. GRIA2 otherwise known as GluA2 is the predominate subunit of the AMPA receptor in the CNS. At synapses, ligand-gated AMPA receptors mediate postsynaptic excitatory currents and are regarded as the fastest responders to neurotransmission through glutamate (Qneibi et al., 2019; Schwenk et al., 2014).

Subsequently, β2-tanycyte showed elevated degrees of the sodium voltage-gated channel alpha subunit 7 (*Scn7a*) transcript which encodes a Na^+-channel protein. Na^+-channels play a crucial role in membrane depolymerization during action potentials in neurons and thus are essential for nerve conduction (Greenstein & Greenstein, 2000). Additionally, a second single-cell RNA-seq investigation detected the enrichment of similar transcripts in tanycytes, namely *Slc17a8* and *Scn7a*. Furthermore, the authors suggest the participation of tanycytes in the modulation of synaptic transmission due to their genetic profile analyzed by a gene ontology term enrichment (GO) analysis (Chen et al., 2017). These findings not only indicate that tanycytes express important proteins necessary for synaptic signaling processes but also empathize the need of a revision of the classic α- and β-subtype classification on a molecular basis due to the detection of highly subtype-specific markers.

Although the results of Campbell et al. and Chen et al., clearly point towards a connection between tanycytes and neurons through synaptic communication, the neuronal subtypes which contact tanycytes still need to be elucidated. Surrounded by a variety of different hypothalamic nuclei the possible candidates targeting tanycytes range from TRH to SST and GnRH neurons just mentioning a few (Müller-Fielitz et al., 2017; Prevot et al., 2010; Rodríguez et al., 2005). My study provides evidence that CRH containing neurons communicate with Vimentin+ tanycytes due to detected CRH punctae in close apposition to tanycytic processes at the rostro-caudal extension of the hypothalamic III-ventricle. If the innervation by CRH+ neurons leads to the release of CNTF by tanycytes, like it was observed in ependymocytes (Alpár et al., 2018), remains to be examined. Besides CRH, I observed TH neuronal terminals at the same territories as tanycytes at the area of the ME during an immunohistochemical staining of coronal hypothalamic brain sections of a RAX-Cre-ER^{T2}-tdTomato mouse (see *Figure 31*). Immunohistochemical approaches using antibodies against other neurotransmitters, neuropeptides and neurohormones should be included in future studies to unmask the synaptoid communication pathways between neurons and tanycytes in the hypothalamic III-ventricular region.

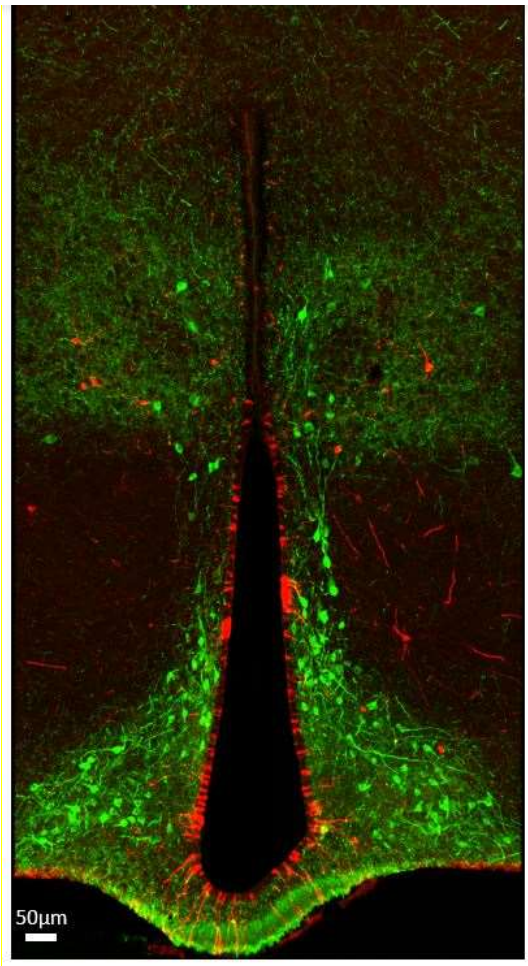

Figure 31 | TH+ neuronal terminals in close proximity to RAX+ tanycytic processes at the area of the ME
TH (green), RAX (red)
Scale bare=50µm

Even though my data provide proof that tanycytes are targeted by neurons, surprisingly not all tanycytes receive synaptic innervation. In accordance with this notion, Alpár et al. reports that just a small fraction of ependymocytes get VGLUT2+ inputs. Notably, ependymocytes residing at the III-ventricular walls form an interconnected network via gap junctions which could allow them to respond in a synchronous way whereas just one cells was initially innervated. CNX43, a protein involved in the formation of gap junctions, is abundantly expressed in tanycytes and localized in their processes and cell bodies (Recabal et al. 2018; Szilvásy-Szabó et al. 2017), an observation which is in agreement with an immunohistochemical staining of a mouse Wild type brain section of the area of the VMH I performed. Like in ependymocytes, gap junctions could contribute to a widespread activation of neighboring tanycytes.

The location of tanycytes within in the brain is restricted to the borders of the III-ventricle in the tuberal and posterior hypothalamus (Robins et al., 2013), the same region I examined in this study. In contrast, a publication by Feng et al. in 2011 describes tanycytes at the walls of the

IV-ventricle at the area of the Locus ceruleus (LoC) in the chicken brain. Moreover, they claimed to have detected a mechanism by which Nerve Growth Factor (NGF) is taken up by β1- and β2-tanycytes residing at the ventricular walls facing the CSF. NGF is further transported through the tanycytic process and accumulates near axonal terminals of noradrenergic LoC neurons. These findings raise the question if other brain regions facing the CSF circulating inside the ventricular system harbor tanycytes and should be addressed urgently in further analysis.

One aspect which should not be underestimated is that female and male bodies differ in its hormonal constitutions and as tanycytes act as hormonal detectors and transporters (Balland et al., 2014; Müller-Fielitz et al., 2017) this could influence their communication with neurons. Especially the female menstrual cycle triggers morphologic changes in tanycytic processes that allow GnRH axonal terminals located at the ME to release their hormonal content into the blood stream during the preovulatory phase, whereas tanycytes normally engulf these terminals and inhibit direct contact of neurons to the fenestrated capillaries (Prevot et al., 2010). In my study I examined male mice, but inclusion of female animals needs to be considered in follow-up studies.

Furthermore, rearrangements of tanycytes organization is diet-dependent and consumption of a high far diet (HFD) induces changes in their linear distribution alongside the III-ventricular walls (Ramalho et al., 2018). Moreover, an HFD has an additionally effect: it significantly increases the neurogenic potential of β2-tanycytes located at the area of the ME in adult mice (Lee et al., 2012). The animals I used in the experiments performed were fed with standard laboratory chow so it would be interesting to explore numbers of synaptic inputs onto tanycytes in mice fed with HFD.

To conclude, this study demonstrates for the first time 3-dimensionally reconstructed hypothalamic brain sections showing tanycytic processes receiving excitatory and inhibitory synaptic innervations. The precise signaling pathways and mechanisms as well as the effects on stress responses, metabolism, reproductive behavior and other regulatory functions of the hypothalamus remain to be elucidated in the future.

References

Agnati, L. F., Zolli, M., Strömberg, I., & Fuxe, K. (1995). Intercellular Communication in the Brain: Wiring versus Volume Transmission. *Neuroscience*, *69*(3), 711–726.

Alberts, B., Johnson, A., Lewis, J., Morgan, D., Raff, M., Robert, K., & Walter, P. (2015). Channels and the Electrical Properties of Membranes. In *The Molecular Biology of the Cell* (Sixth Edit, pp. 611–640). New York: Garland Science.

Alpár, A., Zahola, P., Hanics, J., Hevesi, Z., Korchynska, S., Benevento, M., … Romanov, R. A. (2018). Hypothalamic CNTF volume transmission shapes cortical noradrenergic excitability upon acute stress. *The EMBO Journal*, *37*(21), 1–23. https://doi.org/10.15252/embj.2018100087

Armstrong, W. E. (2015). Hypothalamic Supraoptic and Paraventricular Nuclei. In *The Rat Nervous System* (Fourth Edi, pp. 295–314). Elsevier Inc.

Ausubel, F. M., Brent, R., Kingston, R. E., Moore, D. D., Seidmann, J. G., Smith, J. A., & Struhl, K. (2003). *Current Protocols in Molecular Biology* (Ringbou Ed). John Wiley & Sons, Inc.

Balland, E., Dam, J., Langlet, F., Caron, E., Steculorum, S., Messina, A., … Prévot, V. (2014). Hypothalamic tanycytes are an ERK-gated conduit for leptin into the brain. *Cell Metabolism*, *19*(2), 293–301. https://doi.org/10.1016/j.cmet.2013.12.015

Bolborea, M., & Dale, N. (2013). Hypothalamic tanycytes : potential roles in the control of feeding and energy balance. *Trends in Neurosciences*, *36*(2), 91–100. https://doi.org/10.1016/j.tins.2012.12.008

Bridges, R. J., Natale, N. R., & Patel, S. A. (2012). System x c - cystine / glutamate antiporter : an update on molecular pharmacology and roles within the CNS. *British Journal of Pharmacology*, *165*(1), 20–34. https://doi.org/10.1111/j.1476-5381.2011.01480.x

Campbell, J. N., Macosko, E. Z., Fenselau, H., Pers, T. H., Lyubetskaya, A., Tenen, D., … Tsai, L. (2017). A Molecular Census of Arcuate Hypothalamus and Median Eminence Cell Types. *Nature Neuroscience*, *20*(3), 484–496. https://doi.org/10.1038/nn.4495.A

Canteras, N. S. (2012). Hypothalamic Goal-directed Behavior -Ingestive, Reproductive and Defensive. In C. Watson, G. Paxino, & L. Puelles (Eds.), *The Mouse Nervous System* (pp. 539–562). Academic Press. https://doi.org/10.1016/B978-0-12-369497-3.10020-2

Carmichael, J. D., & Braunstein, G. D. (2009). Diseases of Hypothalamic Origin. In *Hormones, Brain and Behavior* (Second Edi, pp. 3005–3048).

Challa, A. A., & Stefanovic, B. (2011). A Novel Role of Vimentin Filaments : Binding and

Stabilization of Collagen mRNAs □. *Molecular and Cellular Biology*, *31*(18), 3773–3789. https://doi.org/10.1128/MCB.05263-11

Chaudhry, F. A., Reimer, R. J., Bellocchio, E. E., Danbolt, N. C., Osen, K. K., Edwards, R. H., & Storm-mathisen, J. (1998). The Vesicular GABA Transporter , VGAT , Localizes to Synaptic Vesicles in Sets of Glycinergic as Well as GABAergic Neurons. *The Journal of Neuroscience*, *18*(23), 9733–9750.

Chen, R., Wu, X., Jiang, L., & Zhang, Y. (2017). Single-Cell RNA-Seq Reveals Hypothalamic Cell Resource Hypothalamic Cell Diversity. *Cell Reports*, *18*(13), 3227–3241. https://doi.org/10.1016/j.celrep.2017.03.004

Cho, A., Haruyama, N., & Kulkarni, A. (2009). Generation of Transgenic Mice. *Current Protocols in Cell Biology*. https://doi.org/10.1002/0471143030.cb1911s42.Generation

Clasadonte, J., & Prevot, V. (2017). The special relationship : glia – neuron interactions in the neuroendocrine hypothalamus. *Nature Publishing Group*, *14*(1), 25–44. https://doi.org/10.1038/nrendo.2017.124

Corbett, J. J., & Haines, D. E. (2018). The Ventricles, Choroid Plexus, and Cerebrospinal Fluid. In *Fundamental Neuroscience for Basic and Clinical Applications* (pp. 93–106). Elsevier Inc. https://doi.org/10.1016/B978-0-323-39632-5.00006-2

Elizondo-Vega, R., Cortes-Campos, C., Barahona, M. J., Oyarce, K. A., Carril, C. A., & García-Robles, M. A. (2015). The role of tanycytes in hypothalamic glucosensing Morphological characteristics of the hypothalamic region. *J. Cell. Mol. Med*, *19*(7), 1471–1482. https://doi.org/10.1111/jcmm.12590

Felten, D. L., O'Banion, M. K., & Maida, M. S. (2016). Autonomic-Hypothalamic-Limbic Systems. In *Netter's Atlas of Neuroscience* (pp. 421–461). Elsevier Inc.

Feng, C.-Y., Wiggins, L. M., & von Bartheld, C. S. (2011). The Locus Ceruleus Responds to Signaling Molecules Obtained from the CSF by Transfer through Tanycytes. *The Journal of Neuroscience*, *31*(25), 9147–9158. https://doi.org/10.1523/JNEUROSCI.5018-10.2011

Franklin, K. B. J. (1997). *The Mouse Brain in Stereotaxic Coordinates* (second edi). Academic Press.

Garibya, L., & Avashia, N. (2014). Research Techniques Made Simple: Polymerase Chain Reaction (PCR). *J Invest Dermatol.*, *133*(3), 1–8. https://doi.org/10.1038/jid.2013.1.Research

Goldstein, M., & Watkins, S. (2008). Immunohistochemistry. In *Current Protocols in Molecular Biology* (pp. 1–23). https://doi.org/10.1002/0471142727.mb1406s81

Goodman, T., & Hajihosseini, M. K. (2015). Hypothalamic tanycytes — masters and servants of metabolic, neuroendocrine, and neurogenic functions. *Frontiers in Neuroscience*, *9*(October), 1–9. https://doi.org/10.3389/fnins.2015.00387

Greenstein, B., & Greenstein, A. (2000). *Color Atlas of Neuroscience*. Stuttgart, New York: Thieme.

Güldner, F.-H., & Wolff, J. R. (1973). Neurono-glial synaptoid contacts in the median emincen of the rat: ultrastructure, staining properties and distribution on tanycytes. *Brain Research*, *61*, 217–234.

Gundersen, V., Storm-Mathisen, J., & Bergersen, L. H. (2015). Neuroglial Transmission. *Physiological Reviews*, *95*(3), 695–726. https://doi.org/10.1152/physrev.00024.2014

Henning, J. (2001). Hypothalamus. In *International Encyclopedia of the Social and Behavioral Science* (pp. 7112–7118). Elsevier Ltd.

Hofman, M. A., & Swaab, D. F. (2004). Neuroplasticity in the human hypothalamus during ageing. In R. H. Straub & E. Mocchegiani (Eds.), *NeuroImmune Biology* (Vol. 4, pp. 105–121). Elsevier B.V. https://doi.org/10.1016/S1567-7443(04)80009-7

Hofmann, K., Lamberz, C., Piotrowitz, K., Offermann, N., But, D., Scheller, A., … Kuerschner, L. (2017). Tanycytes and a Differential Fatty Acid Metabolism in the Hypothalamus. *Glia*, *65*(2), 231–249. https://doi.org/10.1002/glia.23088

Horstmann, E. (1954). Die Faserglia des Selachiergehirns. *Zeitschrift Für Zellforschung*, *39*, 588–617.

Kumar, T. R., Larson, M., Wang, H., McDermott, J., & Bronshteyn, I. (2009). Transgenic Mouse Technology: Principles and Methods. *Methds Mol Biol.*, *590*, 335–362. https://doi.org/10.1007/978-1-60327-378-7

Langlet, F., Mullier, A., Bouret, S. G., Prevot, V., & Dehouck, B. (2013). Tanycyte-Like Cells Form a Blood – Cerebrospinal Fluid Barrier in the Circumventricular Organs of the Mouse Brain. *The Journal of Comparative Neurology | Research in Systems Neuroscience*, *521*(15), 3389–3405. https://doi.org/10.1002/cne.23355

Lee, D. A., Bedont, J. L., Pak, T., Wang, H., Song, J., Miranda-angulo, A., … Blackshaw, S. (2012). Tanycytes of the hypothalamic median eminence form a diet- responsive neurogenic niche. *Nature Neuroscience*, *15*(5), 700–702. https://doi.org/10.1038/nn.3079

Li, S., Peng, L. C. X., Wang, C., Dan, B. Q., Hua, C. H., Ren, Y. X., … Zhou, X. (2018). Overview of the reporter genes and reporter mouse models. *Animal Models and Experimental Medicin*, *1*(1), 29–35. https://doi.org/10.1002/ame2.12008

Maggi, R., Zasso, J., & Conti, L. (2015). Neurodevelopmental origin and adult neurogenesis

of the neuroendocrine hypothalamus. *Frontiers in Cellular Neuroscience*, *8*, 1–7. https://doi.org/10.3389/fncel.2014.00440

Meunier, A., Sawamoto, K., & Spassky, N. (2013). Ependyma, Choroid. In *Patterning and Cell Type Specification in Developing CNS and PNS: Comprehensive Developmental Neuroscience* (Vol. 1, pp. 819–833). Elsevier Science. https://doi.org/10.1016/B978-0-12-397265-1.00024-1

Miranda-Angulo, A. L., Byerly, M. S., Mesa, J., Wang, H., & Blackshaw, S. (2015). Rax regulates hypothalamic tanycyte differentiation and barrier function in mice. *J Comp Neurol.*, *522*(4), 876–899. https://doi.org/10.1002/cne.23451.Rax

Mirzadeh, Z., Kusne, Y., Duran-moreno, M., Cabrales, E., Gil-perotin, S., Ortiz, C., … Alvarez-buylla, A. (2017). Bi- and uniciliated ependymal cells define continuous floor-plate-derived tanycytic territories. *Nature Communications*, *8*, 1–12. https://doi.org/10.1038/ncomms13759

Müller-Fielitz, H., Stahr, M., Bernau, M., Richter, M., Abele, S., Krajka, V., … Schwaninger, M. (2017). Tanycytes control the hormonal output of the hypothalamic-pituitary-thyroid axis. *Nature Communications*, *8*(481), 1–13. https://doi.org/10.1038/s41467-017-00604-6

Mullier, A., Bouret, S. G., Prevot, V., & Dehouck, B. (2010). Differential Distribution of Tight Junction Proteins Suggests a Role for Tanycytes in Blood-Hypothalamus Barrier Regulation in the Adult Mouse Brain. *The Journal of Comparative Neurology | Research in Systems Neuroscience*, *581*(7), 943–962. https://doi.org/10.1002/cne.22273

Mullis, K. B. (1990). The unusual origin of the polymerade chain reaction. *Scientific American*, *262*(4), 56–61.

Orquera, D. P., Nasif, S., Low, M. J., Rubinstein, M., Souza, J. De, Physiology, I., & Arbor, A. (2017). Essential function of the transcription factor Rax in early patterning of the mammalian hypothalamus. *Dev Biol.*, *416*(1), 212–224. https://doi.org/10.1016/j.ydbio.2016.05.021.Essential

Paddock, S. W. (2000). Principles and Practices of Laser Scanning Confocal Microscopy. *Molecular Biotechnology*, *16*(2), 127–149.

Pak, T., Yoo, S., Miranda-angulo, A. M., Wang, H., & Blackshaw, S. (2014). Rax-CreERT2 Knock-In Mice: A Tool for Selective and Conditional Gene Deletion in Progenitor Cells and Radial Glia of the Retina and Hypothalamus. *PLoS ONE*, *9*(4), 1–13. https://doi.org/10.1371/journal.pone.0090381

Prevot, V., Bellefontaine, N., Baroncini, M., Sharif, A., Hanchate, N. K., Parkash, J., … de

Seranno, S. (2010). Gonadotrophin-releasing hormone nerve terminals, tanycytes and neurohaemal junction remodelling in the adult median eminence: Functional consequences for reproduction and dynamic role of vascular endothelial cells. *Journal of Neuroendocrinology*, *22*(7), 639–649. https://doi.org/10.1111/j.1365-2826.2010.02033.x

Prevot, Vincent, Dehouck, B., Sharif, A., Coifi, P., Giacobini, P., & Clasadonte, J. (2018). The Versatile Tanycyte : A Hypothalamic Integrator of Reproduction and Energy Metabolism. *Endocrine Reviews*, *39*(3), 333–368. https://doi.org/10.1210/er.2017-00235

Prevot, Vincent, Sharif, A., Giacobini, P., & Clasadonte, J. (2018). The Versatile Tanycyte : A Hypothalamic Integrator of Reproduction and Energy Metabolism. *Endocrine Reviews*, *39*(3), 333–368. https://doi.org/10.1210/er.2017-00235

Purves, D., Agustine, G. J., Fitzpatrick, D., Hall, W. C., LaMantia, A.-S., McNamara, J. O., & Wiliams, S. M. (2004). *Neuroscience* (Third Edit). Sinauer Associates, Inc.

Qneibi, M., Hamed, O., Natsheh, A., Fares, O., Jaradat, N., Emwas, N., … Al-Kerm, R. (2019). Inhibition and assessment of the biophysical gating properties of GluA2 and GluA2 / A3 AMPA receptors using curcumin derivatives. *PLoS ONE*, *14*(8), 1–15. https://doi.org/10.1371/journal.pone.0221132

Raikwar, S. P., Bhagavan, S. M., Ramaswamy, S. B., Thangavel, R., Dubova, I., Selvakumar, G. P., … Zaheer, A. (2018). Are Tanycytes the Missing Link Between Type 2 Diabetes and Alzheimer's Disease? *Molecular Neurobiology*, *56*(2), 833–843. https://doi.org/10.1007/s12035-018-1123-8

Ramalho, A. F., Bombassaro, B., Dragano, N. R., Solon, C., Morari, J., Fioravante, M., … Araujo, E. P. (2018). Dietary fats promote functional and structural changes in the median eminence blood / spinal fluid interface — the protective role for BDNF. *Journal of Neuroinflammation*, *15*(1), 1–18. https://doi.org/10.1186/s12974-017-1046-8

Recabal, A., Elizondo-vega, R., Philippot, C., Salgado, M., López, S., Palma, A., … Angeles, M. (2018). Connexin-43 Gap Junctions Are Responsible for the Hypothalamic Tanycyte-Coupled Network. *Frontiers in Cellular Neuroscience*, *12*(November), 1–15. https://doi.org/10.3389/fncel.2018.00406

Rizzoti, K., & Lovell-badge, R. (2017). Pivotal role of median eminence tanycytes for hypothalamic function and neurogenesis. *Molecular and Cellular Endocrinology*, *445*, 7–13. https://doi.org/10.1016/j.mce.2016.08.020

Robins, S. C., Steward, I., McNay, D. E., Taylor, V., Giachio, C., Goetz, M., … Placzek, M. (2013). Alpha-Tanycytes of the adult hypothalamic third ventricle include distinct populations of FGF-responsive neural progenitors. *Nature Communications*, *4*(May), 1–

13. https://doi.org/10.1038/ncomms3049

Rodríguez, E., Guerra, M., Peruzzo, B., & Blázquez, J. L. (2019). Tanycytes : A rich morphological history to underpin future molecular and physiological investigations. *Journal of Neuroendocrinology*, *31*, 1–29. https://doi.org/10.1111/jne.12690

Rodríguez, E. M., Blázquez, J. L., Pastor, F. E., Peláez, B., Pena, P., Peruzzo, B., & Amat, P. (2005). Hypothalamic Tanycytes : A Key Component of Brain – Endocrine Interaction. *International Review of Cytology*, *247*(5), 89–164. https://doi.org/10.1016/S0074-7696(05)47003-5

Salvatierra, J., Lee, X. D. A., Zibetti, C., Duran-moreno, M., Yoo, X. S., Newman, E. A., … Blackshaw, S. (2014). The LIM Homeodomain Factor Lhx2 Is Required for Hypothalamic Tanycyte Specification and Differentiation. *The Journal of Neuroscience*, *34*(50), 16809–16820. https://doi.org/10.1523/JNEUROSCI.1711-14.2014

Sapper, C. B., & Stornetta, R. L. (2015). *Central Autonomic System*. *The Rat Nervous System* (Fourth Edi). Elsevier Inc. https://doi.org/10.1016/B978-0-12-374245-2.00023-1

Sapper, C. B., & Lowell, B. B. (2014). The Hypothalamus. *Currenty Biology*, *24*(23), 1111–1116. https://doi.org/10.1016/B978-0-323-39632-5.00030-X

Schneider, L. (2017). Anatomy and Physiology of Normal Sleep. In M. G. Migilis (Ed.), *Sleep and Neurologic Disease* (pp. 1–28). Academic Press. https://doi.org/10.1016/B978-0-12-804074-4.00001-7.

Schwenk, J., Baehrens, D., Haupt, A., Bildl, W., Boudkkazi, S., & Roeper, J. (2014). Regional Diversity and Developmental Dynamics of the AMPA-Receptor Proteome in the Mammalian Brain. *Neuron*, *84*(1), 41–54. https://doi.org/10.1016/j.neuron.2014.08.044

Scott, D. E., & Paull, W. K. (1979). The Tanycyte of the Rat Median Eminence. *Cell and Tissue Research*, *200*(2), 329–334.

Swaab, D. F. (2004). Neuropeptides in Hypothalamic Neuronal Disorders. *International Review of Cytology*, *240*(SPEC.ISS.), 305–375. https://doi.org/10.1016/S0074-7696(04)40003-5

Szilvásy-Szabó, A., Varga, E., Beliczai, Z., Lechan, R. M., & Fekete, C. (2017). Localization of connexin 43 gap junctions and hemichannels in tanycytes of adult mice. *Brain Research*, *1673*, 64–71. https://doi.org/10.1016/j.brainres.2017.08.010

Takahashi, K., Foster, J. B., & Lin, C. G. (2015). Glutamate transporter EAAT2 : regulation , function , and potential as a therapeutic target for neurological and psychiatric disease. *Cell. Mol. Life Sci.*, *72*(18), 3489–3506. https://doi.org/10.1007/s00018-015-1937-8

Takamori, S., Malherbe, P., Broger, C., & Jahn, R. (2002). Molecular cloning and functional characterization of human vesicular glutamate transporter 3. *EMBO Reports*, *3*(8), 798–803.

Vann, S. D., & Aggleton, J. P. (2004). The mammillary bodies: Two memory systems in one? *Nature Reviews Neuroscience*, *5*(1), 35–44. https://doi.org/10.1038/nrn1299

Wittkowski, W. (1967). Synaptische Strukturen und Elementargranula in der Neurohypophyse des Meerschweinchens. *Zeitschrift Für Zellforschung*, *82*, 434–458.

Yin, W., & Gore, A. C. (2010). The Hypothalamic Median Eminence and its Role in Reproductive Aging. *Annals of the New York Academy of Sciences*, *1204*, 113–122. https://doi.org/10.1111/j.1749-6632.2010.05518.x.The

Yin, W., Sun, Z., Mendenhall, J. M., Walker, D. M., Riha, P. D., Bezner, K. S., & Gore, A. C. (2015). Expression of Vesicular Glutamate Transporter 2 (vGluT2) on Large Dense-Core Vesicles within GnRH Neuroterminals of Aging Female Rats. *PLoS ONE*, *10*(6), 1–20. https://doi.org/10.1371/journal.pone.0129633

Zhang, J., Zhao, J., Jiang, W., Shan, X., Yang, X., & Gao, J. (2012). Conditional gene manipulation: Cre-ating a new biological era. *Journal of Zheijang University - Science B (Biomedicine & Biotechnology)*, *13*(7), 511–524. https://doi.org/10.1631/jzus.B1200042

Appendix

Zusammenfassung **80**

Theoretical localization of selected and analyzed coronal mouse brain sections 82

Gallery of 20x and 40x overview scans of analyzed animals 84

Figure 13 – Values for reconstruction of tanycytic soma and process executed by using the 'Surface Reconstruction' tool 89

Figure 21 – Amount of reconstructed tanycytic processes, tanycytes receiving synaptic inputs and total amount of synaptic inputs in all analyzed mouse lines 93

Figure 22 – Percentage of tanycytes receiving or not receiving synaptic inputs in all analyzed mouse lines 96

Figure 23 – Differences between the amount of synaptic inputs across all positions examined alongside the walls of the hypothalamic III-ventricle 99

Figure 26 – Differences in synaptic inputs between individual subtypes found at the same rostro-caudal position 111

Figure 27 – Differences in synaptic inputs within one tanycytic subtype located at distinct site 113

Figure 28 – Caudal-to-rostral distribution of different tanycytic markers across the borders of the hypothalamic III-ventricle 114

Figure 29 – Percentage of detected tanycytes at position 1 to 13 being either RAX+/GFAP-, RAX-/GFAP+ or RAX+/GFAP+ 116

Zusammenfassung

Im Bereich der mittleren Kerngruppe des Hypothalamus findet man einen besonderen, hoch spezialisierten Zelltyp: den Tanyzyt. Tanyzyten zählen zu den Ependymzellen und teilen mit diesen auch ähnliche Territorien entlang des 3. Ventrikels. Mit ihren zylindrischen Zellkörpern kleiden sie Teile des 3. Ventrikels aus, in welchem die Cerebrospinalflüssigkeit kontinuierlich zirkuliert. Die auffallendste morphologische Eigenschaft der Tanyzyten ist ihr langer, radialer Fortsatz der tief in das umliegende Parenchym empordringt und mit den Kapillaren des Hypothalamus-Hypophysen-Pfortader-Systems Kontakte ausbildet. Aufgrund dieser einzigartigen Morphologie und der vorteilhaften Lage nimmt man an, dass Tanyzyten den Austausch von Hormonen und anderen biologisch aktiven Substanzen zwischen der CSF und dem Blutsystem regulieren. Sie werden weiters als wichtige Elemente bzw. Modulatoren von zentralen Aufgaben des Hypothalamus erachtet. Darüber hinaus wird vermutet, dass Tanyzyten sogenannte ‚synaptische Neuron-Glia Kontakte' mit neurosekretorischen Axonen im Bereich der Eminentia mediana ausbilden. Durch die Detektion und die darauffolgende Quantifizierung von erregenden und inhibierenden synaptischen Inputs von Neuronen an Tanyzyten in topografisch definierten Regionen um den 3. Ventrikel im Bereich des Hypothalamus untersucht die vorliegende Studie die Hypothese, dass Tanyzyten fähig sind, neuronale elektrochemische Signale weiter zu leiten. Dazu wurden immunhistochemisch gefärbte koronale Hirnschnitte von Wildtyp, CRH-Cre-tdTomato und RAX-Cre-ER^{T2}-tdTomato Mäusen verwendet, die im nächsten Schritt durch ein konfokales Laser-scanning-Mikroskop untersucht und 13 zuvor definierte Bereiche mit einer 63x Vergrößerung aufgenommen und fotografiert wurden. Darauffolgend wurde unter Verwendung des Programms IMARIS ein geeigneter Rekonstruktions-Ablauf etabliert um an den ventrikulären Grenzen entspringende tanyzytische Fortsätze und gegebenenfalls synaptische Inputs 3-dimensional zu rekonstruieren. Mit dieser neu entwickelten Methode konnte erfolgreich gezeigt werden, dass Tanyzyten synaptische Inputs von umliegenden hypothalamischen Neuronen erhalten. Durch die Untersuchung der gesamten rostro-kaudalen Verlängerung des Hypothalamus konnte ein leichter Trend hin zu einer höheren Anzahl an synaptischen Inputs in kaudalen Regionen beobachtet werden. Interessanterweise erhielten an sämtlichen analysierten Positionen nicht alle detektierten Tanyzyten synaptische Inputs. Des Weiteren konnte auf Grund der Verwendung von verschiedenen Markern zur Lokalisierung von Tanyzyten im hypothalamischen Parenchym um den 3. Ventrikel verschiedene Subtypen identifiziert werden: RAX+ Tanyzyten besiedelten mehr kaudal gelegene Regionen wohingegen GFAP+ Tanyzyten genau komplementär in mehr rostralen Bereichen entdeckt wurden.

Zusammenfassend unterstreicht die Beobachtung von erregenden sowie inhibierenden synaptischen Inputs im Rahmen dieser Studie die Vermutung, dass Tanyzyten an der synaptischen Signalübertragung beteiligt sind und die Kommunikation mit Neuronen unterschiedlicher hypothalamischer Kerngebiete wird vermutet.

keywords: *Tanyzyten, Hypothalamus, 3. Ventrikel, Synapsen, synaptische Kontakte, synaptische Kommunikation, Neurotransmission, 3D Rekonstruktionen*

Theoretical localization of selected and analyzed coronal mouse brain sections

Reference: The Mouse Brain in Stereotaxic Coordinates, Franklin 1997

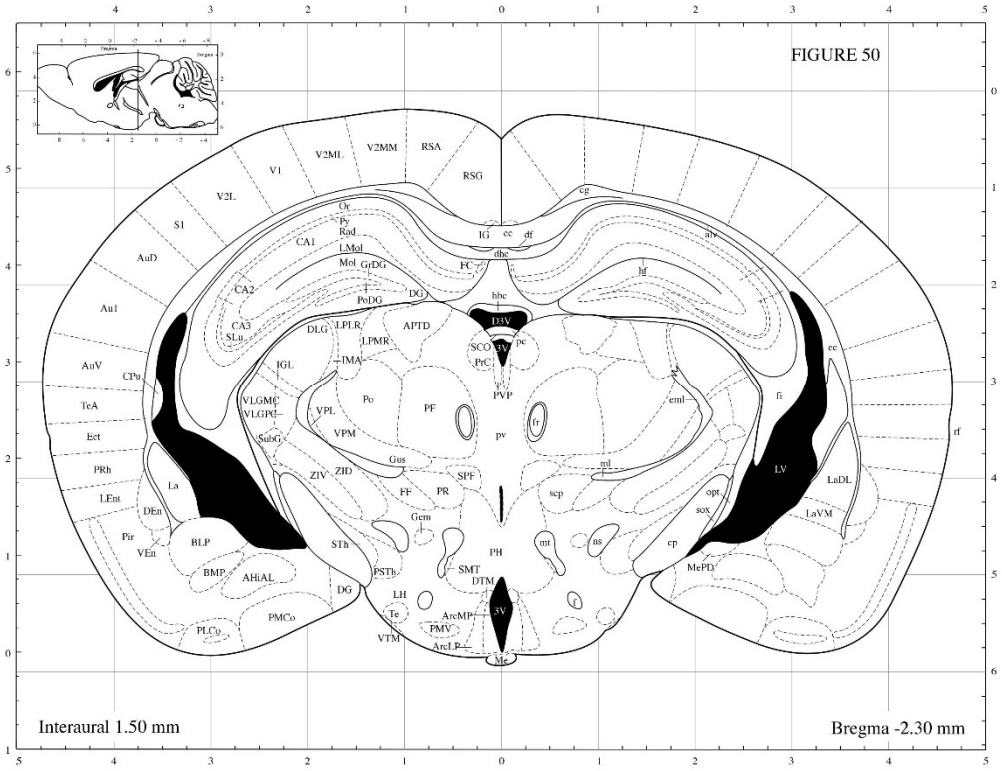

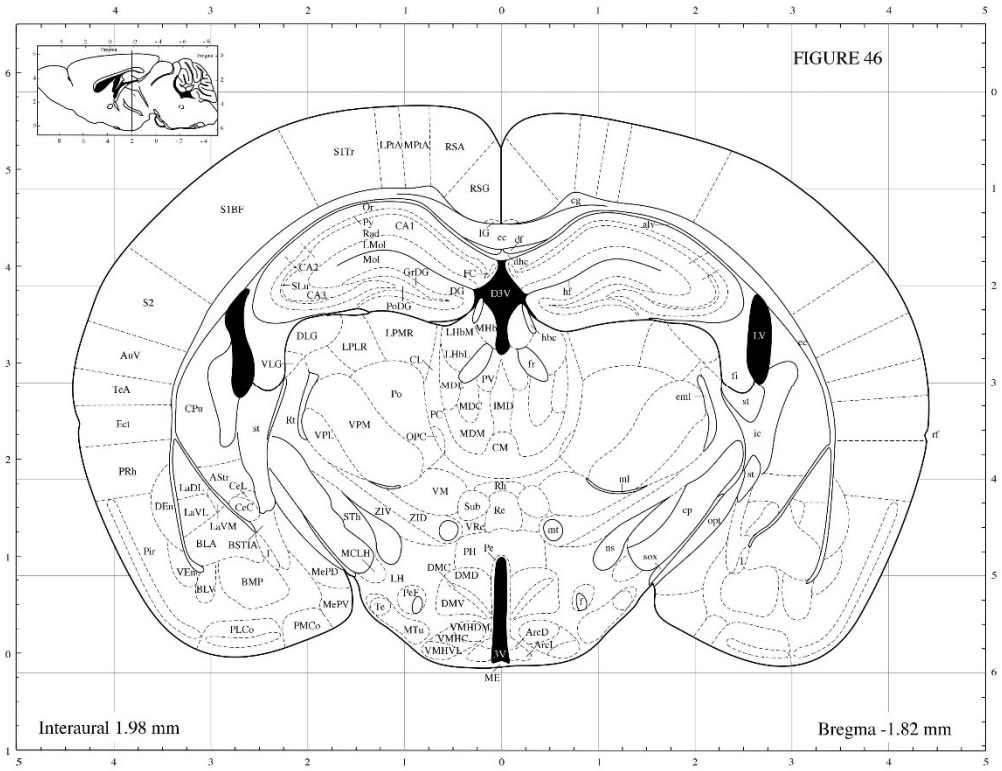

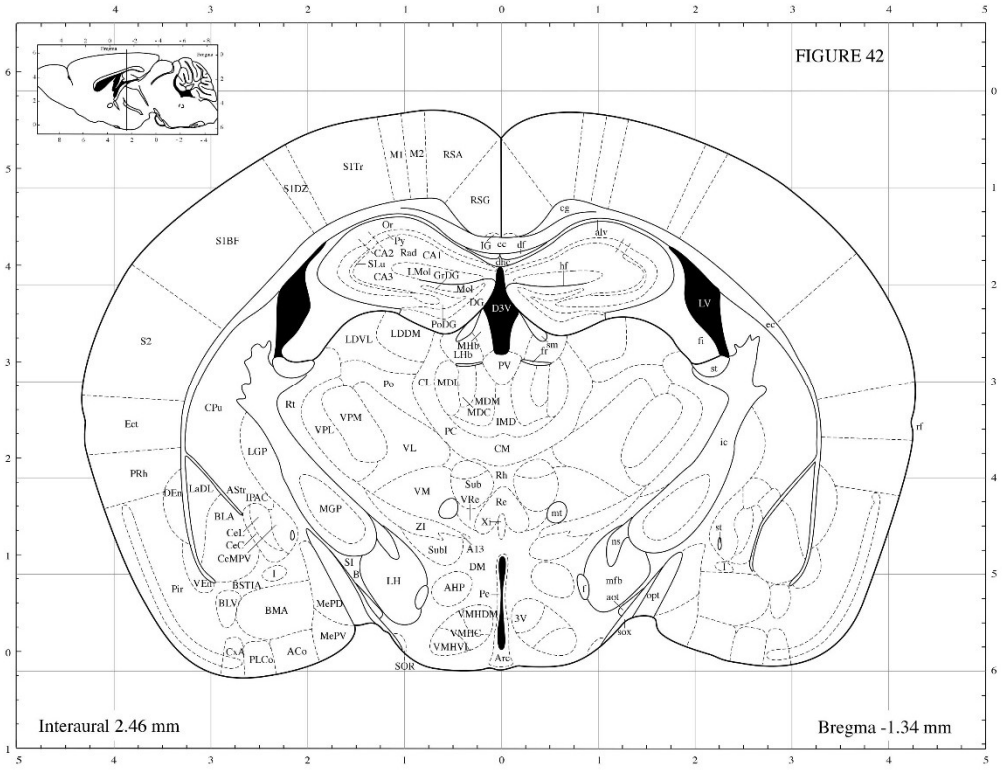
FIGURE 42
S1Tr
M1
M2
RSA
S1DZ
RSG
S1BF
Or
Py
CA2
Rad
CA1
SLu
CA3
LMol
GrDG
Mol
DG
D3V
LV
PoDG
LDVL
LDDM
MHb
LHb
PV
S2
Po
CI
MDL
CPu
Rt
MDM
MDC
IMD
VPM
VPL
PC
VL
CM
Ect
LGP
PRh
LaDL
AStr
IPAC
VM
Sub
Rh
VRe
Re
MGP
BLA
Xi
Cel
CeC
CeMPV
ZI
SubI
A13
SI
LH
DM
AHP
Pe
Pir
VEn
BSTIA
BLV
BMA
MePD
VMHDM
3V
MePV
VMHC
VMHVL
CxA
PLCo
ACo
SOR
Arc
Interaural 2.46 mm
Bregma -1.34 mm

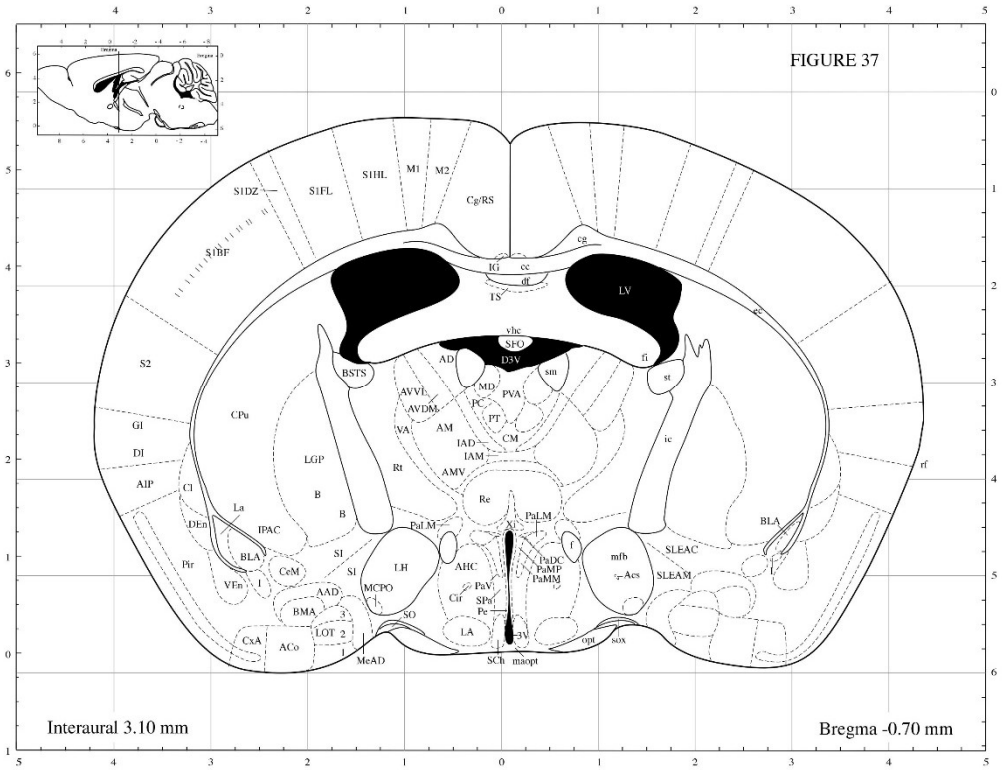
FIGURE 37
S1HL
M1
M2
S1DZ
S1FL
Cg/RS
S1BF
IG
cc
dlf
IS
LV
vhc
SFO
D3V
AD
fi
S2
BSTS
sm
st
AVVL
MD
AVDM
PC
PVA
CPu
PT
GI
VA
AM
CM
IAD
DI
LGP
IAM
ic
Rt
AMV
AIP
Cl
B
Re
La
PaLM
BLA
DEn
IPAC
SI
LH
AHC
SLEAC
Pir
BLA
CeM
mfb
Acs
SLEAM
VEn
MCPO
PaDC
PaMP
PaMM
AAD
Cir
SPa
Pe
BMA
SO
LOT
LA
3V
opt
sox
CxA
ACo
MeAD
SCh
maopt
Interaural 3.10 mm
Bregma -0.70 mm

Gallery of 20x and 40x overview scans of analyzed animals

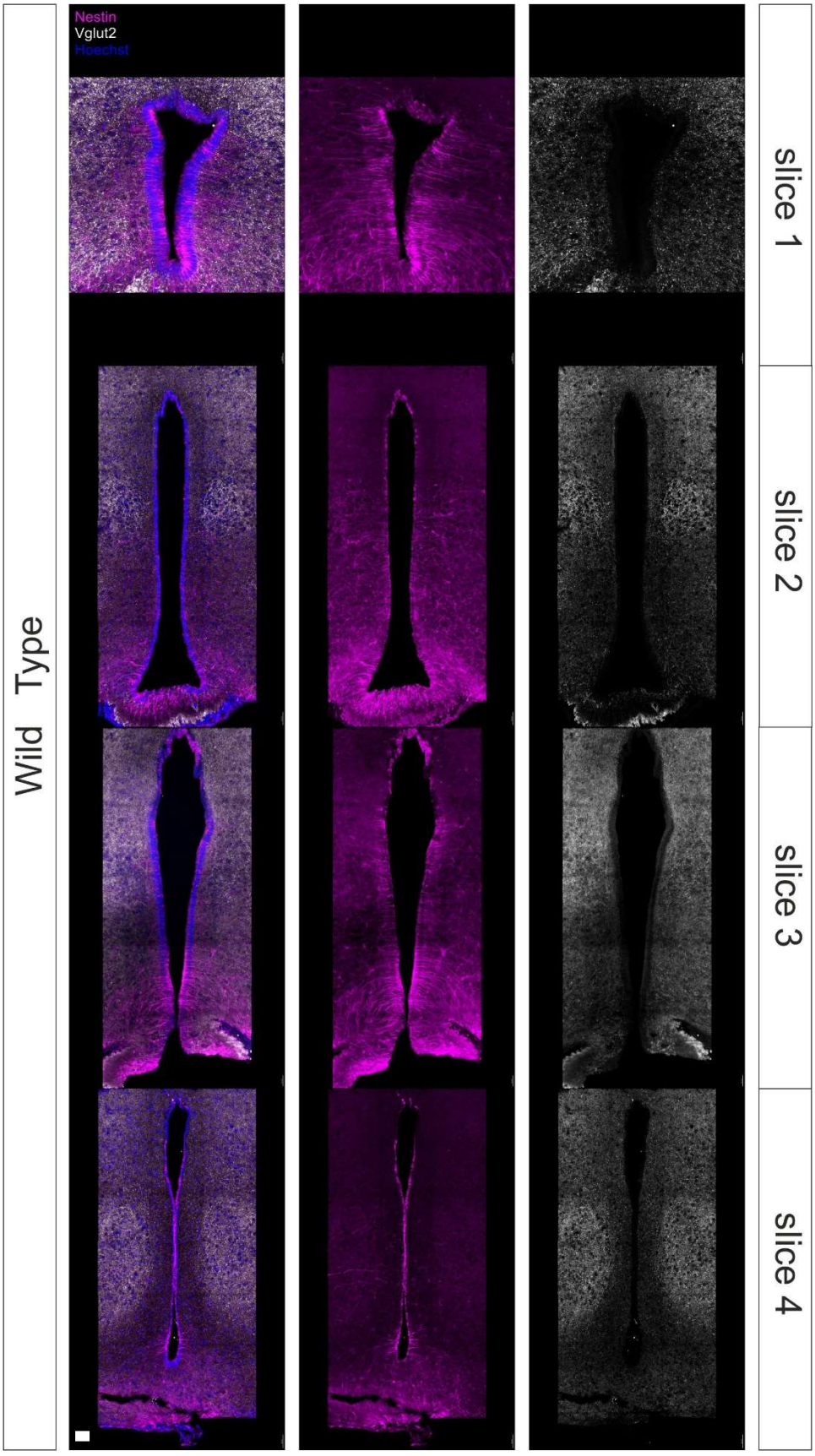

Scale bar 30µm

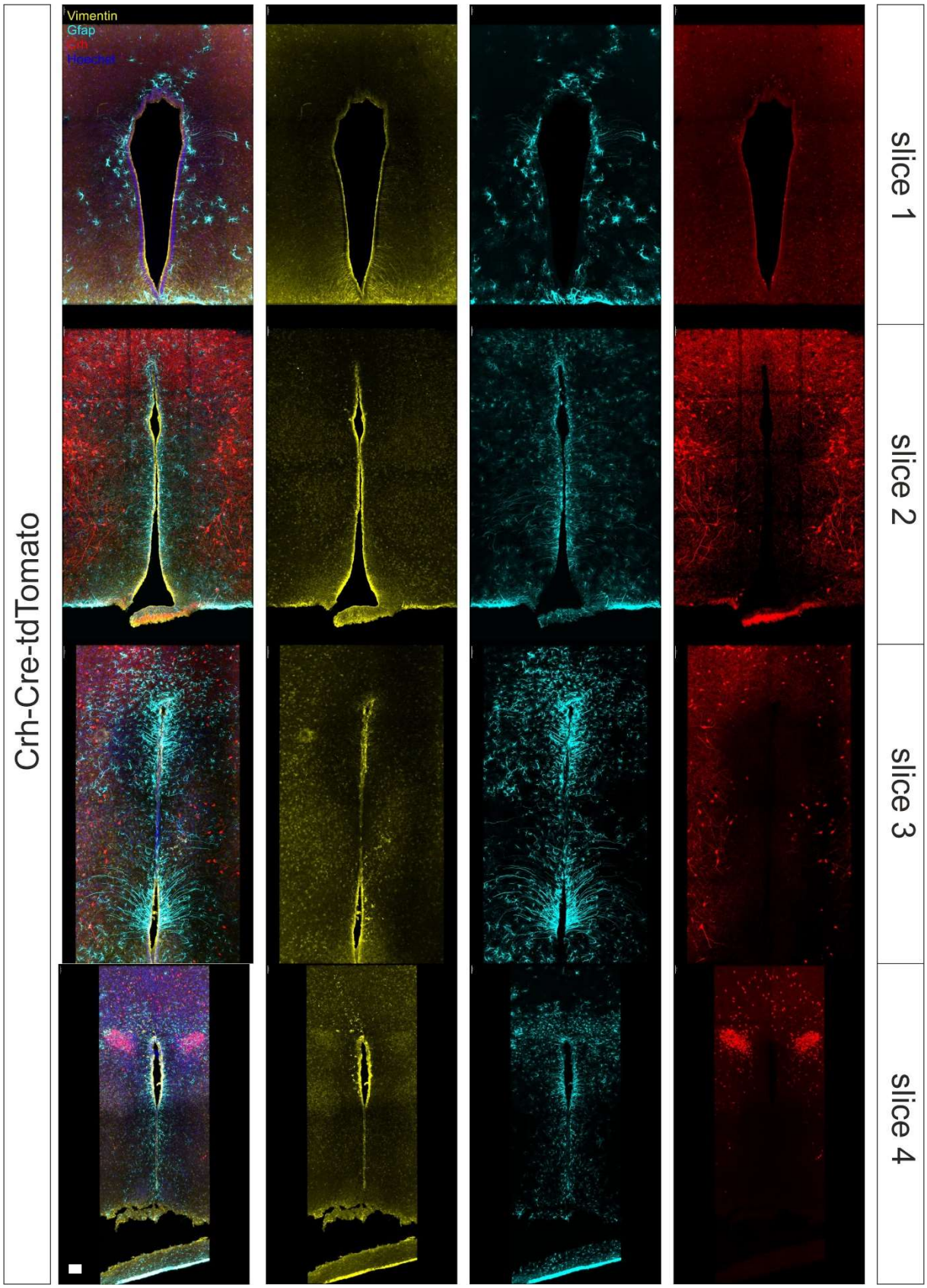

Scale bar 30µm

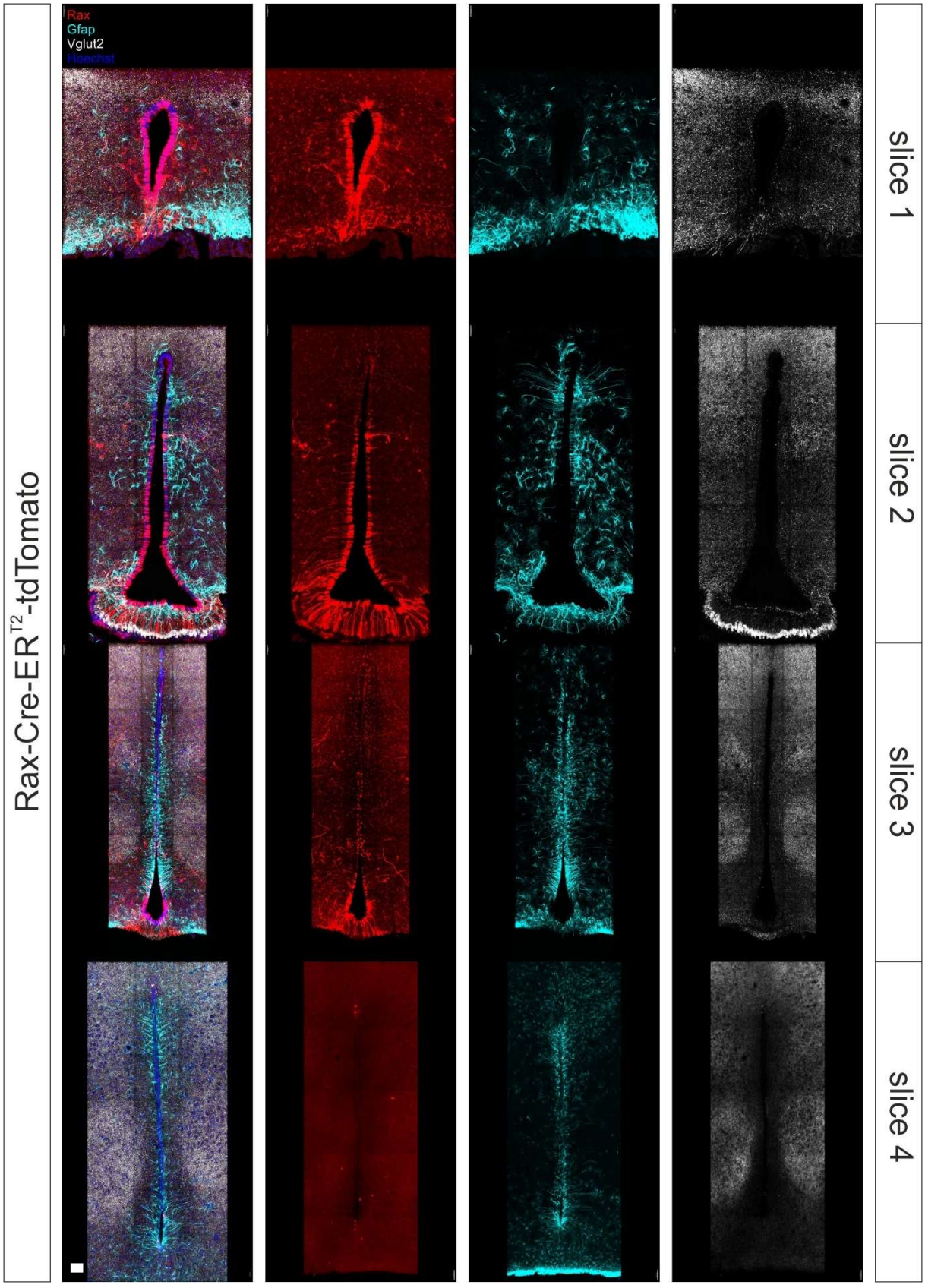

Scale bar 30µm

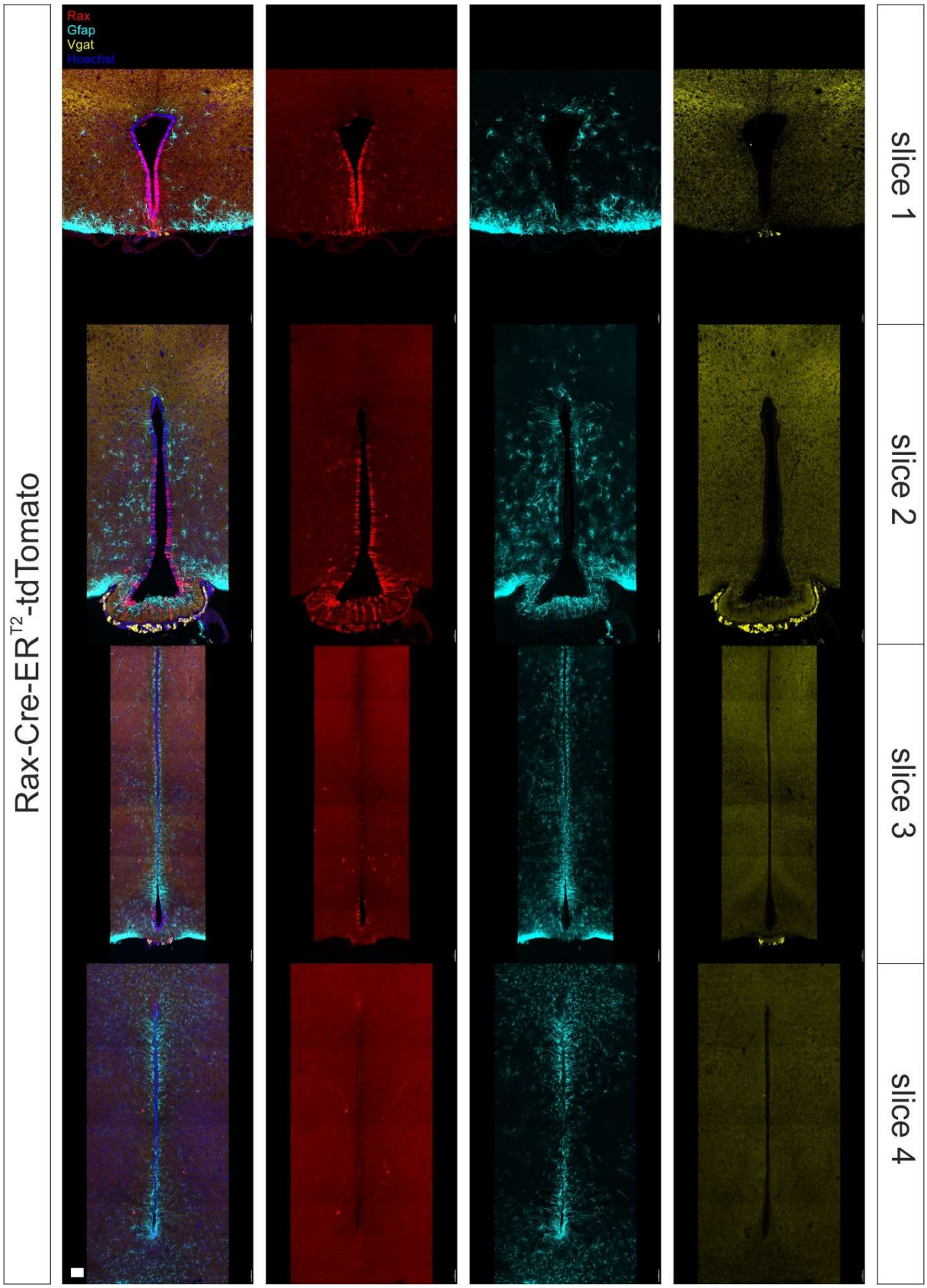

Scale bar 30µm

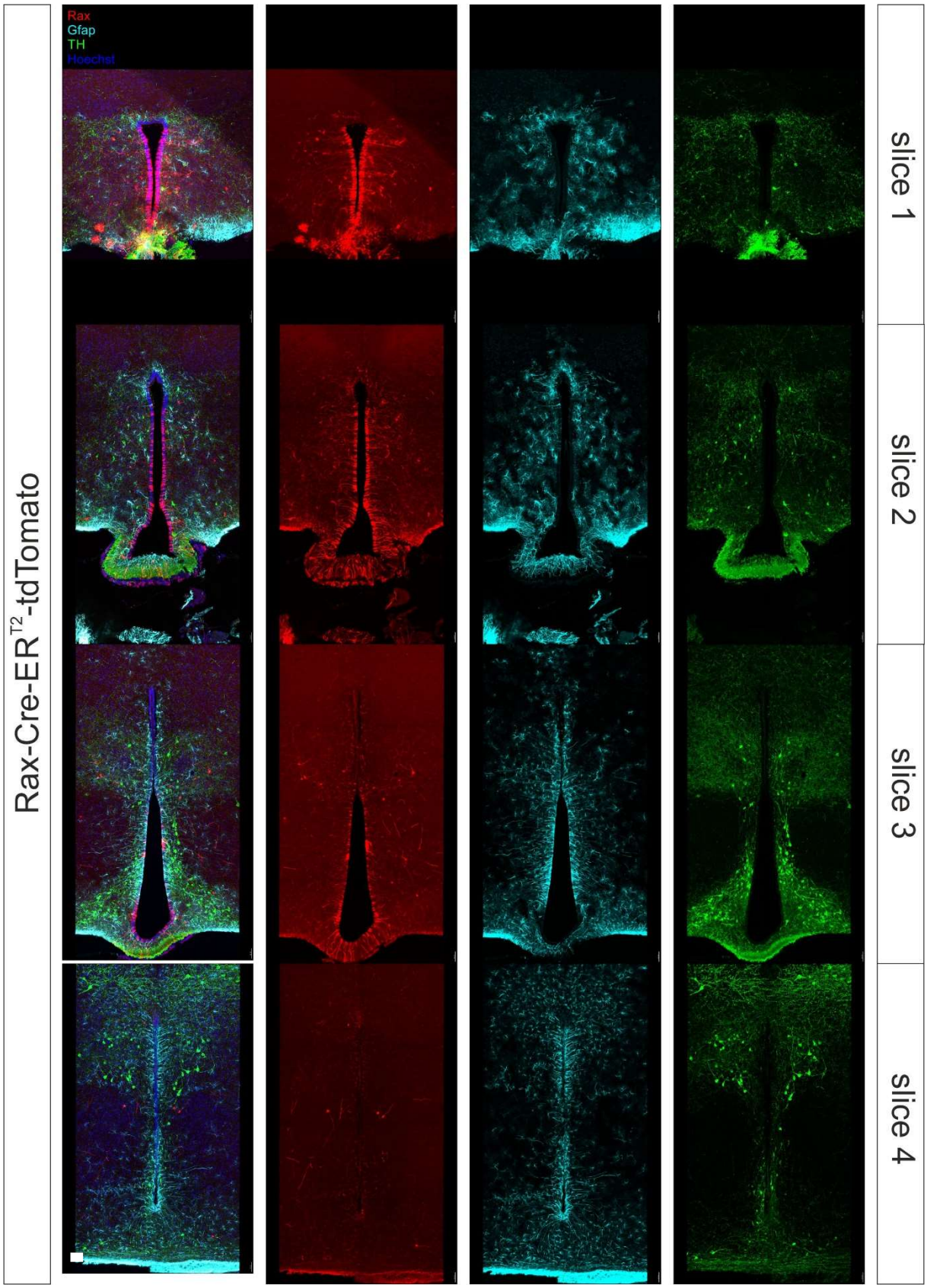

Scale bar 30µm

Figure 13 – Values for reconstruction of tanycytic soma and process executed by using the 'Surface Reconstruction' tool

Position 1				
Animal	Cell type	Structure	Volume in µm^3	Spots <0.8µm
1	Tanycytes	*Soma*	2820.102	0
			1.70E+03	0
		Process	1810.219	256
			1472.323	27
			646.735	56
2	Tanycytes	*Soma*	214	3
		Process	251	38
3	Tanycytes	*Soma*	2045.058	0
		Process	1090.946	26
4	Tanycytes	*Soma*	3913.245	0
		Process	5258.622	94
5	Tanycytes	*Soma*	5912	13
		Process	7786.575	71
Position 2				
Animal	Cell type	Structure	Volume in µm^3	Spots <0.8µm
1	Tanycytes	*Soma*	2940	0
			3501.675	11
		Process	6838.445	101
			4908.025	211
2	not possible			
3	Tanycytes	*Soma*	474.7868	0
		Process	596.9634	8
			132.692	1
4	Tanycytes	*Soma*	7557.497	0
		Process	33834.86	573
5	Tanycytes	*Soma*	7952.398	2
		Process	35813.91	768
Position 3				

Animal	Cell type			
1, 2, 3, 4, 5	Ependymocytes			
Position 4				
Animal	Cell type	Structure	Volume µm^3	Spots <0.8µm
1	Tanycytes	*Soma*	1313.467	15
		Process	1711.557	118
2	Tanycytes	*Soma*	691.241	0
			1364	0
		Process	903.4939	35
			2060.184	119
3	Tanycytes	*Soma*	3280.399	2
			553.1518	2
		Process	2960.133	47
			418.194	8
4	Tanycytes	*Soma*	12282.42	6
		Process	22998.37	1045
5	Ependymocytes			
		Position 5		
Animal	Cell type	Structure	Volume in µm^3	Spots <0.8µm
1	Tanycytes	*Soma*	1461.512	6
		Process	1869.926	57
			600	28
2	Tanycytes	*Soma*	9797	3
		Process	8594.839	290
			1634.117	91
3	Tanycytes	*Soma*	3068	1
		Process	912.0057	11
			451	12
			433	11
			2007	22
			2632	7
4	Tanycytes	*Soma*	2046.354	0
		Process	8470.402	301

5	not possible			
		Position 6		
Animal	Cell type	Structure	Volume in µm^3	Spots <0.8µm
1	not possible			
2	Tanycytes	*Soma*	677.0123	0
			118	0
		Process	2348.696	72
			1492.964	114
			648.667	27
3	Ependymocytes			
4	Tanycytes	*Soma*	33265.85	34
		Process	39810.62	1511
5	Tanycytes	*Soma*	3504.189	1
		Process	7971.873	66
		Position 7		
Animal	Cell type			
1, 2, 3, 4, 5	Ependymocytes			
		Position 8		
Animal	Cell type	Structure	Volume in µm^3	Spots <0.8µm
1	Ependymocytes			
2	Tanycytes	*Soma*	2582.58	3
		Process	489.8635	13
			1064.547	39
3	Tanycytes	*Soma*	3711.966	3
		Process	4318.014	99
4, 5	not possible			
		Position 9		
Animal	Cell type	Structure	Volume in µm^3	Spots <0.8µm
1	Ependymocytes			
2	Tanycytes	*Soma*	1876.47	1
			469.3586	0
		Process	3701.566	106
			719.271	27

3	Tanycytes	*Soma* + *Process*	22845.27	321
4	Tanycytes	*Soma*	5710.212	4
		Process	10153.32	402
5	not possible			
Position 10				
Animal	Cell type	Structure	Volume in µm^3	Spots <0.8µm
1	Ependymocytes			
2	Tanycytes	*Soma*	5625	1
		Process	5041.949	148
			5144.776	249
3	Ependymocytes			
4	Tanycytes	*Soma*	11630.422	20
		Process	40369.67	1263
5	Tanycytes	*Soma*	3984.511	1
		Process	3017.748	66
Position 11				
Animal	Cell type			
1, 2, 3, 4, 5	Ependymocytes			
Position 12				
Animal	Cell type	Structure	Volume in µm^3	Spots <0.8µm
1	Tanycytes	*Soma*	1617.55	8
			1326.825	1
		Process	481.6914	17
			551.5189	26
			663.645	13
2, 3, 4, 5	Ependymocytes			
Position 13				
Animal	Cell type	Structure	Volume in µm^3	Spots <0.8µm
1	Ependymocytes			
2	Ependymocytes & tanycytes	*Soma*	9955.885	11
		Process	1946.235	35

Figure 21 – Amount of reconstructed tanycytic processes, tanycytes receiving synaptic inputs and total amount of synaptic inputs in all analyzed mouse lines

Wild Type VGLUT2+ inputs onto Nestin+ tanycytes N=5						
	Total amount of detected tanycytes		**Amount of tanycytes receiving VGLUT2+ inputs**		**Total amount of detected VGLUT2+ inputs**	
Position	Mean	SEM	Mean	SEM	Mean	SEM
1	14.8	1.744	8.6	1.288	23.4	6.713
2	17.8	2.800	11.8	1.985	32.4	8.029
3	0.6	0.600	0.6	0.600	0.6	0.600
4	16.8	4.641	9	2.408	21	6.870
5	16.2	5.064	11.2	3.625	34	15.258
6	15	4.347	7.6	2.315	16.6	5.741
7	0	0.000	0	0.000	0	0.000
8	0.667	0.333	0.333	0.333	2	2.000
9	10.2	4.716	6.8	3.513	18	10.104
10	13.6	3.187	7.4	1.077	16.4	2.694
11	6	5.282	3.4	3.400	6.4	6.400
12	4	2.098	2.4	1.122	4	1.924
13	13.6	3.995	8.8	3.056	23.8	12.651

RAX-CreER^{T2}-tdTomato VGLUT2+ inputs onto RAX+ or GFAP+ tanycytes N=3						
	Total amount of detected tanycytes		**Amount of tanycytes receiving VGLUT2+ inputs**		**Total amount of detected VGLUT2+ inputs**	
Position	Mean	SEM	Mean	SEM	Mean	SEM
1	15.667	1.453	8.667	1.333	19	2
2	14.333	0.667	7	0.577	23.667	6.360
3	27.667	1.333	17	1.528	44	10.970

4	25	4.163	18.667	2.906	48.667	2.728
5	19.333	1.202	11.667	2.186	33.667	8.969
6	9.667	2.333	5.333	0.882	23.333	5.239
7	1.333	1.333	1.333	1.333	3.333	3.333
8	25.667	6.119	10	0.577	18.333	2.906
9	28	1.528	11.667	1.202	19	4.619
10	16.333	4.372	12.667	4.667	45	21.008
11	0	0	0	0	0	0
12	7	1.528	1.667	1.202	2	1.528
13	20	7.211	9.333	0.333	22.667	5.783

RAX-CreER^{T2}-tdTomato VGAT+ inputs onto RAX+ or GFAP+ tanycytes N=3						
	Total amount of detected tanycytes		**Amount of tanycytes receiving VGAT+ inputs**		**Total amount of detected VGAT+ inputs**	
Position	Mean	SEM	Mean	SEM	Mean	SEM
1	19.667	1.202	15	0.577	42	6.807
2	25.333	2.963	18.667	3.528	45.667	12.811
3	38.667	8.373	21	8.021	50.667	23.068
4	32.667	2.728	22	2.309	76.333	15.720
5	20.667	2.603	13.333	2.404	57	11.504
6	9.667	2.603	7	1.732	28.667	10.588
7	0	0	0	0	0	0
8	28	3.464	10	1.732	16.667	2.186
9	35.667	5.783	16.333	5.239	28.667	8.988
10	14.333	2.963	9	2.646	30.667	11.552
11	0	0	0	0	0	0
12	4	4	2.333	2.333	3.333	3.333
13	16.333	1.856	12.667	2.404	47.667	14.518

CRH-Cre-tdTomato CRH+ inputs onto Vimentin+ tanycytes N=2						
	Total amount of detected tanycytes		**Amount of tanycytes receiving CRH+ inputs**		**Total amount of detected CRH+ inputs**	
Position	Mean	SEM	Mean	SEM	Mean	SEM
1	7.5	7.5	3.5	3.5	7.5	7.5
2	14	1	9.5	0.5	20	3
3	0	0	0	0	0	0
4	21.5	0.5	11	2	27	3
5	24	6	13	6	22.5	10.5
6	5.5	5.5	3.5	3.5	20	20
7	5	5	2	2	4	4
8	4	4	1.5	1.5	1.5	1.5
9	15.5	9.5	4.5	3.5	5	4
10	18.5	6.5	7	3	10	6
11	8.5	1.5	8	1	21.5	0.5
12	14.5	4.5	7	0	10	1
13	11	0	1	1	1.5	1.5

Figure 22 – Percentage of tanycytes receiving or not receiving synaptic inputs in all analyzed mouse lines

Wild Type VGLUT2+ inputs onto Nestin+ tanycytes N=5				
	% of tanycytes receiving synaptic inputs		% of tanycytes not receiving synaptic inputs	
Positions	Mean	SEM	Mean	SEM
1	59.222	6.929	40.778	6.929
2	65.440	3.613	34.560	3.613
3	20	20	80	20
4	43.292	10.913	56.708	10.913
5	68.062	2.896	31.938	2.896
6	40.118	10.375	59.882	10.375
7	0	0	100	0
8	20	20	80	20
9	38.422	16.262	61.578	16.262
10	59.359	8.460	40.641	8.460
11	12.593	12.593	87.407	12.593
12	42.5	19.203	57.500	19.203
13	50.961	15.142	49.039	15.142

RAX-Cre-ER^{T2}-tdTomato VGLUT2+ inputs onto RAX+ or GFAP+ tanycytes N=3				
	% of tanycytes receiving synaptic inputs		% of tanycytes not receiving synaptic inputs	
Positions	Mean	SEM	Mean	SEM
1	54.736	4.736	45.264	4.736
2	49.060	4.532	50.940	4.532
3	62.299	8.906	37.701	8.906
4	74.891	1.708	25.109	1.708
5	59.711	8.284	40.289	8.284

6	60	11.097	40	11.097
7	33.333	33.333	66.667	33.333
8	42.549	7.668	57.451	7.668
9	41.533	2.636	58.467	2.636
10	74.089	7.669	25.911	7.669
11	0	0	100	0
12	30	25.166	70	25.166
13	59.657	18.394	40.343	18.394

RAX-Cre-ER^{T2}-tdTomato VGAT+ inputs onto RAX+ or GFAP+ tanycytes N=3				
	% of tanycytes receiving synaptic inputs		% of tanycytes not receiving synaptic inputs	
Positions	Mean	SEM	Mean	SEM
1	77.158	7.345	22.842	7.345
2	72.632	7.930	27.368	7.930
3	50.196	16.245	49.804	16.245
4	67.449	5.161	32.551	5.161
5	63.881	4.344	36.119	4.344
6	73.810	3.123	26.190	3.123
7	0	0	100	0
8	35.256	1.867	64.744	1.867
9	43.383	7.439	56.617	7.439
10	62.821	12.517	37.179	12.517
11	0	0	100	0
12	19.444	19.444	80.556	19.444
13	76.825	10.567	23.175	10.567

CRH-Cre-tdTomato CRH+ inputs onto Vimentin+ tanycytes N=2		
Positions	% of tanycytes receiving synaptic inputs	% of tanycytes not receiving synaptic inputs

	Mean	SEM	Mean	SEM
1	23.333	23.333	76.667	23.333
2	67.949	1.282	32.051	1.282
3	0	0	100	0
4	50.974	8.117	49.026	8.117
5	51.111	12.222	48.889	12.222
6	31.818	31.818	68.182	31.818
7	20	20	80	20
8	18.750	18.750	81.250	18.750
9	24.333	7.667	75.667	7.667
10	36.667	3.333	63.333	3.333
11	95	5	5	5
12	53.421	16.579	46.579	16.579
13	9.091	9.091	90.909	9.091

Figure 23 – Differences between the amount of synaptic inputs across all positions examined alongside the walls of the hypothalamic III-ventricle

Wild Type total VGLUT2+ inputs onto Nestin+ tanycytes N=5					
ANOVA summary					
source	**df**	**SS**	**MS**	**F**	**p-value**
Between groups	12	7919	659.9	F (12, 50) = 2.235	p=0.0238
Within groups	50	14762	295.2		
total	62	22681			
Are differences among means statistically significant? (p < 0.05)			Yes, *		
R square			0.3492		
Tukey's multiple comparisons test					
Number of families			1		
Number of comparisons per family			78		
Alpha			0.05		
Compared positions	Mean 1	Mean 2	Mean Differences	95% CI of Differences	Significant?
1 vs. 2	23.40.	32.4	-9	-46.79 to 28.79	ns
1 vs. 3	23.40	0.6	22.8	-14.99 to 60.59	ns
1 vs. 4	23.40	21	2.4	-35.39 to 40.19	ns
1 vs. 5	23.40	34	-10.6	-48.39 to 27.19	ns
1 vs. 6	23.40	16.6	6.8	-30.99 to 44.59	ns
1 vs. 7	23.40	0	23.4	-14.39 to 61.19	ns
1 vs. 8	23.40	2	21.4	-22.23 to 65.03	ns
1 vs. 9	23.40	18	5.4	-32.39 to 43.19	ns
1 vs. 10	23.40	16.4	7	-30.79 to 44.79	ns
1 vs. 11	23.40	6.4	17	-20.79 to 54.79	ns
1 vs. 12	23.40	4	19.40	-18.39 to 57.19	ns
1 vs. 13	23.40	23.8	-0.4	-38.19 to 37.39	ns
2 vs. 3	32.40	0.6	31.8	-5.988 to 69.59	ns
2 vs. 4	32.40	21	11.4	-26.39 to 49.19	ns

2 vs. 5	32.40	34	-1.6	-39.39 to 36.19	ns
2 vs. 6	32.40	16.6	15.8	-21.99 to 53.59	ns
2 vs. 7	32.40	0	32.4	-5.388 to 70.19	ns
2 vs. 8	32.40	2	30.4	-13.23 to 74.03	ns
2 vs. 9	32.40	18	14.4	-23.39 to 52.19	ns
2 vs. 10	32.40	16.4	16	-21.79 to 53.79	ns
2 vs. 11	32.40	6.4	26	-11.79 to 63.79	ns
2 vs. 12	32.40	4	28.4	-9.388 to 66.19	ns
2 vs. 13	32.40	23.8	8.6	-29.19 to 46.39	ns
3 vs. 4	0.6000	21	-20.4	-58.19 to 17.39	ns
3 vs. 5	0.6000	34	-33.4	-71.19 to 4.388	ns
3 vs. 6	0.6000	16.6	-16	-53.79 to 21.79	ns
3 vs. 7	0.6000	0	0.6	-37.19 to 38.39	ns
3 vs. 8	0.6000	2	-1.4	-45.03 to 42.23	ns
3 vs. 9	0.6000	18	-17.4	-55.19 to 20.39	ns
3 vs. 10	0.6000	16.4	-15.8	-53.59 to 21.99	ns
3 vs. 11	0.6000	6.4	-5.8	-43.59 to 31.99	ns
3 vs. 12	0.6000	4	-3.4	-41.19 to 34.39	ns
3 vs. 13	0.6000	23.8	-23.2	-60.99 to 14.59	ns
4 vs. 5	21	34	-13	-50.79 to 24.79	ns
4 vs. 6	21	16.6	4.4	-33.39 to 42.19	ns
4 vs. 7	21	0	21	-16.79 to 58.79	ns
4 vs. 8	21	2	19	-24.63 to 62.63	ns
4 vs. 9	21	18	3	-34.79 to 40.79	ns
4 vs. 10	21	16.4	4.6	-33.19 to 42.39	ns
4 vs. 11	21	6.4	14.6	-23.19 to 52.39	ns
4 vs. 12	21	4	17	-20.79 to 54.79	ns
4 vs. 13	21	23.8	-2.8	-40.59 to 34.99	ns
5 vs. 6	34	16.6	17.4	-20.39 to 55.19	ns
5 vs. 7	34	0	34	-3.788 to 71.79	ns
5 vs. 8	34	2	32	-11.63 to 75.63	ns
5 vs. 9	34	18	16	-21.79 to 53.79	ns
5 vs. 10	34	16.4	17.6	-20.19 to 55.39	ns

5 vs. 11	34	6.4	27.6	-10.19 to 65.39	ns
5 vs. 12	34	4	30	-7.788 to 67.79	ns
5 vs. 13	34	23.8	10.2	-27.59 to 47.99	ns
6 vs. 7	16.6	0	16.6	-21.19 to 54.39	ns
6 vs. 8	16.6	2	14.6	-29.03 to 58.23	ns
6 vs. 9	16.6	18	-1.4	-39.19 to 36.39	ns
6 vs. 10	16.6	16.4	0.2	-37.59 to 37.99	ns
6 vs. 11	16.6	6.4	10.2	-27.59 to 47.99	ns
6 vs. 12	16.6	4	12.6	-25.19 to 50.39	ns
6 vs. 13	16.6	23.8	-7.2	-44.99 to 30.59	ns
7 vs. 8	0	2	-2	-45.63 to 41.63	ns
7 vs. 9	0	18	-18	-55.79 to 19.79	ns
7 vs. 10	0	16.4	-16.4	-54.19 to 21.39	ns
7 vs. 11	0	6.4	-6.4	-44.19 to 31.39	ns
7 vs. 12	0	4	-4	-41.79 to 33.79	ns
7 vs. 13	0	23.8	-23.8	-61.59 to 13.99	ns
8 vs. 9	2	18	-16	-59.63 to 27.63	ns
8 vs. 10	2	16.4	-14.4	-58.03 to 29.23	ns
8 vs. 11	2	6.4	-4.4	-48.03 to 39.23	ns
8 vs. 12	2	4	-2	-45.63 to 41.63	ns
8 vs. 13	2	238	-21.8	-65.43 to 21.83	ns
9 vs. 10	18	16.4	1.6	-36.19 to 39.39	ns
9 vs. 11	18	6.4	11.6	-26.19 to 49.39	ns
9 vs. 12	18	4	14	-23.79 to 51.79	ns
9 vs. 13	18	23.8	-5.8	-43.59 to 31.99	ns
10 vs. 11	16.4	6.4	10	-27.79 to 47.79	ns
10 vs. 12	16.4	4	12.4	-25.39 to 50.19	ns
10 vs. 13	16.4	23.8	-7.4	-45.19 to 30.39	ns
11 vs. 12	6.4	4	2.4	-35.39 to 40.19	ns
11 vs. 13	6.4	23.8	-17.4	-55.19 to 20.39	ns
12 vs. 13	4	23.8	-19.8	-57.59 to 17.99	ns

RAX-CreER^{T2}-tdTomato VGLUT2+ inputs onto RAX+ or GFAP+ tanycytes N=3					
ANOVA summary					
source	**df**	**SS**	**MS**	**F**	**p-value**
Between groups	12	9323	776.9	F (12, 26) = 4.218	p=0.0010
Within groups	26	4789	184.2		
total	38	14112			
Are differences among means statistically significant? (p < 0.05)			Yes, **		
R square			0.6607		
Tukey's multiple comparisons test					
Number of families			1		
Number of comparisons per family			78		
Alpha			0.05		
Compared positions	Mean 1	Mean 2	Mean Differences	95% CI of Differences	Significant?
1 vs. 2	19	23.67	-4.667	-44.94 to 35.60	ns
1 vs. 3	19	44	-25	-65.27 to 15.27	ns
1 vs. 4	19	48.67	-29.67	-69.94 to 10.60	ns
1 vs. 5	19	33.67	-14.67	-54.94 to 25.60	ns
1 vs. 6	19	23.33	-4.333	-44.6 to 35.94	ns
1 vs. 7	19	3.333	15.67	-24.6 to 55.94	ns
1 vs. 8	19	18.33	0.6667	-39.6 to 40.94	ns
1 vs. 9	19	19	0	-40.27 to 40.27	ns
1 vs. 10	19	45	-26	-66.27 to 14.27	ns
1 vs. 11	19	0	19	-21.27 to 59.27	ns
1 vs. 12	19	2	17	-23.27 to 57.27	ns
1 vs. 13	19	22.67	-3.667	-43.94 to 36.60	ns
2 vs. 3	23.67	44	-20.33	-60.6 to 19.94	ns
2 vs. 4	23.67	48.67	-25	-65.27 to 15.27	ns
2 vs. 5	23.67	33.67	-10	-50.27 to 30.27	ns
2 vs. 6	23.67	23.33	0.3333	-39.94 to 40.60	ns
2 vs. 7	23.67	3.333	20.33	-19.94 to 60.60	ns

2 vs. 8	23.67	18.33	5.333	-34.94 to 45.60	ns
2 vs. 9	23.67	19	4.667	-35.6 to 44.94	ns
2 vs. 10	23.67	45	-21.33	-61.6 to 18.94	ns
2 vs. 11	23.67	0	23.67	-16.6 to 63.94	ns
2 vs. 12	23.67	2	21.67	-18.6 to 61.94	ns
2 vs. 13	23.67	22.67	1	-39.27 to 41.27	ns
3 vs. 4	44	48.67	-4.667	-44.94 to 35.60	ns
3 vs. 5	44	33.67	10.33	-29.94 to 50.60	ns
3 vs. 6	44	23.33	20.67	-19.6 to 60.94	ns
3 vs. 7	44	3.333	40.67	0.3983 to 80.94	*
3 vs. 8	44	18.33	25.67	-14.6 to 65.94	ns
3 vs. 9	44	19	25	-15.27 to 65.27	ns
3 vs. 10	44	45	-1	-41.27 to 39.27	ns
3 vs. 11	44	0	44	3.732 to 84.27	*
3 vs. 12	44	2	42	1.732 to 82.27	*
3 vs. 13	44	22.67	21.33	-18.94 to 61.60	ns
4 vs. 5	48.67	33.67	15	-25.27 to 55.27	ns
4 vs. 6	48.67	23.33	25.33	-14.94 to 65.60	ns
4 vs. 7	48.67	3.333	45.33	5.065 to 85.60	*
4 vs. 8	48.67	18.33	30.33	-9.935 to 70.60	ns
4 vs. 9	48.67	19	29.67	-10.6 to 69.94	ns
4 vs. 10	48.67	45	3.667	-36.6 to 43.94	ns
4 vs. 11	48.67	0	48.67	8.398 to 88.94	**
4 vs. 12	48.67	2	46.67	6.398 to 86.94	*
4 vs. 13	48.67	22.67	26	-14.27 to 66.27	ns
5 vs. 6	33.67	23.33	10.33	-29.94 to 50.60	ns
5 vs. 7	33.67	3.333	30.33	-9.935 to 70.60	ns
5 vs. 8	33.67	18.33	15.33	-24.94 to 55.60	ns
5 vs. 9	33.67	19	14.67	-25.6 to 54.94	ns
5 vs. 10	33.67	45	-11.33	-51.6 to 28.94	ns
5 vs. 11	33.67	0	33.67	-6.602 to 73.94	ns
5 vs. 12	33.67	2	31.67	-8.602 to 71.94	ns
5 vs. 13	33.67	22.67	11	-29.27 to 51.27	ns

6 vs. 7	23.33	3.333	20	-20.27 to 60.27	ns
6 vs. 8	23.33	18.33	5	-35.27 to 45.27	ns
6 vs. 9	23.33	19	4.333	-35.94 to 44.60	ns
6 vs. 10	23.33	45	-21.67	-61.94 to 18.60	ns
6 vs. 11	23.33	0	23.33	-16.94 to 63.60	ns
6 vs. 12	23.33	2	21.33	-18.94 to 61.60	ns
6 vs. 13	23.33	22.67	0.6667	-39.6 to 40.94	ns
7 vs. 8	3.333	18.33	-15	-55.27 to 25.27	ns
7 vs. 9	3.333	19	-15.67	-55.94 to 24.60	ns
7 vs. 10	3.333	45	-41.67	-81.94 to -1.398	*
7 vs. 11	3.333	0	3.333	-36.94 to 43.60	ns
7 vs. 12	3.333	2	1.333	-38.94 to 41.60	ns
7 vs. 13	3.333	22.67	-19.33	-59.6 to 20.94	ns
8 vs. 9	18.33	19	-0.6667	-40.94 to 39.60	ns
8 vs. 10	18.33	45	-26.67	-66.94 to 13.60	ns
8 vs. 11	18.33	0	18.33	-21.94 to 58.60	ns
8 vs. 12	18.33	2	16.33	-23.94 to 56.60	ns
8 vs. 13	18.33	22.67	-4.333	-44.6 to 35.94	ns
9 vs. 10	19	45	-26	-66.27 to 14.27	ns
9 vs. 11	19	0	19	-21.27 to 59.27	ns
9 vs. 12	19	2	17	-23.27 to 57.27	ns
9 vs. 13	19	22.67	-3.667	-43.94 to 36.60	ns
10 vs. 11	45	0	45	4.732 to 85.27	*
10 vs. 12	45	2	43	2.732 to 83.27	*
10 vs. 13	45	22.67	22.33	-17.94 to 62.60	ns
11 vs. 12	0	2	-2	-42.27 to 38.27	ns
11 vs. 13	0	22.67	-22.67	-62.94 to 17.60	ns
12 vs. 13	2	22.67	-20.67	-60.94 to 19.60	ns

RAX-CreER^{T2}-tdTomato VGAT+ inputs onto RAX+ or GFAP+ tanycytes N=3
ANOVA summary

source	**df**	**SS**	**MS**	**F**	**p-value**
Between groups	12	19770	1648	F (12, 26) = 4.262	p=0.0010
Within groups	26	10050	386.5		
total	38	29820			

Are differences among means statistically significant? ($p < 0.05$)	Yes; ***
R square	0.6630

Tukey's multiple comparisons test	
Number of families	1
Number of comparisons per family	78
Alpha	0.05

Compared positions	Mean 1	Mean 2	Mean Differences	95% CI of Differences	Significant?
1 vs. 2	42	45.67	-3.667	-62 to 54.67	ns
1 vs. 3	42	50.67	-8.667	-67 to 49.67	ns
1 vs. 4	42	76.33	-34.33	-92.67 to 24	ns
1 vs. 5	42	57	-15	-73.34 to 43.34	ns
1 vs. 6	42	28.67	13.33	-45 to 71.67	ns
1 vs. 7	42	0	42	-16.34 to 100.3	ns
1 vs. 8	42	16.67	25.33	-33 to 83.67	ns
1 vs. 9	42	28.67	13.33	-45 to 71.67	ns
1 vs. 10	42	30.67	11.33	-47 to 69.67	ns
1 vs. 11	42	0	42	-16.34 to 100.3	ns
1 vs. 12	42	3.333	38.67	-19.67 to 97	ns
1 vs. 13	42	47.67	-5.667	-64 to 52.67	ns
2 vs. 3	45.67	50.67	-5	-63.34 to 53.34	ns
2 vs. 4	45.67	76.33	-30.67	-89 to 27.67	ns
2 vs. 5	45.67	57	-11.33	-69.67 to 47	ns
2 vs. 6	45.67	28.67	17	-41.34 to 75.34	ns
2 vs. 7	45.67	0	45.67	-12.67 to 104	ns
2 vs. 8	45.67	16.67	29	-29.34 to 87.34	ns
2 vs. 9	45.67	28.67	17	-41.34 to 75.34	ns
2 vs. 10	45.67	30.67	15	-43.34 to 73.34	ns
2 vs. 11	45.67	0	45.67	-12.67 to 104	ns

2 vs. 12	45.67	3.333	42.33	-16 to 100.7	ns
2 vs. 13	45.67	47.67	-2	-60.34 to 56.34	ns
3 vs. 4	50.67	76.33	-25.67	-84 to 32.67	ns
3 vs. 5	50.67	57	-6.333	-64.67 to 52	ns
3 vs. 6	50.67	28.67	22	-36.34 to 80.34	ns
3 vs. 7	50.67	0	50.67	-7.670 to 109	ns
3 vs. 8	50.67	16.67	34	-24.34 to 92.34	ns
3 vs. 9	50.67	28.67	22	-36.34 to 80.34	ns
3 vs. 10	50.67	30.67	20	-38.34 to 78.34	ns
3 vs. 11	50.67	0	50.67	-7.670 to 109	ns
3 vs. 12	50.67	3.333	47.33	-11 to 105.7	ns
3 vs. 13	50.67	47.67	3	-55.34 to 61.34	ns
4 vs. 5	76.33	57	19.33	-39 to 77.67	ns
4 vs. 6	76.33	28.67	47.67	-10.67 to 106	ns
4 vs. 7	76.33	0	76.33	18 to 134.7	**
4 vs. 8	76.33	16.67	59.67	1.330 to 118	*
4 vs. 9	76.33	28.67	47.67	-10.67 to 106	ns
4 vs. 10	76.33	30.67	45.67	-12.67 to 104	ns
4 vs. 11	76.33	0	76.33	18 to 134.7	**
4 vs. 12	76.33	3.333	73	14.66 to 131.3	**
4 vs. 13	76.33	47.67	28.67	-29.67 to 87	ns
5 vs. 6	57	28.67	28.33	-30 to 86.67	ns
5 vs. 7	57	0	57	-1.336 to 115.3	ns
5 vs. 8	57	16.67	40.33	-18 to 98.67	ns
5 vs. 9	57	28.67	28.33	-30 to 86.67	ns
5 vs. 10	57	30.67	26.33	-32 to 84.67	ns
5 vs. 11	57	0	57	-1.336 to 115.3	ns
5 vs. 12	57	3.333	53.67	-4.670 to 112	ns
5 vs. 13	57	47.67	9.333	-49 to 67.67	ns
6 vs. 7	28.67	0	28.67	-29.67 to 87	ns
6 vs. 8	28.67	16.67	12	-46.34 to 70.34	ns
6 vs. 9	28.67	28.67	0	-58.34 to 58.34	ns
6 vs. 10	28.67	30.67	-2	-60.34 to 56.34	ns

6 vs. 11	28.67	0	28.67	-29.67 to 87	ns
6 vs. 12	28.67	3.333	25.33	-33 to 83.67	ns
6 vs. 13	28.67	47.67	-19	-77.34 to 39.34	ns
7 vs. 8	0	16.67	-16.67	-75 to 41.67	ns
7 vs. 9	0	28.67	-28.67	-87 to 29.67	ns
7 vs. 10	0	30.67	-30.67	-89 to 27.67	ns
7 vs. 11	0	0	0	-58.34 to 58.34	ns
7 vs. 12	0	3.333	-3.333	-61.67 to 55	ns
7 vs. 13	0	47.67	-47.67	-106 to 10.67	ns
8 vs. 9	16.67	28.67	-12	-70.34 to 46.34	ns
8 vs. 10	16.67	30.67	-14	-72.34 to 44.34	ns
8 vs. 11	16.67	0	16.67	-41.67 to 75	ns
8 vs. 12	16.67	3.333	13.33	-45 to 71.67	ns
8 vs. 13	16.67	47.67	-31	-89.34 to 27.34	ns
9 vs. 10	28.67	30.67	-2	-60.34 to 56.34	ns
9 vs. 11	28.67	0	28.67	-29.67 to 87	ns
9 vs. 12	28.67	3.333	25.33	-33 to 83.67	ns
9 vs. 13	28.67	47.67	-19	-77.34 to 39.34	ns
10 vs. 11	30.67	0	30.67	-27.67 to 89	ns
10 vs. 12	30.67	3.333	27.33	-31 to 85.67	ns
10 vs. 13	30.67	47.67	-17	-75.34 to 41.34	ns
11 vs. 12	0	3.333	-3.333	-61.67 to 55	ns
11 vs. 13	0	47.67	-47.67	-106 to 10.67	ns
12 vs. 13	3.333	47.67	-44.33	-102.7 to 14	ns

CRH-Cre-tdTomato CRH+ inputs onto Vimentin+ tanycytes N=2					
ANOVA summary					
source	**df**	**SS**	**MS**	**F**	**p-value**
Between groups	12	2114	176.2	F (12, 13) = 1.739	p=0.1676
Within groups	13	1317	101.3		
total	25	3430			

Are differences among means statistically significant? ($p < 0.05$)	No
R square	0.6162
Tukey's multiple comparisons test	
Number of families	1
Number of comparisons per family	78
Alpha	0.05

Compared positions	Mean 1	Mean 2	Mean Differences	95% CI of Differences	Significant?
1 vs. 2	7.5	20	-12.5	-52.53 to 27.53	ns
1 vs. 3	7.5	0	7.5	-32.53 to 47.53	ns
1 vs. 4	7.5	27	-19.5	-59.53 to 20.53	ns
1 vs. 5	7.5	22.5	-15	-55.03 to 25.03	ns
1 vs. 6	7.5	20	-12.5	-52.53 to 27.53	ns
1 vs. 7	7.5	4	3.5	-36.53 to 43.53	ns
1 vs. 8	7.5	1.5	6	-34.03 to 46.03	ns
1 vs. 9	7.5	5	2.5	-37.53 to 42.53	ns
1 vs. 10	7.5	10	-2.5	-42.53 to 37.53	ns
1 vs. 11	7.5	21.5	-14	-54.03 to 26.03	ns
1 vs. 12	7.5	10	-2.5	-42.53 to 37.53	ns
1 vs. 13	7.5	1.5	6	-34.03 to 46.03	ns
2 vs. 3	20	0	20	-20.03 to 60.03	ns
2 vs. 4	20	27	-7	-47.03 to 33.03	ns
2 vs. 5	20	22.5	-2.5	-42.53 to 37.53	ns
2 vs. 6	20	20	0	-40.03 to 40.03	ns
2 vs. 7	20	4	16	-24.03 to 56.03	ns
2 vs. 8	20	1.5	18.5	-21.53 to 58.53	ns
2 vs. 9	20	5	15	-25.03 to 55.03	ns
2 vs. 10	20	10	10	-30.03 to 50.03	ns
2 vs. 11	20	21.5	-1.5	-41.53 to 38.53	ns
2 vs. 12	20	10	10	-30.03 to 50.03	ns
2 vs. 13	20	1.5	18.5	-21.53 to 58.53	ns
3 vs. 4	0	27	-27	-67.03 to 13.03	ns
3 vs. 5	0	22.5	-22.5	-62.53 to 17.53	ns

3 vs. 6	0	20	-20	-60.03 to 20.03	ns
3 vs. 7	0	4	-4	-44.03 to 36.03	ns
3 vs. 8	0	1.5	-1.5	-41.53 to 38.53	ns
3 vs. 9	0	5	-5	-45.03 to 35.03	ns
3 vs. 10	0	10	-10	-50.03 to 30.03	ns
3 vs. 11	0	21.5	-21.5	-61.53 to 18.53	ns
3 vs. 12	0	10	-10	-50.03 to 30.03	ns
3 vs. 13	0	1.5	-1.5	-41.53 to 38.53	ns
4 vs. 5	27	22.5	4.5	-35.53 to 44.53	ns
4 vs. 6	27	20	7	-33.03 to 47.03	ns
4 vs. 7	27	4	23	-17.03 to 63.03	ns
4 vs. 8	27	1.5	25.5	-14.53 to 65.53	ns
4 vs. 9	27	5	22	-18.03 to 62.03	ns
4 vs. 10	27	10	17	-23.03 to 57.03	ns
4 vs. 11	27	21.5	5.5	-34.53 to 45.53	ns
4 vs. 12	27	10	17	-23.03 to 57.03	ns
4 vs. 13	27	1.5	25.5	-14.53 to 65.53	ns
5 vs. 6	22.5	20	2.5	-37.53 to 42.53	ns
5 vs. 7	22.5	4	18.5	-21.53 to 58.53	ns
5 vs. 8	22.5	1.5	21	-19.03 to 61.03	ns
5 vs. 9	22.5	5	17.5	-22.53 to 57.53	ns
5 vs. 10	22.5	10	12.5	-27.53 to 52.53	ns
5 vs. 11	22.5	21.5	1	-39.03 to 41.03	ns
5 vs. 12	22.5	10	12.5	-27.53 to 52.53	ns
5 vs. 13	22.5	1.5	21	-19.03 to 61.03	ns
6 vs. 7	20	4	16	-24.03 to 56.03	ns
6 vs. 8	20	1.5	18.5	-21.53 to 58.53	ns
6 vs. 9	20	5	15	-25.03 to 55.03	ns
6 vs. 10	20	10	10	-30.03 to 50.03	ns
6 vs. 11	20	21.5	-1.5	-41.53 to 38.53	ns
6 vs. 12	20	10	10	-30.03 to 50.03	ns
6 vs. 13	20	1.5	18.5	-21.53 to 58.53	ns
7 vs. 8	4	1.5	2.5	-37.53 to 42.53	ns

7 vs. 9	4	5	-1	-41.03 to 39.03	ns
7 vs. 10	4	10	-6	-46.03 to 34.03	ns
7 vs. 11	4	21.5	-17.5	-57.53 to 22.53	ns
7 vs. 12	4	10	-6	-46.03 to 34.03	ns
7 vs. 13	4	1.5	2.5	-37.53 to 42.53	ns
8 vs. 9	1.5	5	-3.5	-43.53 to 36.53	ns
8 vs. 10	1.5	10	-8.5	-48.53 to 31.53	ns
8 vs. 11	1.5	21.5	-20	-60.03 to 20.03	ns
8 vs. 12	1.5	10	-8.5	-48.53 to 31.53	ns
8 vs. 13	1.5	1.5	0	-40.03 to 40.03	ns
9 vs. 10	5	10	-5	-45.03 to 35.03	ns
9 vs. 11	5	21.5	-16.5	-56.53 to 23.53	ns
9 vs. 12	5	10	-5	-45.03 to 35.03	ns
9 vs. 13	5	1.5	3.5	-36.53 to 43.53	ns
10 vs. 11	10	21.5	-11.5	-51.53 to 28.53	ns
10 vs. 12	10	10	0	-40.03 to 40.03	ns
10 vs. 13	10	1.5	8.5	-31.53 to 48.53	ns
11 vs. 12	21.5	10	11.5	-28.53 to 51.53	ns
11 vs. 13	21.5	1.5	20	-20.03 to 60.03	ns
12 vs. 13	10	1.5	8.5	-31.53 to 48.53	ns

Figure 26 – Differences in synaptic inputs between individual subtypes found at the same rostro-caudal position

RAX-CreER^{T2}-tdTomato VGLUT2+ inputs onto RAX+ or GFAP+ tanycytes N=3					
Two-way ANOVA summary					
Source of variation	**df**	**SS**	**MS**	**F**	**p-value**
Interaction	2	2135	1067	F (2, 12) = 3.640	0.0581
Row Factor (diff. rostro-caudal position)	1	272.2	272.2	F (1, 12) = 0.9284	0.3543
Column Factor (diff. tanycytic subtypes)	2	226.3	113.2	F (2, 12) = 0.3859	0.6880
Residual	12	3519	293.2		
Sidak's multiple comparison test (within each row, compare columns)					
Number of families	2				
Number of comparisons per family	3				
Alpha	0.05				
	Mean 1	Mean 2	Mean Differences	95% CI of Differences	Significant?
Bregma -1.82mm (slice2)					
α1 vs. α2/β1	48.67	33.67	15.00	-23.73 to 53.73	ns
α1 vs. β2	48.67	23.33	25.33	-13.40 to 64.07	ns
α2/β1 vs. β2	33.67	23.33	10.33	-28.40 to 49.07	ns
Bregma -1.34mm (slice3)					
α1 vs. α2/β1	18,33	19,00	-0,6667	-39,40 to 38,07	ns
α1 vs. β2	18,33	45,00	-26,67	-65,40 to 12,07	ns
α2/β1 vs. β2	19,00	45,00	-26,00	-64,73 to 12,73	ns

RAX-CreER^{T2}-tdTomato VGAT+ inputs onto RAX+ or GFAP+ tanycytes N=3					
Two-way ANOVA summary					
Source of variation	**df**	**SS**	**MS**	**F**	**p-value**
Interaction	2	2852	1426	F (2, 12) = 4,014	0,0463
Row Factor	1	3698	3698	F (1, 12) = 10,41	0,0073

(diff. rostro-caudal position)					
Column Factor (diff. tanycytic subtypes)	2	940,3	470,2	F (2, 12) = 1,323	0,3024
Residual	12	4263	355,3		

Tukey's multiple comparison test (within each row, compare columns)					
Number of families	2				
Number of comparisons per family	3				
Alpha	0,05				
	Mean 1	Mean 2	Mean Differences	95% CI of Differences	Significant?
Bregma -1.82mm (slice2)					
α1 vs. α2/β1	76.33	57	19.33	-21.73 to 60.39	ns
α1 vs. β2	76.33	28.67	47.67	6.608 to 88.73	*
α2/β1 vs. β2	57	28.67	28.33	-12.73 to 69.39	ns
Bregma -1.34mm (slice3)					
α1 vs. α2/β1	16.67	28.67	-12	-53.06 to 29.06	ns
α1 vs. β2	16.67	30.67	-14	-55.06 to 27.06	ns
α2/β1 vs. β2	28.67	30.67	-2	-43.06 to 39.06	ns

Figure 27 – Differences in synaptic inputs within one tanycytic subtype located at distinct site

RAX-CreER^{T2}-tdTomato VGLUT2+ inputs onto RAX+ or GFAP+ tanycytes N=3								
Multiple t-test								
Discovery determined using the Original FDR method of Benjamini and Hochberg, with Q = 1%								
Each row was analyzed individually without assuming a consistent SD								
Number of t test: 3								
	Discovery?	**p-value**	**Mean 1**	**Mean 2**	**Differences**	**SE of difference**	**t ratio**	df
α1	*	0.0016	48.6667	18.3333	30.3333	3.9861	7.6098	4
α2/β1	ns	0.2197	33.6667	19	14.6667	10.0885	1.4538	4
β2	ns	0.3736	23.3333	45	-21.6667	21.6513	1.0007	4

RAX-CreER^{T2}-tdTomato VGAT+ inputs onto RAX+ or GFAP+ tanycytes N=3								
Multiple t-test								
Discovery determined using the Original FDR method of Benjamini and Hochberg, with Q = 1%								
Each row was analyzed individually without assuming a consistent SD								
Number of t test: 3								
	Discovery?	**p-value**	**Mean 1**	**Mean 2**	**Differences**	**SE of difference**	**t ratio**	df
α1	ns	0.0198	76.3333	16.6667	59.6667	15.871	3.7595	4
α2/β1	ns	0.1243	57	28.6667	28.3333	14.5983	1.9409	4
β2	ns	0.9046	28.6667	30.6667	-2	15.6702	0.1276	4

Figure 28 – Caudal-to-rostral distribution of different tanycytic markers across the borders of the hypothalamic III-ventricle

Position	Signal					
	Nestin N=5		**Vimentin N=3**		**RAX N=6**	
	Mean	SEM	Mean	SEM	Mean	SEM
1	14.8	1.744	8.333	4.410	17.667	1.229
2	17.8	2.8	11.333	3.180	19.833	2.810
3	0.6	0.6	2.333	2.333	14.333	1.430
4	16.8	4.641	4.667	3.283	18.667	2.753
5	16.2	5.064	10	7.211	17.667	1.202
6	15	4.347	9	4.726	9.667	1.563
7	0	0	0	0	0	0.000
8	0.667	0.333	1.667	1.667	7.667	2.642
9	10.2	4.716	5.667	4.256	11.5	3.019
10	13.6	3.187	10.333	5.548	15.333	2.404
11	6	5.282	0.667	0.667	0	0
12	4	2.098	1	1	0	0
13	13.6	3.995	0	0	1.333	0.715

Position	Signal					
	GFAP N=9		RAX + GFAP N=6		Vimentin + GFAP N=3	
	Mean	SEM	Mean	SEM	Mean	SEM
1	0.778	0.572	0	0	1.667	1.667
2	0.667	0.667	0	0	1.667	0.882
3	12.556	3.735	0.333	0.333	8.333	8.333
4	7.889	2.176	1.5	0.563	10.667	3.756
5	1.778	0.683	0	0	13.333	8.452
6	0	0	0	0	0	0
7	1.111	0.754	0	0	9	4.933
8	12.556	3.087	1	0.632	6.667	4.410

9	13.444	3.5	0.333	0.333	11	5.292
10	0	0	0	0	8.333	8.333
11	0.111	0.111	0	0	4.667	2.333
12	4.778	1.665	0	0	9	4.726
13	11.222	3.539	0	0	7.333	3.667

Figure 29 – Percentage of detected tanycytes at position 1 to 13 being either RAX+/GFAP-, RAX-/GFAP+ or RAX+/GFAP+

RAX-CreER^{T2}-tdTomato % of RAX+/GFAP-, RAX-/GFAP+ and RAX+/GFAP+ tanycytes N=6						
	RAX+/GFAP- tanycytes		RAX-/GFAP+ tanycytes		RAX+/GFAP+ tanycytes	
Positions	Mean	SEM	Mean	SEM	Mean	SEM
1	100	1.229	0	0	0	0
2	100	2.81	0	0	0	0
3	43.216	1.43	55.779	3.490	1.005	0.334
4	64.740	2.753	30.058	2.765	5.202	0.563
5	88.333	1.202	11.667	0.955	0	0
6	100	1.563	0	0	0	0
7	0	0	100	0.667	0	0
8	28.571	2.642	67.702	1.956	3.727	0.632
9	36.126	3.019	62.827	1.897	1.047	0.334
10	100	2.404	0	0	0	0
11	0	0	0	0	0	0
12	0	0	100	2.029	0	0
13	7.339	0.715	92.661	3.341	0	0